

NONLINEAR DYNAMICS AND SYSTEMS THEORY

An International Journal of Research and Surveys

Volume 24

Number 4

2024

CONTENTS

Existence of Solution for a General Class of Strongly Nonlinear Elliptic Problems.....	321
<i>Y. Akdim and M. Ouboufettal</i>	
Optimization of Hotel Y Management through Application of Occupancy Forecasting by Support Vector Machine and K-Nearest Neighbors Methods.....	331
<i>M. Y. Anshori, I. H. Santoso, P. Katias, T. Herlambang, H. Arof, B. Suharto and K. Oktafianto</i>	
A New Numerical Scheme for Solving Time-Fractional Variable-Order Partial Differential Equations.....	340
<i>Soufiane Benyoussef, Oumkeltoum Benhamouda, Mohamed Dalah and Khaled Zennir</i>	
Application of Discrete Event Simulation and System Dynamics Modeling in Optimizing the Performance of OutPatient Department.....	354
<i>Amina Boukoftane, Muhammad Ahmed Kalwar, Nadia Oukid, Khaled Zennir, Muhammad Saad Memon and Muhammad Ali Khan</i>	
Sharing Keys Using Some Toeplitz Matrices and Logistic Maps.....	366
<i>Benzeghli Brahim and Adoui Salah</i>	
Analysis and Existence of Rumor Spreading with Campaign and Punishment Control	380
<i>Irma Fitria, Subchan Subchan, Dinda Anisa Maulina and Alvian Alif Hidayatullah</i>	
Square Root Ensemble Kalman Filter for Forefinger Motion Estimation as Post-Stroke Patients' Medical Rehabilitation.....	392
<i>T. Herlambang, F. A. Susanto, H. Nurhadi, K. Oktafianto, H. Arof and R. S. Marjianto</i>	
On the Synchronization of a Novel Chaotic System with Two Control Methods.....	400
<i>Lakehal Nadjet and Fareh Hannachi</i>	
An Efficient DCA Algorithm for Solving Non-Monotone Affine Variational Inequality Problem.....	410
<i>A. Noui, Z. Kebaili and M. Achache</i>	
A Novel Numerical Approach for Solving Nonlinear Volterra Integral Equation with Constant Delay.....	419
<i>K. Rouibah, S. Kaouache and A. Bellour</i>	

NONLINEAR DYNAMICS & SYSTEMS THEORY

Volume 24, No. 4, 2024

Nonlinear Dynamics and Systems Theory

An International Journal of Research and Surveys

EDITOR-IN-CHIEF A.A.MARTYNYUK

*S.P.Timoshenko Institute of Mechanics
National Academy of Sciences of Ukraine, Kiev, Ukraine*

MANAGING EDITOR I.P.STAVROULAKIS

Department of Mathematics, University of Ioannina, Greece

REGIONAL EDITORS

S.G. GEORGIEV, Paris, France

A.OKNIŃSKI, Kielce, Poland
Europe

M.BOHNER, Rolla, USA

HAO WANG, Edmonton, Canada
USA and Canada

T.A.BURTON, Port Angeles, USA

C.CRUZ-HERNANDEZ, Ensenada, Mexico
Central and South America

M.ALQURAN, Irbid, Jordan

Jordan and Middle East

T.HERLAMANG, Surabaya, Indonesia

Indonesia and New Zealand

Nonlinear Dynamics and Systems Theory

An International Journal of Research and Surveys

EDITOR-IN-CHIEF A.A.MARTYNYUK

The S.P. Timoshenko Institute of Mechanics, National Academy of Sciences of Ukraine,
Nesterov Str. 3, 03057, Kyiv-57, UKRAINE / e-mail: journalndst@gmail.com

MANAGING EDITOR I.P.STAVROULAKIS

Department of Mathematics, University of Ioannina
451 10 Ioannina, HELLAS (GREECE) / e-mail: ipstav@cc.uoi.gr

ADVISORY EDITOR A.G.MAZKO,

Institute of Mathematics of NAS of Ukraine, Kiev (Ukraine)
e-mail: mazko@imath.kiev.ua

REGIONAL EDITORS

S.G. GEORGIEV, France, e-mail: svetlingeorgiev1@gmail.com
A. OKNINSKI, Poland, e-mail: fizao@tu.kielce.pl
M. BOHNER, USA, e-mail: bohner@mst.edu
HAO WANG, Edmonton, Canada, e-mail: hao8@ualberta.ca
T.A. BURTON, USA, e-mail: taburton@olypen.com
C. CRUZ-HERNANDEZ, Mexico, e-mail: ccruz@cicese.mx
M. ALQURAN, Jordan, e-mail: marwan04@just.edu.jo
T. HERLAMBANG, Indonesia, e-mail: teguh@unusa.ac.id

EDITORIAL BOARD

Adzkiya, D. (Indonesia)	Kloedon, P. (Germany)
Artstein, Z. (Israel)	Kokologiannaki, C. (Greece)
Awrejcewicz, J. (Poland)	Kouzou A. (Algeria)
Braiek, N. B. (Tunisia)	Krishnan, E. V. (Oman)
Chen Ye-Hwa (USA)	Kryzhevich, S. (Poland)
De Angelis, M. (Italy)	Limarchenko, O. S. (Ukraine)
Denton, Z. (USA)	Lopez Gutierrez R. M. (Mexico)
Djemai, M. (France)	Lozi, R. (France)
Dshalalow, J. H. (USA)	Peterson, A. (USA)
Gajic Z. (USA)	Radziszewski, B. (Poland)
Georgiou, G. (Cyprus)	Shi Yan (Japan)
Honglei Xu (Australia)	Sivasundaram, S. (USA)
Jafari, H. (South African Republic)	Staicu V. (Portugal)
Khusainov, D. Ya. (Ukraine)	Vatsala, A. (USA)

ADVISORY COMPUTER SCIENCE EDITORS

A.N.CHERNIENKO and A.S.KHOROSHUN, Kiev, Ukraine

ADVISORY LINGUISTIC EDITOR

S.N.RASSHYVALOVA, Kiev, Ukraine

© 2024, InforMath Publishing Group, ISSN 1562-8353 print, ISSN 1813-7385 online, Printed in Ukraine
No part of this Journal may be reproduced or transmitted in any form or by any means without
permission from InforMath Publishing Group.

INSTRUCTIONS FOR CONTRIBUTORS

(1) General. Nonlinear Dynamics and Systems Theory (ND&ST) is an international journal devoted to publishing peer-refereed, high quality, original papers, brief notes and review articles focusing on nonlinear dynamics and systems theory and their practical applications in engineering, physical and life sciences. Submission of a manuscript is a representation that the submission has been approved by all of the authors and by the institution where the work was carried out. It also represents that the manuscript has not been previously published, has not been copyrighted, is not being submitted for publication elsewhere, and that the authors have agreed that the copyright in the article shall be assigned exclusively to InforMath Publishing Group by signing a transfer of copyright form. Before submission, the authors should visit the website:

<http://www.e-ndst.kiev.ua>

for information on the preparation of accepted manuscripts. Please download the archive Sample_NDST.zip containing example of article file (you can edit only the file Samplefilename.tex).

(2) Manuscript and Correspondence. Manuscripts should be in English and must meet common standards of usage and grammar. To submit a paper, send by e-mail a file in PDF format directly to

*Professor A.A. Martynyuk, Institute of Mechanics,
Nesterov str.3, 03057, Kiev-57, Ukraine
e-mail: journalndst@gmail.com*

or to one of the Regional Editors or to a member of the Editorial Board. Final version of the manuscript must typeset using LaTeX program which is prepared in accordance with the style file of the Journal. Manuscript texts should contain the title of the article, name(s) of the author(s) and complete affiliations. Each article requires an abstract not exceeding 150 words. Formulas and citations should not be included in the abstract. AMS subject classifications and key words must be included in all accepted papers. Each article requires a running head (abbreviated form of the title) of no more than 30 characters. The sizes for regular papers, survey articles, brief notes, letters to editors and book reviews are: (i) 10-14 pages for regular papers, (ii) up to 24 pages for survey articles, and (iii) 2-3 pages for brief notes, letters to the editor and book reviews.

(3) Tables, Graphs and Illustrations. Each figure must be of a quality suitable for direct reproduction and must include a caption. Drawings should include all relevant details and should be drawn professionally in black ink on plain white drawing paper. In addition to a hard copy of the artwork, it is necessary to attach the electronic file of the artwork (preferably in PCX format).

(4) References. Each entry must be cited in the text by author(s) and number or by number alone. All references should be listed in their alphabetic order. Use please the following style:

Journal: [1] H. Poincare, Title of the article. *Title of the Journal* volume (issue) (year) pages. [Language]

Book: [2] A.M. Lyapunov, *Title of the Book*. Name of the Publishers, Town, year.

Proceeding: [3] R. Bellman, Title of the article. In: *Title of the Book*. (Eds.). Name of the Publishers, Town, year, pages. [Language]

(5) Proofs and Sample Copy. Proofs sent to authors should be returned to the Editorial Office with corrections within three days after receipt. The corresponding author will receive a sample copy of the issue of the Journal for which his/her paper is published.

(6) Editorial Policy. Every submission will undergo a stringent peer review process. An editor will be assigned to handle the review process of the paper. He/she will secure at least two reviewers' reports. The decision on acceptance, rejection or acceptance subject to revision will be made based on these reviewers' reports and the editor's own reading of the paper.

NONLINEAR DYNAMICS AND SYSTEMS THEORY

An International Journal of Research and Surveys
Published by InforMath Publishing Group since 2001

Volume 24

Number 4

2024

CONTENTS

- Existence of Solution for a General Class of Strongly Nonlinear Elliptic Problems 321
Y. Akdim and M. Ouboufettal
- Optimization of Hotel Y Management through Application of Occupancy Forecasting by Support Vector Machine and K-Nearest Neighbors Methods 331
M. Y. Anshori, I. H. Santoso, P. Katias, T. Herlambang, H. Arof, B. Suharto and K. Oktafianto
- A New Numerical Scheme for Solving Time-Fractional Variable-Order Partial Differential Equations 340
Soufiane Benyoussef, Oumkeltoum Benhamouda, Mohamed Dalah and Khaled Zennir
- Application of Discrete Event Simulation and System Dynamics Modeling in Optimizing the Performance of OutPatient Department 354
Amina Boukoftane, Muhammad Ahmed Kalwar, Nadia Oukid, Khaled Zennir, Muhammad Saad Memon and Muhammad Ali Khan
- Sharing Keys Using Some Toeplitz Matrices and Logistic Maps 366
Benzeghli Brahim and Adoui Salah
- Analysis and Existence of Rumor Spreading with Campaign and Punishment Control 380
Irma Fitria, Subchan Subchan, Dinda Anisa Maulina and Alvian Alif Hidayatullah
- Square Root Ensemble Kalman Filter for Forefinger Motion Estimation as Post-Stroke Patients' Medical Rehabilitation 392
T. Herlambang, F. A. Susanto, H. Nurhadi, K. Oktafianto, H. Arof and R. S. Marjianto
- On the Synchronization of a Novel Chaotic System with Two Control Methods 400
Lakehal Nadjet and Fareh Hannachi
- An Efficient DCA Algorithm for Solving Non-Monotone Affine Variational Inequality Problem 410
A. Noui, Z. Kebaili and M. Achache
- A Novel Numerical Approach for Solving Nonlinear Volterra Integral Equation with Constant Delay 419
K. Rouibah, S. Kaouache and A. Bellour

Founded by A.A. Martynyuk in 2001.

Registered in Ukraine Number: KB No 5267 / 04.07.2001.

NONLINEAR DYNAMICS AND SYSTEMS THEORY

An International Journal of Research and Surveys

Impact Factor from SCOPUS for 2022: SJR – 0.293, SNIP – 0.784 and CiteScore – 1.5

Nonlinear Dynamics and Systems Theory (ISSN 1562–8353 (Print), ISSN 1813–7385 (Online)) is an international journal published under the auspices of the S.P. Timoshenko Institute of Mechanics of National Academy of Sciences of Ukraine and Curtin University of Technology (Perth, Australia). It aims to publish high quality original scientific papers and surveys in areas of nonlinear dynamics and systems theory and their real world applications.

AIMS AND SCOPE

Nonlinear Dynamics and Systems Theory is a multidisciplinary journal. It publishes papers focusing on proofs of important theorems as well as papers presenting new ideas and new theory, conjectures, numerical algorithms and physical experiments in areas related to nonlinear dynamics and systems theory. Papers that deal with theoretical aspects of nonlinear dynamics and/or systems theory should contain significant mathematical results with an indication of their possible applications. Papers that emphasize applications should contain new mathematical models of real world phenomena and/or description of engineering problems. They should include rigorous analysis of data used and results obtained. Papers that integrate and interrelate ideas and methods of nonlinear dynamics and systems theory will be particularly welcomed. This journal and the individual contributions published therein are protected under the copyright by International InforMath Publishing Group.

PUBLICATION AND SUBSCRIPTION INFORMATION

Nonlinear Dynamics and Systems Theory will have 6 issues in 2024, printed in hard copy (ISSN 1562–8353) and available online (ISSN 1813–7385), by InforMath Publishing Group, Nesterov str., 3, Institute of Mechanics, Kiev, MSP 680, Ukraine, 03057. Subscription prices are available upon request from the Publisher, EBSCO Information Services (<mailto:journals@ebSCO.com>), or website of the Journal: <http://e-ndst.kiev.ua>. Subscriptions are accepted on a calendar year basis. Issues are sent by airmail to all countries of the world. Claims for missing issues should be made within six months of the date of dispatch.

ABSTRACTING AND INDEXING SERVICES

Papers published in this journal are indexed or abstracted in: Mathematical Reviews / MathSciNet, Zentralblatt MATH / Mathematics Abstracts, PASCAL database (INIST–CNRS) and SCOPUS.



Existence of Solution for a General Class of Strongly Nonlinear Elliptic Problems

Y. Akdim* and M. Ouboufettal

LAMA Laboratory, Department of Mathematics, Faculty of Sciences Dhar El Mahraz, University Sidi Mohamed Ben Abdellah, P.O. Box 1796 Atlas Fez, Morocco.

Received: April 27, 2020; Revised: May 30, 2024

Abstract: In this paper, we study the existence of solution for a general class of strongly nonlinear elliptic problems associated with the differential inclusion $\beta(u) + A(u) + g(x, u, Du) \ni f$, where A is a Leray-Lions operator from $W_0^{1,p}(\Omega)$ into its dual, β is a maximal monotone mapping such that $0 \in \beta(0)$, while $g(x, s, \xi)$ is a nonlinear term which has a growth condition with respect to ξ and no growth with respect to s but it satisfies a sign condition on s . The right-hand side f is assumed to belong to $L^\infty(\Omega)$.

Keywords: inclusion problems; Leray-Lions operator; maximal monotone mapping; Sobolev spaces; truncation.

Mathematics Subject Classification (2010): 35J60, 35J70, 70K99.

1 Introduction

Let Ω be a bounded domain in $\mathbb{R}^N (N \geq 1)$ with sufficiently smooth boundary $\partial\Omega$. Our aim is to show the existence of solutions for the following strongly nonlinear elliptic inclusion:

$$(E, f) \quad \begin{cases} \beta(u) + A(u) + g(x, u, Du) \ni f \text{ in } \mathcal{D}'(\Omega), \\ u \in W_0^{1,p}(\Omega), g(x, u, Du) \in L^1(\Omega), g(x, u, Du)u \in L^1(\Omega), \end{cases}$$

where A is a Leray-Lions operator from $W_0^{1,p}(\Omega)$ into its dual $W^{-1,p'}(\Omega)$ ($1 < p < \infty$) defined as $A(u) = -\text{div}(a(x, u, Du))$, $f \in L^\infty(\Omega)$, β is a maximal monotone mapping

* Corresponding author: <mailto:youssef.akdim@usmba.ac.ma>

such that $0 \in \beta(0)$ and g is a nonlinear lower term having "natural growth" (of order p) with respect to Du , with respect to u , we do not assume any growth restrictions, but we assume the "sign condition" $g(x, s, \xi)s \geq 0$.

The particular instances of the problem (E, f) have been studied for $\beta \equiv 0$, Boccardo, Gallouët and Murat in [7] have proved the existence of at least one solution for the problem. Let us point out that another work in this direction can be found in [6].

For $g \equiv 0$, it is known (cf. [5, 10, 18, 20]) that the problem (E, f) has a solution in the standard sense, the so-called weak solution, that is, a couple $(u, b) \in W_0^{1,p}(\Omega) \times L^1(\Omega)$ such that $b \in \beta(u)$ a.e. in Ω and

$$\int_{\Omega} b\varphi + \int_{\Omega} a(x, u, Du) \cdot D\varphi = \int_{\Omega} f\varphi, \quad \forall \varphi \in W_0^{1,p}(\Omega) \cap L^{\infty}(\Omega).$$

In another important work [2], Akdim and Allalou have proved the existence of a renormalized solution for an elliptic problem of diffusion-convection type in the framework of weighted variable exponent Sobolev spaces

$$(E) \begin{cases} \beta(u) - \operatorname{div}(a(x, Du) + F(u)) \ni f & \text{in } \Omega, \\ u = 0 & \text{on } \partial\Omega. \end{cases}$$

We also refer the reader to [1, 3, 4, 8, 12, 13, 17, 19] for more results on problems in this direction. One of the motivations for studying (E, f) comes from applications to rheological fluids (see [16] for more details) as an important class of non-Newtonian fluids.

The present paper is organized as follows. In Section 2, we give assumptions and the statement of result. The proof of the theorem is given in Section 3, it consists of the following steps. First, we define approximation equations. We then prove an a priori estimate in $W_0^{1,p}(\Omega)$ for the solutions u_{ε} of these approximate equations. Finally, we prove that the truncations $T_k(u_{\varepsilon})$ are relatively compact in the strong topology of $W_0^{1,p}(\Omega)$, a result which allows us to pass to the limit and obtain the existence result. In the last Section 4, we will present an example for illustrating our abstract result.

2 Assumptions and Main Result

2.1 Assumptions

Let Ω be a bounded domain in \mathbb{R}^N ($N \geq 1$) with sufficiently smooth boundary $\partial\Omega$ and $1 < p < \infty$ be fixed.

Let A be a nonlinear operator from $W_0^{1,p}(\Omega)$ into its dual $W^{-1,p'}(\Omega)$ ($\frac{1}{p} + \frac{1}{p'} = 1$) defined by $A(u) = -\operatorname{div}(a(x, u, Du))$, where $a : \Omega \times \mathbb{R} \times \mathbb{R}^N \rightarrow \mathbb{R}^N$ is the Carathéodory function satisfying the following assumptions:

(H_1)

$$a(x, s, \xi) \cdot \xi \geq \lambda|\xi|^p, \quad \text{where } \lambda > 0, \quad (1)$$

$$|a(x, s, \xi)| \leq \alpha(k(x) + |s|^{p-1} + |\xi|^{p-1}), \quad \text{where } k(x) \in L^{p'}(\Omega), \quad k \geq 0, \quad \alpha > 0, \quad (2)$$

$$(a(x, s, \xi) - a(x, s, \eta)) \cdot (\xi - \eta) > 0 \quad \text{for } \xi \neq \eta \in \mathbb{R}^N. \quad (3)$$

Let $g : \Omega \times \mathbb{R} \times \mathbb{R}^N \rightarrow \mathbb{R}$ be the Carathéodory function such that
 (H₂)

$$g(x, s, \xi)s \geq 0, \tag{4}$$

$$|g(x, s, \xi)| \leq h(|s|)(c(x) + |\xi|^p), \tag{5}$$

where $h : \mathbb{R}^+ \rightarrow \mathbb{R}^+$ is a continuous increasing function and $c(x)$ is a positive function which is in $L^1(\Omega)$.

Let $\beta : \mathbb{R} \rightarrow 2^{\mathbb{R}}$ be a set valued, maximal monotone mapping such that $0 \in \beta(0)$ and consider

(H₃) $f \in L^\infty(\Omega)$.

2.2 Main result

Consider the strongly nonlinear elliptic inclusion problem with the Dirichlet boundary conditions

$$(E, f) \begin{cases} \beta(u) + A(u) + g(x, u, Du) \ni f \text{ in } \mathcal{D}'(\Omega), \\ u \in W_0^{1,p}(\Omega), g(x, u, Du) \in L^1(\Omega), g(x, u, Du)u \in L^1(\Omega). \end{cases}$$

Definition 2.1 A weak solution to (E, f) is a pair of functions $(u, b) \in W_0^{1,p}(\Omega) \times L^1(\Omega)$ satisfying $b(x) \in \beta(u(x))$ a.e. in Ω , $g(x, u, Du) \in L^1(\Omega)$, $g(x, u, Du)u \in L^1(\Omega)$ and

$$b - \operatorname{div}(a(x, u, Du)) + g(x, u, Du) = f \text{ in } \mathcal{D}'(\Omega).$$

Our objective is to prove the following existence theorem.

Theorem 2.1 *Under the assumptions (H₁) – (H₃), there exists at least one weak solution of (E, f) in the sense of Definition 2.1.*

3 Proof of Theorem 2.1

Step 1: Approximate problems

From now on, we will use the standard truncation function $T_k, k \geq 0$, defined for all $s \in \mathbb{R}$ by $T_k(s) = \max\{-k, \min\{s, k\}\}$.

Let $0 < \varepsilon \leq 1$, we introduce the approximate problem

$$(E_\varepsilon, f) \begin{cases} \beta_\varepsilon(T_{\frac{1}{\varepsilon}}(u_\varepsilon)) - \operatorname{div}(a(x, u_\varepsilon, Du_\varepsilon)) + g_\varepsilon(x, u_\varepsilon, Du_\varepsilon) = f, \\ u_\varepsilon \in W_0^{1,p}(\Omega), \end{cases}$$

where

$$g_\varepsilon(x, s, \xi) = \frac{g(x, s, \xi)}{1 + \varepsilon|g(x, s, \xi)|}$$

satisfies

$$g_\varepsilon(x, s, \xi)s \geq 0, |g_\varepsilon(x, s, \xi)| \leq |g(x, s, \xi)|, |g_\varepsilon(x, s, \xi)| \leq \frac{1}{\varepsilon}$$

and where $\beta_\varepsilon : \mathbb{R} \rightarrow \mathbb{R}$ is the Yosida approximation of β . Note that, for any $u \in W_0^{1,p}(\Omega)$, we have

$$\langle \beta_\varepsilon(u), u \rangle \geq 0, \quad |\beta_\varepsilon(u)| \leq \frac{1}{\varepsilon}|u| \quad \text{and} \quad \lim_{\varepsilon \rightarrow 0} \beta_\varepsilon(u) = \beta(u).$$

We refer the reader to [9] for more details about the maximal monotone mapping.

Since $|\beta_\varepsilon(T_{\frac{1}{\varepsilon}}(u_\varepsilon))| \leq \frac{1}{\varepsilon^2}$ and g_ε is bounded for any fixed $\varepsilon > 0$, there exists at least one solution u_ε of (E_ε, f) (cf. [14], [15]), i.e., for each $0 < \varepsilon \leq 1$ and $f \in W^{-1,p'}(\Omega)$, there exists at least one solution $u_\varepsilon \in W_0^{1,p}(\Omega)$ such that

$$\int_{\Omega} \beta_\varepsilon(T_{\frac{1}{\varepsilon}}(u_\varepsilon))\varphi + \int_{\Omega} a(x, u_\varepsilon, Du_\varepsilon) \cdot D\varphi + \int_{\Omega} g_\varepsilon(x, u_\varepsilon, Du_\varepsilon)\varphi = \langle f, \varphi \rangle \quad (6)$$

holds for all $\varphi \in W_0^{1,p}(\Omega)$, where $\langle \cdot, \cdot \rangle$ denotes the duality pairing between $W_0^{1,p}(\Omega)$ and $W^{-1,p'}(\Omega)$.

Step 2: A priori estimates

Taking u_ε as a test function in (6), we obtain

$$\int_{\Omega} \beta_\varepsilon(T_{\frac{1}{\varepsilon}}(u_\varepsilon))u_\varepsilon + \int_{\Omega} a(x, u_\varepsilon, Du_\varepsilon) \cdot Du_\varepsilon + \int_{\Omega} g_\varepsilon(x, u_\varepsilon, Du_\varepsilon)u_\varepsilon = \int_{\Omega} f u_\varepsilon, \quad (7)$$

as the first term on the left-hand side is nonnegative and since g_ε verifies the sign condition, by (1), we have

$$\lambda \|u_\varepsilon\|_{W_0^{1,p}(\Omega)}^p \leq C \|f\|_{L^\infty(\Omega)} \|u_\varepsilon\|_{W_0^{1,p}(\Omega)},$$

where C is a positive constant coming from the Hölder and Poincaré inequalities, then

$$\|u_\varepsilon\|_{W_0^{1,p}(\Omega)} \leq C_1. \quad (8)$$

Moreover, from (7) and (8), we infer that

$$0 \leq \int_{\Omega} g_\varepsilon(x, u_\varepsilon, Du_\varepsilon)u_\varepsilon \leq C_2. \quad (9)$$

For $\delta > 0$, we define $H_\delta^+ : \mathbb{R} \rightarrow \mathbb{R}$ by

$$H_\delta^+(r) = \begin{cases} 1 & \text{if } r > \delta, \\ \frac{r}{\delta} & \text{if } 0 \leq r \leq \delta, \\ 0 & \text{if } r < 0. \end{cases}$$

Clearly, H_δ^+ is an approximation of $sign_0^+$.

We use the test function $\varphi = H_\delta^+(\beta_\varepsilon(T_{\frac{1}{\varepsilon}}(u_\varepsilon)) - k)$ in (6), we obtain

$$\int_\Omega \beta_\varepsilon(T_{\frac{1}{\varepsilon}}(u_\varepsilon))H_\delta^+(\beta_\varepsilon(T_{\frac{1}{\varepsilon}}(u_\varepsilon)) - k) + \int_\Omega a(x, u_\varepsilon, Du_\varepsilon) \cdot D(H_\delta^+(\beta_\varepsilon(T_{\frac{1}{\varepsilon}}(u_\varepsilon)) - k)) + \int_\Omega g_\varepsilon(x, u_\varepsilon, Du_\varepsilon)H_\delta^+(\beta_\varepsilon(T_{\frac{1}{\varepsilon}}(u_\varepsilon)) - k) = \int_\Omega fH_\delta^+(\beta_\varepsilon(T_{\frac{1}{\varepsilon}}(u_\varepsilon)) - k).$$

By using (1) and the fact that β_ε is monotone increasing with $\beta_\varepsilon(0) = 0$, we have

$$\int_\Omega a(x, u_\varepsilon, Du_\varepsilon)(H_\delta^+)'(\beta_\varepsilon(T_{\frac{1}{\varepsilon}}(u_\varepsilon)) - k)\beta_\varepsilon'(T_{\frac{1}{\varepsilon}}(u_\varepsilon)) \cdot Du_\varepsilon \geq 0.$$

Since g_ε verifies the sign condition, we obtain

$$\int_\Omega g_\varepsilon(x, u_\varepsilon, Du_\varepsilon)H_\delta^+(\beta_\varepsilon(T_{\frac{1}{\varepsilon}}(u_\varepsilon)) - k) \geq 0.$$

Consequently, we get

$$\int_\Omega (\beta_\varepsilon(T_{\frac{1}{\varepsilon}}(u_\varepsilon)) - k)H_\delta^+(\beta_\varepsilon(T_{\frac{1}{\varepsilon}}(u_\varepsilon)) - k) \leq \int_\Omega (f - k)H_\delta^+(\beta_\varepsilon(T_{\frac{1}{\varepsilon}}(u_\varepsilon)) - k).$$

Taking $\delta \rightarrow 0$ yields

$$\int_\Omega (\beta_\varepsilon(T_{\frac{1}{\varepsilon}}(u_\varepsilon)) - k)^+ \leq \int_\Omega (f - k)^+. \tag{10}$$

Similarly, one can show

$$\int_\Omega (\beta_\varepsilon(T_{\frac{1}{\varepsilon}}(u_\varepsilon)) + k)^- \leq \int_\Omega (f + k)^-. \tag{11}$$

Combining (10) and (11) gives

$$\int_\Omega (|\beta_\varepsilon(T_{\frac{1}{\varepsilon}}(u_\varepsilon))| - k)^+ \leq \int_\Omega (|f| - k)^+.$$

Choosing $k > \|f\|_\infty$, we obtain

$$\|\beta_\varepsilon(T_{\frac{1}{\varepsilon}}(u_\varepsilon))\|_\infty \leq \|f\|_\infty. \tag{12}$$

Step 3: Basic convergence results

By (12), there exists $b \in L^\infty(\Omega)$ such that

$$\beta_\varepsilon(T_{\frac{1}{\varepsilon}}(u_\varepsilon)) \overset{*}{\rightharpoonup} b \text{ in } L^\infty(\Omega). \tag{13}$$

Since u_ε remains bounded in $W_0^{1,p}(\Omega)$, we can extract a subsequence, still denoted by u_ε , such that

$$u_\varepsilon \rightharpoonup u \text{ weakly in } W_0^{1,p}(\Omega)$$

and

$$u_\varepsilon \rightarrow u \text{ a.e. in } \Omega.$$

We already know that for any fixed $k \in \mathbb{R}^{*+}$,

$$T_k(u_\varepsilon) \rightharpoonup T_k(u) \text{ weakly in } W_0^{1,p}(\Omega).$$

Our objective is to prove that

$$T_k(u_\varepsilon) \rightarrow T_k(u) \text{ strongly in } W_0^{1,p}(\Omega).$$

We shall use in (6) the test function

$$v_\varepsilon = \varphi(z_\varepsilon),$$

where

$$z_\varepsilon = T_k(u_\varepsilon) - T_k(u) \text{ and } \varphi(s) = se^{\lambda s^2}.$$

We get

$$\int_{\Omega} \beta_\varepsilon(T_{\frac{1}{\varepsilon}}(u_\varepsilon))v_\varepsilon + \int_{\Omega} a(x, u_\varepsilon, Du_\varepsilon) \cdot Dv_\varepsilon + \int_{\Omega} g_\varepsilon(x, u_\varepsilon, Du_\varepsilon)v_\varepsilon = \int_{\Omega} f v_\varepsilon.$$

From now on, we denote by $\eta^1(\varepsilon), \eta^2(\varepsilon), \dots$ various sequences of real numbers which converge to zero when ε tends to zero.

Since v_ε converges to zero weakly* in $L^\infty(\Omega)$, we have

$$\int_{\Omega} f v_\varepsilon \rightarrow 0,$$

this implies that

$$\eta^1(\varepsilon) = \int_{\Omega} \beta_\varepsilon(T_{\frac{1}{\varepsilon}}(u_\varepsilon))v_\varepsilon + \int_{\Omega} a(x, u_\varepsilon, Du_\varepsilon) \cdot Dv_\varepsilon + \int_{\Omega} g_\varepsilon(x, u_\varepsilon, Du_\varepsilon)v_\varepsilon \rightarrow 0.$$

Note that

$$\int_{\Omega} \beta_\varepsilon(T_{\frac{1}{\varepsilon}}(u_\varepsilon))v_\varepsilon = \int_{\{|u_\varepsilon| \leq k\}} \beta_\varepsilon(T_{\frac{1}{\varepsilon}}(u_\varepsilon))v_\varepsilon + \int_{\{|u_\varepsilon| > k\}} \beta_\varepsilon(T_{\frac{1}{\varepsilon}}(u_\varepsilon))v_\varepsilon.$$

The fact that the second term on the right-hand side is nonnegative and $\chi_{\{|u_\varepsilon| \leq k\}} \beta_\varepsilon(T_{\frac{1}{\varepsilon}}(u_\varepsilon))$ is uniformly bounded, together with the Lebesgue dominated convergence theorem provide that

$$\int_{\{|u_\varepsilon| \leq k\}} \beta_\varepsilon(T_{\frac{1}{\varepsilon}}(u_\varepsilon))v_\varepsilon \rightarrow 0.$$

This implies that

$$\int_{\Omega} a(x, u_\varepsilon, Du_\varepsilon) \cdot Dv_\varepsilon + \int_{\Omega} g_\varepsilon(x, u_\varepsilon, Du_\varepsilon)v_\varepsilon \leq \eta^2(\varepsilon).$$

Using the same arguments as in [7], we obtain

$$0 \leq \int_{\Omega} [a(x, T_k(u_\varepsilon), DT_k(u_\varepsilon)) - a(x, T_k(u), DT_k(u))] \cdot D(T_k(u_\varepsilon) - T_k(u)) \leq \eta^3(\varepsilon).$$

Finally, a result in [8] (see also [11]) implies

$$T_k(u_\varepsilon) \rightarrow T_k(u) \text{ strongly in } W_0^{1,p}(\Omega). \tag{14}$$

Step 4: Passing to the limit

In virtue of (14), we have for the subsequence

$$Du_\varepsilon \rightarrow Du \text{ a.e. in } \Omega,$$

which with

$$u_\varepsilon \rightarrow u \text{ a.e. in } \Omega$$

yields, since $a(x, u_\varepsilon, Du_\varepsilon)$ is bounded in $(L^{p'}(\Omega))^N$,

$$a(x, u_\varepsilon, Du_\varepsilon) \rightharpoonup a(x, u, Du) \text{ weakly in } (L^{p'}(\Omega))^N \tag{15}$$

as well as

$$g_\varepsilon(x, u_\varepsilon, Du_\varepsilon) \rightarrow g(x, u, Du) \text{ a.e. in } \Omega. \tag{16}$$

We now use the classical trick in order to prove that $g_\varepsilon(x, u_\varepsilon, Du_\varepsilon)$ is uniformly equi-integrable.

For any measurable subset E of Ω and for any $m \in \mathbb{R}^+$, we have

$$\begin{aligned} \int_E |g_\varepsilon(x, u_\varepsilon, Du_\varepsilon)| &= \int_{E \cap \{|u_\varepsilon| \leq m\}} |g_\varepsilon(x, u_\varepsilon, Du_\varepsilon)| + \int_{E \cap \{|u_\varepsilon| > m\}} |g_\varepsilon(x, u_\varepsilon, Du_\varepsilon)| \\ &\leq \int_E |g_\varepsilon(x, T_m(u_\varepsilon), DT_m(u_\varepsilon))| + \frac{1}{m} \int_E g_\varepsilon(x, u_\varepsilon, Du_\varepsilon)u_\varepsilon. \end{aligned}$$

Using (5) and (9), we obtain

$$\int_E |g_\varepsilon(x, u_\varepsilon, Du_\varepsilon)| \leq h(m) \int_E (c(x) + |DT_m(u_\varepsilon)|^p) + \frac{C_2}{m}.$$

Since the sequence $(DT_m(u_\varepsilon))$ converges strongly in $(L^p(\Omega))^N$, the above inequality implies the equi-integrability of $g_\varepsilon(x, u_\varepsilon, Du_\varepsilon)$.

In view of (16), we thus have

$$g_\varepsilon(x, u_\varepsilon, Du_\varepsilon) \rightarrow g(x, u, Du) \text{ strongly in } L^1(\Omega). \tag{17}$$

From (13), (15) and (17), we can pass to the limit in (6):

$$\int_\Omega \beta_\varepsilon(T_{\frac{1}{\varepsilon}}(u_\varepsilon))\varphi + \int_\Omega a(x, u_\varepsilon, Du_\varepsilon) \cdot D\varphi + \int_\Omega g_\varepsilon(x, u_\varepsilon, Du_\varepsilon)\varphi = \int_\Omega f\varphi,$$

we obtain

$$\int_\Omega b\varphi + \int_\Omega a(x, u, Du) \cdot D\varphi + \int_\Omega g(x, u, Du)\varphi = \int_\Omega f\varphi \text{ for any } \varphi \in W_0^{1,p}(\Omega) \cap L^\infty(\Omega).$$

Moreover, since $g_\varepsilon(x, u_\varepsilon, Du_\varepsilon)u_\varepsilon \geq 0$, $g_\varepsilon(x, u_\varepsilon, Du_\varepsilon)u_\varepsilon \rightarrow g(x, u, Du)u$ a.e. in Ω and

$$0 \leq \int_\Omega g_\varepsilon(x, u_\varepsilon, Du_\varepsilon)u_\varepsilon \leq C,$$

by Fatou's lemma, we have

$$g(x, u, Du)u \in L^1(\Omega).$$

Step 5: Subdifferential argument

It remains to prove that $u(x) \in D(\beta(x))$ and $b(x) \in \beta(u(x))$ for almost all $x \in \Omega$. Since β is a maximal monotone graph, there exists a convex, l.s.c and proper function

$$j : \mathbb{R} \rightarrow [0, \infty] \text{ such that } \beta(r) = \partial j(r) \text{ for all } r \in \mathbb{R}.$$

According to [9], for $0 < \varepsilon \leq 1$, $j_\varepsilon : \mathbb{R} \rightarrow \mathbb{R}$ defined by $j_\varepsilon(r) = \int_0^r \beta_\varepsilon(s) ds$ has the following properties:

- i) For any $0 < \varepsilon \leq 1$, j_ε is convex and differentiable for all $r \in \mathbb{R}$ so that $j'_\varepsilon(r) = \beta_\varepsilon(r)$ for all $r \in \mathbb{R}$ and any $0 < \varepsilon \leq 1$.
- ii) $j_\varepsilon(r) \rightarrow j(r)$ for all $r \in \mathbb{R}$ as $\varepsilon \rightarrow 0$.

From i), it follows that for any $0 < \varepsilon \leq 1$,

$$j_\varepsilon(r) \geq j_\varepsilon(T_{\frac{1}{\varepsilon}}(u_\varepsilon)) + (r - T_{\frac{1}{\varepsilon}}(u_\varepsilon))\beta_\varepsilon(T_{\frac{1}{\varepsilon}}(u_\varepsilon)) \quad (18)$$

holds for all $r \in \mathbb{R}$ and almost everywhere in Ω .

Let $E \subset \Omega$ be an arbitrary measurable set and χ_E be its characteristic function. Let $h_l : \mathbb{R} \rightarrow \mathbb{R}$ be defined by $h_l(r) = \min(1, (l+1-|r|)^+)$ for each $r \in \mathbb{R}$.

We fix $\varepsilon_0 > 0$, multiplying (18) by $h_l(u_\varepsilon)\chi_E$, integrating over Ω and using ii), we obtain

$$j(r) \int_E h_l(u_\varepsilon) \geq \int_E j_{\varepsilon_0}(T_{l+1}(u_\varepsilon))h_l(u_\varepsilon) + (r - T_{l+1}(u_\varepsilon))h_l(u_\varepsilon)\beta_\varepsilon(T_{\frac{1}{\varepsilon}}(u_\varepsilon)) \quad (19)$$

for all $r \in \mathbb{R}$ and all $0 < \varepsilon < \min(\varepsilon_0, \frac{1}{l})$. As $\varepsilon \rightarrow 0$, taking into account that E is arbitrary, we obtain from (19)

$$j(r)h_l(u) \geq j_{\varepsilon_0}(T_{l+1}(u))h_l(u) + bh_l(u)(r - T_{l+1}(u)) \quad (20)$$

for all $r \in \mathbb{R}$ and almost everywhere in Ω .

Passing to the limit with $l \rightarrow \infty$ and then with $\varepsilon_0 \rightarrow 0$ in (20) finally yields

$$j(r) \geq j(u(x)) + b(x)(r - u(x)) \quad (21)$$

for all $r \in \mathbb{R}$ and almost everywhere in Ω , hence $u \in D(\beta)$ and $b \in \beta(u)$ for almost everywhere in Ω .

With this last step, the proof of Theorem 2.1 is concluded.

4 Example

Let Ω be a bounded domain of \mathbb{R}^N ($N \geq 1$). Let us consider the Carathéodory functions

$$a(x, s, \xi) = |\xi|^{p-2}\xi,$$

$$g(x, s, \xi) = \rho s|s|^r|\xi|^p, \quad \rho > 0, \quad r > 0,$$

and β is the maximal monotone mapping defined by

$$\beta(s) = (s - 1)^+ - (s + 1)^-.$$

It is easy to show that the Carathéodory function $a(x, s, \xi)$ satisfies the growth condition (2), the coercivity condition (1) and the strict monotonicity condition (3). Also, the Carathéodory function $g(x, s, \xi)$ satisfies the conditions (4) and (5).

Finally, the hypotheses of Theorem 2.1 are satisfied, therefore, for all $f \in L^\infty(\Omega)$, the following problem

$$\begin{cases} \beta(u) - \Delta_p(u) + g(x, u, Du) \ni f \text{ in } \mathcal{D}'(\Omega), \\ u \in W_0^{1,p}(\Omega), g(x, u, Du) \in L^1(\Omega), g(x, u, Du)u \in L^1(\Omega), \end{cases}$$

has at least one solution.

5 Conclusion

This paper focuses on establishing the existence of solution for a general class of strongly nonlinear elliptic problems associated with the differential inclusion $\beta(u) + A(u) + g(x, u, Du) \ni f$, where A is a Leray-Lions operator from $W_0^{1,p}(\Omega)$ into its dual, β is a maximal monotone mapping such that $0 \in \beta(0)$, while $g(x, s, \xi)$ is a nonlinear term which has a growth condition with respect to ξ and no growth with respect to s but it satisfies a sign condition on s . The right-hand side f is assumed to belong to $L^\infty(\Omega)$. In the future, we aim to expand this study for a measure or L^1 sources.

Acknowledgment

The authors would like to thank the anonymous reviewer for offering valuable suggestions to improve this paper.

References

- [1] A. Abbassi, C. Allalou and A. Kassidi. Existence of weak solutions for nonlinear p -elliptic problem by topological degree. *Nonlinear Dynamics and Systems Theory* **20** (3) (2020) 229–241.
- [2] Y. Akdim and C. Allalou. Renormalized solutions of Stefan degenerate elliptic nonlinear problems with variable exponent. *Journal of Nonlinear Evolution Equations and Applications* **2015** (7) (2016) 105–119.
- [3] Y. Akdim, R. Elharch, M. C. Hassib and S. Lalaoui Rhali. Capacity and anisotropic Sobolev spaces with zero boundary values. *Nonlinear Dynamics and Systems Theory* **22** (1) (2022) 1–12.
- [4] F. Andreu, N. Igbida, J. M. Mazón and J. Toledo. L^1 existence and uniqueness results for quasi-linear elliptic equations with nonlinear boundary conditions. *Annales de l'Institut Henri Poincaré C. Analyse Non Linéaire* **24** (1) (2007) 61–89.
- [5] P. Bénilan, L. Boccardo, T. Gallouët, R. Gariepy, M. Pierre and J.L. Vázquez. An L^1 -theory of existence and uniqueness of solutions of nonlinear elliptic equations. *Annali della Scuola Normale Superiore di Pisa. Classe di Scienze. Serie IV* **22** (2) (1995) 241–273.

- [6] A. Bensoussan, L. Boccardo and F. Murat. On a nonlinear partial differential equation having natural growth terms and unbounded solution. *Annales de l'Institut Henri Poincaré. Analyse Non Linéaire* **5** (4) (1988) 347–364.
- [7] L. Boccardo, T. Gallouët and F. Murat. A unified presentation of two existence results for problems with natural growth. In: *Progress in partial differential equations: the Metz surveys, 2 (1992)* Pitman Res. Notes Math. Ser. Longman Sci. Tech., Harlow **296** (1993) 127–137.
- [8] L. Boccardo, F. Murat and J.-P. Puel. Existence of bounded solutions for nonlinear elliptic unilateral problems. *Annali di Matematica Pura ed Applicata. Serie Quarta* **152** (1988) 183–196.
- [9] H. Brézis. *Opérateurs maximaux monotones et semi-groupes de contractions dans les espaces de Hilbert*. North-Holland Mathematics Studies, No. 5. North-Holland Publishing Co., Amsterdam-London; American Elsevier Publishing Co., Inc., New York, 1973.
- [10] H. Brézis and W. Strauss. Semi-linear second-order elliptic equations in L^1 . *Journal of the Mathematical Society of Japan* **25** (1973) 565–590.
- [11] F. E. Browder. Existence theorems for nonlinear partial differential equations. *Global Analysis (Proc. Sympos. Pure Math., Vol. XVI, Berkeley, Calif., 1968)* Amer. Math. Soc., Providence, R.I. (1970) 1–60.
- [12] P. Gwiazda, P. Wittbold, A. Wróblewska and A. Zimmermann. Renormalized solutions of nonlinear elliptic problems in generalized Orlicz spaces. *Journal of Differential Equations* **253** (2) (2012) 635–666.
- [13] A. Kumar, A. K. Singh and Rajeev. A phase change problem including space-dependent latent heat and periodic heat flux. *Nonlinear Dynamics and Systems Theory* **19** (1-SI) (2019) 178–185.
- [14] J. Leray and J.-L. Lions. Quelques résultats de Višik sur les problèmes elliptiques non-linéaires par les méthodes de Minty-Browder. *Bulletin de la Société Mathématique de France* **93** (1965) 97–107.
- [15] J.-L. Lions. *Quelques méthodes de résolution des problèmes aux limites non linéaires*. Dunod, Paris; Gauthier-Villars, Paris, 1969.
- [16] M. Růžička. *Electrorheological Fluids: Modeling and Mathematical Theory*. Lecture Notes in Mathematics. Springer-Verlag, Berlin **1748**, 2000.
- [17] K. I. Saffidine and S. Mesbahi. Existence result for positive solution of a degenerate reaction-diffusion system via a method of upper and lower solutions. *Nonlinear Dynamics and Systems Theory* **21** (4) (2021) 434–445.
- [18] G. Stampacchia. Le problème de Dirichlet pour les équations elliptiques du second ordre à coefficients discontinus. *Université de Grenoble. Annales de l'Institut Fourier* **15** (1) (1965) 189–258.
- [19] P. Wittbold and A. Zimmermann. Existence and uniqueness of renormalized solutions to nonlinear elliptic equations with variable exponents and L^1 -data. *Nonlinear Analysis. Theory, Methods & Applications* **72** (6) (2010) 2990–3008.
- [20] X. Xu. Existence and convergence theorems for doubly nonlinear partial differential equations of elliptic-parabolic type. *Journal of Mathematical Analysis and Applications* **150** (1) (1990) 205–223.



Optimization of Hotel Y Management through Application of Occupancy Forecasting by Support Vector Machine and K-Nearest Neighbors Methods

M. Y. Anshori¹, I. H. Santoso², P. Katias¹, T. Herlambang³, H. Arof⁴,
B. Suharto^{5*} and K. Oktafianto⁶

¹ Department of Management, Universitas Nahdlatul Ulama Surabaya, Indonesia.

² Department of Accounting Magister, University of Wijaya Kusuma, Surabaya, Indonesia.

³ Department of Information System, Universitas Nahdlatul Ulama Surabaya, Indonesia.

⁴ Department of Electrical Engineering, University of Malaya, Malaysia.

^{5*} The Tourism and Hospitality Department, Faculty of Applied Sciences,
Airlangga University, Indonesia.

⁶ Department of Mathematics, University of PGRI Ronggolawe, Indonesia.

Received: October 28, 2023; Revised: June 22, 2024

Abstract: Almost all countries in the world, including Indonesia [1], strive to develop their tourism potential to earn as much foreign exchange as possible. The role of tourism is very important for a country/region because it has a very broad multiplier effect. Efficiently managed hotels are able to win the competition. Therefore, making the right forecasting and estimation model is of great help for hotel managers to manage hotels effectively and efficiently. For that reason, software development is needed for forecasting and estimation systems. This research tries to synergize management discipline and mathematics so that it can be used more easily, accurately, effectively and efficiently in hotel management. Some reliable forecasting methods among others are Support Vector Machine (SVM) and K-Nearest Neighbors (K-NN). This paper optimizes hotel management through the application of occupancy forecasting by using the SVM and K-NN methods. The simulation results by the RapidMiner software and both methods using 90% of training data and 10% of testing data show that the RMSE produced by the SVM method is 0.011, while the RMSE produced by the KNN method is 0.116. Thus, the SVM method has higher accuracy than the K-NN.

Keywords: *occupancy; forecast; SVM; K-NN.*

Mathematics Subject Classification (2010): 68T45, 68T10.

* Corresponding author: <mailto:bambang.suharto@vokasi.unair.ac.id>

1 Introduction

Almost all countries in the world, including Indonesia [1], strive to develop their tourism potential to earn as much foreign exchange as possible. The role of tourism is very important for a country/region because it has a very broad multiplier effect. Efficiently managed hotels are able to win the competition. Therefore, making the right forecasting and estimation model is of a great help for hotel managers to manage hotels effectively and efficiently, so software development is needed for forecasting and estimation systems [2–4].

In general, forecasting can be grouped into quantitative forecasting and qualitative forecasting. Qualitative forecasting which is based on intuition and empirical experience becomes subjective. Subjective forecasting is difficult to implement due to the limitations of the human brain in analyzing information and causal relationships that affect the business. If such qualitative forecasting is done by several people separately, the results are likely to have considerable variation. On the other hand, if it is carried out jointly, it is likely that there is no similarity in the forecasting results, or an influential person in the group determines the results [5].

Some previous research used Forecast to help predict the desired number or data. In 2021, the one conducted by Rini et al. [6] used forecast to predict the number of dengue cases, in 2022, Anshori [7] forecasted the number of restaurants to be closed using ANFIS, while Susanto et al. [2] used Backpropagation Neural Network. In 2023, Anshori [1], did a hotel forecast using Linear Support Vector Machine [8,9]. As for the estimation methods, many were applied in the fields of robotics such as AUV motion, mobile robots and finger arm robots [10,11].

Some reliable forecasting methods among others are Support Vector Machine (SVM) and K-Nearest Neighbors (K-NN). SVM is a machine learning method able to analyze data and sort it into one of two categories [12]. SVM works to find the best hyperplane or decision boundary function to separate two or more classes in the input space. The hyperplane can be a line in two dimensions and can be a flat plane in multiple planes. Meanwhile, K-NN is an algorithm functioning to classify data based on training data sets, taken from K-Nearest Neighbors. With k , the number of nearest neighbors, the study in this paper is to optimize hotel management through the application of occupancy forecasting by the SVM and K-NN methods [13].

2 Occupancy Data of Hotel Y

Occupancy data of hotel Y are presented in Tables 1-3.

3 Algorithm of K-Nearest Neighbors

K-Nearest Neighbors is a classification algorithm for data grouping into several classes based on the closest distance or similarity of the data to the training data. K-NN performs classification based on the closest distance calculated from Euclidean. Euclidean Distance is a calculation used to find the distance between 2 points in Euclidean space. Euclidean distance calculation is shown in the equation

$$Euc = \sqrt{(x_2 - x_1)^2 + (y_2 - y_1)^2}. \quad (1)$$

Notes:

$d(x_1, x_j)$: Euclidean distance;

	2017		2018			2019			
	Room Available	Occ (%)	Room Sold	Room Available	Occ (%)	Room Sold	Room Available	Occ (%)	Room Sold
January	7,006	48.6%	3,262	7,006	46.6%	3,262	7,006	50.5%	3,536
February	4,480	63.7%	2,853	6,328	61.3%	3,880	6,328	63.6%	4,027
March	7,006	72.3%	5,066	7,006	72.3%	5,066	7,006	66.6%	4,663
April	6,780	64.9%	4,402	6,780	64.9%	4,402	6,780	69.9%	4,736
May	7,006	63.4%	4,444	7,006	63.4%	4,444	7,006	57.5%	4,025
June	6,780	61.2%	4,150	6,780	61.2%	4,150	6,780	75.3%	5,106
July	7,006	76.4%	5,351	7,006	76.4%	5,351	7,006	74.6%	5,223
August	7,006	73.8%	5,172	7,006	73.8%	5,172	7,006	61.6%	4,316
September	6,780	70.6%	4,787	6,780	70.6%	4,787	6,780	58.7%	3,977
October	7,006	81.7%	5,723	7,006	81.7%	5,723	7,006	72.3%	5,068
November	6,780	80.3%	5,443	6,780	80.3%	5,443	6,780	79.7%	5,406
December	7,006	70.6%	4,943	7,006	70.6%	4,943	7,006	77.1%	5,401

Table 1: The occupancy data of Hotel Y for 2017–2019.

	2020		2021			2022			
	Room Available	Occ (%)	Room Sold	Room Available	Occ (%)	Room Sold	Room Available	Occ (%)	Room Sold
January	7,006	49.8%	3,487	7,006	44.5%	3,118	7,006	51.1%	3,582
February	6,554	59.8%	3,921	6,328	50.9%	3,224	6,328	49.5%	3,132
March	7,006	42.7%	2,992	7,006	65.9%	4,614	7,006	57.4%	4,023
April	6,780	16.8%	1,140	6,780	61.9%	4,200	6,780	42.6%	2,891
May	7,006	18.7%	1,308	7,006	52.8%	3,698	7,006	76.4%	5,353
June	6,780	27.0%	1,830	6,780	70.6%	4,790	6,780	65.7%	4,455
July	7,006	37.1%	2,600	7,006	32.0%	2,242	7,006	60.6%	4,246
August	7,006	46.1%	3,227	7,006	40.6%	2,845	7,006	52.1%	3,650
September	6,780	45.3%	3,070	6,780	68.7%	4,658	6,780	53.4%	3,618
October	7,006	62.0%	4,341	7,006	80.7%	5,652	7,006	62.2%	4,360
November	6,780	76.9%	5,212	6,780	71.0%	4,816	6,780	68.6%	4,652
December	7,006	66.8%	4,682	7,006	81.0%	5,672	7,006	71.2%	4,985

Table 2: The occupancy data of Hotel Y for 2020–2022.

	2023		
	Room Available	Occ (%)	Room Sold
January	7,006	48.1%	3,372
February	6,328	52.1%	3,294
March	7,006	57.4%	4,023
April	6,780	36.0%	2,441
May	7,006	62.0%	4,345

Table 3: The occupancy data of Hotel W for 2023.

x_i : record data to i ;
 x_j : record data to j ;
 a_r : data to-r from i, j .

3.1 Algorithm of Support Vector Machine

Since then, SVMs have been used in text, hypertext and image classification. SVMs can work with handwritten characters and the algorithm has been used in biology labs to perform tasks such as protein sorting. SVMs work to find the best hyperplane or decision boundary function to separate two or more classes in the input space. The hyperplane can be a line in two dimensions and can be a flat plane in multiple planes.

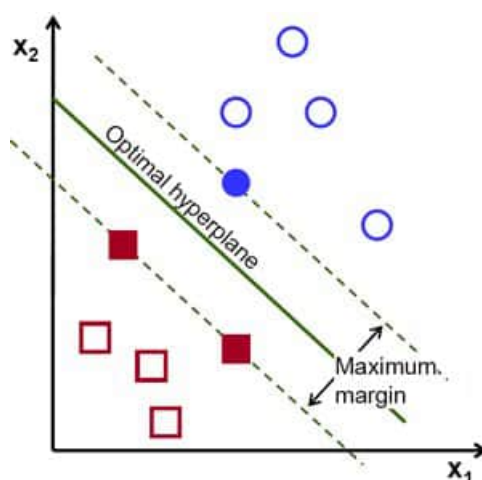


Figure 1: Support Vector Machine Model.

The algorithm of SVM is shown in Figure 2.

3.2 Implementation of the K-Nearest Neighbors Algorithm on data

The implementation of the K-NN algorithm on hotel occupancy data in the RapidMiner software is shown in Figure 3.

3.3 Implementation of Support Vector Machine Algorithm on Data

The application of the SVM method to the occupancy data model is shown in Figure 4.

4 Simulation Results

In this paper, the simulation used two algorithms, where both the SVM and K-NN methods were compared when using several types of training data and testing data. There are 3 types of training and testing data grouping cases, that is, the first case (case 1) in which the training data is 70% and the testing data is 30%, the second case in which the training data is 80% and the testing data is 20%, and the third case in which the training data is 90% and the testing data is 10%. After modeling in the RapidMiner software using the occupancy data of Hotel Y, the SVM and K-NN methods were implemented, resulting in Figures 5 – 7.

Figure 5 is as an explanation related to case 1, with 70% of training data and 30% of the testing data. It can be seen that the forecasting results by the SVM method have a

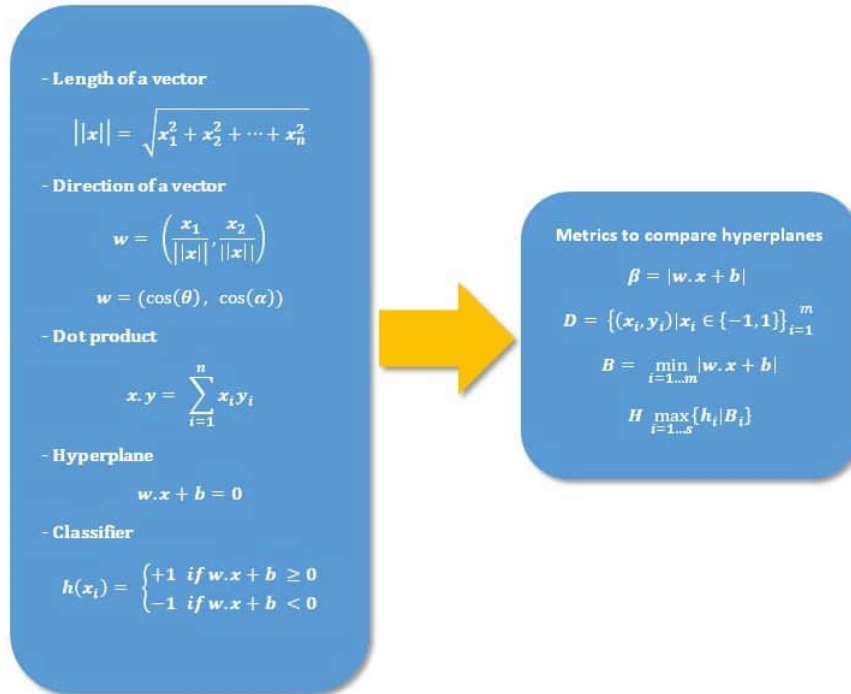


Figure 2: Algorithm of Support Vector Machine.

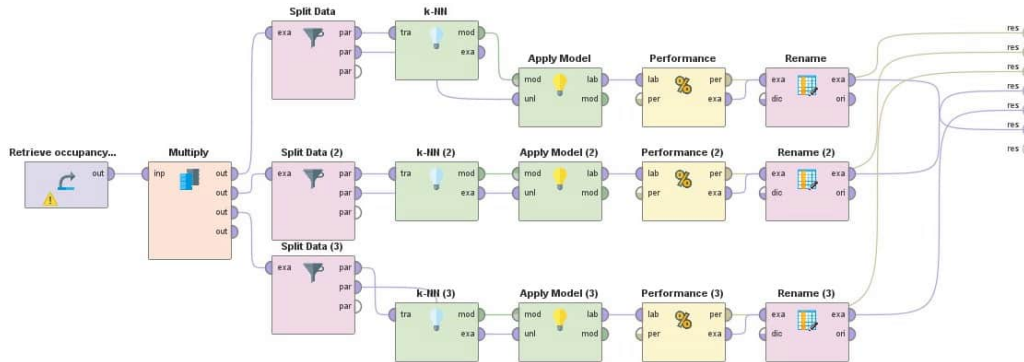


Figure 3: Implementation of the K-NN algorithm on occupancy data of hotel Y.

smaller error than those by the K-NN because the simulation-resulted graph shows that the SVM method has almost the same value as the real data. It can be seen in Table 2 that the RMSDE by the SVM method is 0.014 and that by the K-NN method is 0.137. So, the SVM method has a smaller error of about 0.1.

Figure 6 is as an explanation related to the first case (case 1) with 80% of training data and 20% of testing data, it can be seen that the forecasting results by the SVM method have a smaller error than those by the K-NN because the simulation-resulted

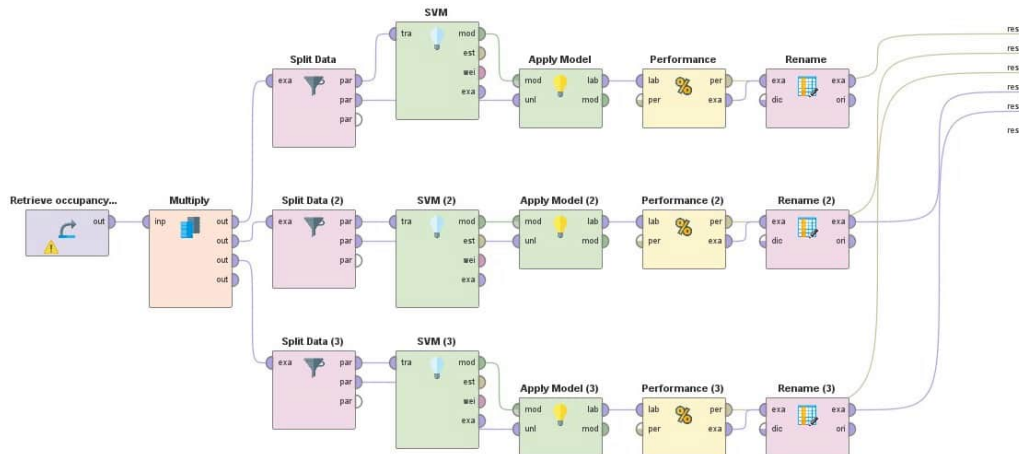


Figure 4: Implementation of the SVM Algorithm on occupancy data of Hotel Y.

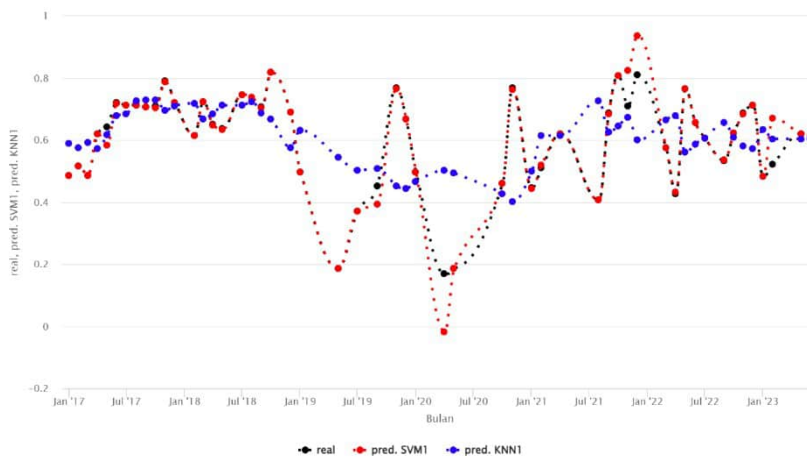


Figure 5: Simulation Results of hotel Y occupancy forecast using 70% of training data and 30% of testing data.

graph shows that the SVM method has almost the same value as the real data. It can be seen in Table 2 that the RMSE by the SVM method is 0.029 and that by the K-NN method is 0.134. So, the SVM method has a smaller error of about 0.1.

Figure 7 is as an explanation related to the first case (case 1), with 90% of training data and 10% of testing data. It can be seen that the results of forecasting by the SVM method have a smaller error than those by K-NN because the simulation-resulted graph shows that the SVM method has almost the same value as the real data. It can be seen in Table 2 that the RMSE by the SVM method is 0.011 and the RMSE by the K-NN method is 0.116. So, the SVM method has a smaller error of about 0.1.

Table 4 above shows that the SVM method has a higher accuracy and a smaller error

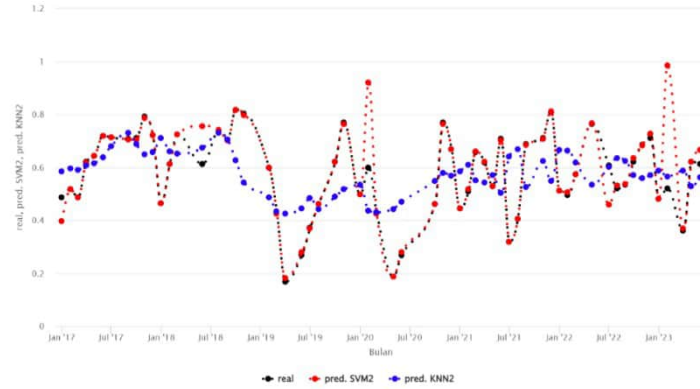


Figure 6: Simulation results of hotel Y occupancy forecast using 80% of training data and 20% of testing data.

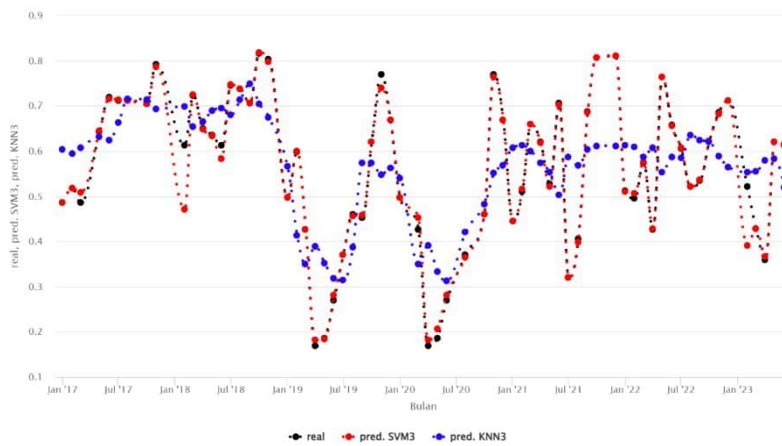


Figure 7: Simulation results of hotel Y occupancy forecast occupancy using 90% of training data and 10% of testing data.

	SVM			KNN		
	70% Training data and 30% Testing data	80% Training data and 20% Testing data	90% Training data and 10% Testing data	70% Training data and 30% Testing data	80% Training data and 20% Testing data	90% Training data and 10% Testing data
RMSE of Forecasting results	0.014	0.029	0.011	0.137	0.134	0.116

Table 4: The RMSE comparison using SVM and K-NN.

than the K-NN for all three cases. When compared, overall, it is clear that using SMV in case 3 shows the smallest RMSE value. When considering the SMV method alone, case 3 has the smallest RMSE value because the training data is larger than those of cases 1 and 2. Likewise, for the K-NN, case 3 has a smaller RMSE value than cases 1 and 2.

5 Conclusion

Based on the results of the discussion above and the forecasting results as in the graph above, it can be concluded that the SVM method has a higher accuracy and a smaller error than the K-NN method for all three cases. When compared, as a whole, using SMV in case 3 shows the smallest RMSE value. When considering the SVM method alone, case 3 has the smallest RMSE value because the training data is larger than those of cases 1 and 2. Likewise, for K-NN, case 3 has a smaller RMSE value than cases 1 and 2. Thus, the SVM method is highly reliable for hotel occupancy forecasting.

Acknowledgment

High appreciation to the Kemdikbudristek for the very fund support for the completion of the research conducted in the year of 2024 with contract number 109/E5/PG.02.00.PL/2024, 054/SP2H/PT/LL7/2024, and 1104/UNUSA-LPPM/Adm.I/VI/2024.

References

- [1] M. Y. Anshori, I. H. Santoso, T. Herlambang, D. Rahmalia, K. Oktafianto and P. Katias. Forecasting of Occupied Rooms in the Hotel Using Linear Support Vector Machine. *Nonlinear Dynamics and Systems Theory* **23** (2) (2023) 129–140.
- [2] F. A. Susanto, M. Y. Anshori, D. Rahmalia, K. Oktafianto, D. Adzkiya, P. Katias and T. Herlambang. Estimation of Closed Hotels and Restaurants in Jakarta as Impact of Corona Virus Disease (Covid-19) Spread Using Backpropagation Neural Network. *Nonlinear Dynamics and Systems Theory* **22** (4) (2022) 457–467.
- [3] M. Y. Anshori, T. Shawyuni, D. V. Madrigal, D. Rahmalia, F. A. Susanto, T. Herlambang and D. Adzkiya. Estimation of closed hotels and restaurants in Jakarta as impact of corona virus disease spread using adaptive neuro fuzzy inference system. *International Journal of Artificial Intelligence (IJAI)* **11** (2) (2022).
- [4] D. Rahmalia, T. Herlambang, A. S. Kamil, R. A. Rasyid, F. Yudianto, L. Muzdalifah and E. F. Kurniawati. Profitability estimation of XYZ company using H-infinity and Ensemble Kalman Filter. In: *The Third International Conference on Combinatorics, Graph Theory and Network Topology* University of Jember-Indonesia, 26-27 Oct. 2019.
- [5] D. B. Maghfira, R. Sarno, F. A. Susanto, T. Herlambang, K. Oktafianto, W. Hartawan and I. W. Farid. Electronic Nose for Classifying Civet Coffee and Non-Civet Coffee. *Nonlinear Dynamics and Systems Theory* **23** (3) (2023) 323–337.
- [6] F. S. Rini, T. D. Wulan and T. Herlambang. Forecasting The Number of Demam Berdarah Dengue (DBD) Patients Using The Fuzzy Method At The Siwalankerto Public Health Center. In: *The 1st International Conference on Neuroscience and Learning Technology (ICONSATIN 2021)* Jember, Indonesia, 18-19 September 2021.
- [7] M. Y. Anshori, D. Rahmalia, T. Herlambang and D. F. Karya. Optimizing Adaptive Neuro Fuzzy Inference System (ANFIS) parameters using Cuckoo Search (Case study of world crude oil price estimation). In: *The 4th International Conference on Combinatorics, Graph Theory, and Network Topology (ICCGANT) 2020* East Java, Indonesia, 22-23 August 2020.
- [8] M. Y. Anshori, D. Rahmalia and T. Herlambang. Comparison Backpropagation (BP) and Learning Vector Quantification (LVQ) on classifying price range of smartphone in market. In: *The 4th International Conference on Combinatorics, Graph Theory, and Network Topology (ICCGANT) 2020* East Java, Indonesia, 22-23 August 2020.

- [9] M. Y. Anshori, T. Herlambang, P. Katias, F. A. Susanto and R. R. Rasyid. Profitability estimation of XYZ company using H-infinity and Ensemble Kalman Filter. In: *The 5th International Conference of Combinatorics, Graph Theory, and Network Topology (ICCGANT 2021)* Jember, Indonesia, 21-22 August 2021.
- [10] V. N. Vapnik and A. Y. Lerner. Pattern recognition using generalized portraits. *Automation and Remote Control* **24** (1963) 709–715.
- [11] T. Herlambang, S. Syamsuar, F. Yudianto, A. Basuki, G. Wijiatmoko, A. Roschyntawati, H. Hendrato, K. Oktafianto and R. S. Marjianto. Trajectory Estimation of Amphibious Aircraft Using H-Infinity and Ensemble Kalman Filter Methods. *Nonlinear Dynamics and System Theory* **24** (3) (2024) 259–266.
- [12] M. Y. Anshori, T. Herlambang, V. Asyari, H. Arof, A. A. Firdaus, K. Oktafianto and B. Suharto. Optimization of Hotel W Management through Performance Comparison of Support Vector Machine and Linear Regression Algorithm in Forecasting Occupancy. *Nonlinear Dynamics and System Theory* **24** (3) (2024) 228–235.
- [13] A. Muhith, I. H. Susanto, D. Rahmalia, D. Adzkiya and T. Herlambang. The Analysis of Demand and Supply of Blood in Hospital in Surabaya City Using Panel Data Regression. *Nonlinear Dynamics and System Theory* **22** (5) (2022) 550–560.



A New Numerical Scheme for Solving Time-Fractional Variable-Order Partial Differential Equations

Soufiane Benyoussef^{1*}, Oumkeltoum Benhamouda², Mohamed Dalah³
and Khaled Zennir^{4,5}

^{1*} *Department of Science and Technology, Faculty of Applied Sciences,
University of Ibn Khaldoun, Tiaret 14000, Algeria.*

² *Faculté des Sciences et de la Technologie,
USTHB, B. P. 32, El-Alia 16111, Bab-Ezzouar, Alger, Algeria.*

³ *Department of Mathematics, Faculty of Exact Sciences,
University Constantine 1, Frères Mentouri,*

Applied Mathematics and Modeling Laboratory, Constantine 25 017, Algeria.

⁴ *Department of Mathematics, College of Science, Qassim University, SAudi Arabia.*

⁵ *Department of Mathematics, Faculty of Science, University of 20 Aout 1955 - Skikda, Algeria.*

Received: October 22, 2023; Revised: June 9, 2024

Abstract: In this work, we study approximations of solutions of fractional differential equations of order α by using an implicit finite difference scheme (IFDS). A discretization and development of the scheme is obtained by using different approaches to fractional derivatives. The implicit finite difference scheme (IFDS) approach is followed in order to derive a simple discretization of the space fractional derivatives. The consistency, stability and convergence of the method are proved. Several examples illustrating the accuracy of the method are given. Moreover, we study the stability and convergence of the implicit finite difference scheme (IFDS) applied to the numerical solution of the fractional differential equations of order α . Two tests for our problem are solved numerically to verify the effectiveness of the proposed numerical scheme.

Keywords: *fractional derivatives; stability; consistence; convergence; numerical scheme.*

Mathematics Subject Classification (2010): 93A30, 26A33, 65N06, 34K28.

* Corresponding author: <mailto:soufiane.benyoussef@univ-tiaret.dz>

1 Introduction

In viscous boundary problems, there is a viscodynamic operator in the Biot poroviscoelastic theory which may be formulated with a fractional derivative (see [9, 10, 13, 14]). The power law and stretched exponential temporal responses of nonideal capacitors can also be shown to relate to the electro-elastic and electro-visco-elastic models. A fractional-order differential equation is a generalized form of an integer-order differential equation. This one is useful in many areas, e.g., for the depiction of physical, mechanical and biological models of several phenomena in pure mathematics and applied science. Numerical analysis (see for more details [5, 15, 16]) is a very important branch of mathematics in which we analyse and solve several problems which require calculations with different techniques. The important role of numerical methods for fractional calculus is how to apply numerical methods for fractional integrals and fractional derivatives (see [2, 4, 14]), for example, finite element methods (FEM), finite difference methods, Multi-Grid methods (MGM) for fractional partial and ordinary differential equations. The development of fractional differential equations and their solutions are carried out by using the Simulink Matlab Program (see for more details [1, 3, 7, 17]), which calculates the approximate solutions of fractional differential equations of order α by using the implicit finite difference scheme (IFDS). The structure of this paper is organized as follows. Section 2 includes the basic concepts of the implicit finite difference scheme (IFDS) and we present the steps of discretization and development of the scheme and several techniques of the proposed approach. Section 3 discusses the stability of the approximate scheme presented in Section 2. In Section 4, we prove the convergence of the approximate scheme for the fractional differential equations of order α . In Section 5, we focus on the solvability of the approximate scheme. Finally, Section 6 includes the examples of specific algorithms for a variety of boundary and initial conditions and conclusions are presented in Section 7.

2 Discretization and Development of the Implicit Finite Difference Scheme

In this section, we apply the NSFD to obtain the numerical solution for the linear partial differential equations with time-fractional derivative

$$\begin{cases} \frac{\partial^\alpha u}{\partial t^\alpha} + a(x, t) \frac{\partial^2 u}{\partial x^2}(x, t) + c(x, t) \frac{\partial u}{\partial x} = f(x, t) & 0 < x < L, \quad t > 0, \quad 0 < \alpha < 1, \\ u(0, t) = q(t), \\ u(L, t) = p(t), \\ u(x, 0) = s(x). \end{cases} \tag{1}$$

Let $\phi_1(h)$ and $\phi_2(k)$ be two strictly positive functions and $[0, L]$ be the interval of interest. For the numerical scheme, define $x_i = i\phi_1(h)$, where $i = \overline{0, M}$ and $t_j = j\phi_2(k)$, where $j = \overline{0, N}$. The parameters $\phi_1(h)$ and $\phi_2(k)$ are the space and time steps, respectively. Now, let us assume that

$$u(x_i, t_j) = u_i^j \text{ and } f(x_i, t_j) = f_i^j, \tag{2}$$

and

$$a(x_i, t_j) = a_i^j \text{ and } c(x_i, t_j) = c_i^j,$$

where u_i^j is the numerical approximation of $u(x_i, t_j)$ and f_i^j is the numerical approximation of $f(x_i, t_j)$.

There exist different approaches to fractional derivatives [11]. For simplification, we consider the interval $[0, t]$,

$$\frac{\partial^{\alpha(x,t)} u(x,t)}{\partial t^{\alpha(x,t)}} = \begin{cases} \frac{1}{\Gamma(1-\alpha(x,t))} \int_0^t \frac{u_\xi(x,\xi)}{(t-\xi)^{\alpha(x,t)}} d\xi & \text{if } 0 < \alpha < 1, \\ u_t(x,t) & \text{if } \alpha(x,t) = 1. \end{cases} \quad (3)$$

Initially, as the boundary value problem needs to be discretized to be able to solve (1), it is first necessary to discretize the variable-order time-fractional derivative (3) as follow:

$$\begin{aligned} \frac{\partial^{\alpha(x_i,t_{j+1})} u(x_i,t_{j+1})}{\partial t^{\alpha(x_i,t_{j+1})}} &= \frac{1}{\Gamma(1-\alpha(x_i,t_{j+1}))} \int_0^{t_{j+1}} \frac{u_\xi(x_i,\xi)}{(t_{j+1}-\xi)^{\alpha(x_i,t_{j+1})}} d\xi \\ &= \frac{1}{\Gamma(1-\alpha(x_i,t_{j+1}))} \sum_{s=0}^j \int_{s\phi_2(k)}^{(s+1)\phi_2(k)} \frac{u_\xi(x_i,\xi)}{(t_{j+1}-\xi)^{\alpha(x_i,t_{j+1})}} d\xi. \end{aligned}$$

Then we obtain

$$\frac{\partial^{\alpha(x_i,t_{j+1})} u(x_i,t_{j+1})}{\partial t^{\alpha(x_i,t_{j+1})}} = \frac{1}{\Gamma(1-\alpha(x_i,t_{j+1}))} \sum_{s=0}^j \int_{s\phi_2(k)}^{(s+1)\phi_2(k)} \left(\frac{\partial u}{\partial \xi} \right)_i^{s+1} \frac{d\xi}{(t_{j+1}-\xi)^{\alpha(x_i,t_{j+1})}}.$$

The first-order spatial derivative can be approximated by the following expression:

$$\left(\frac{\partial u}{\partial \xi} \right)_i^{s+1} = \frac{u_i^{s+1} - u_i^{s-1}}{\phi_2(k)} + \Delta(\phi_2(k)). \quad (4)$$

Adopting the discrete scheme given in (9), we discretize the variable-order time-fractional derivative as

$$\begin{aligned} \frac{\partial^{\alpha(x_i,t_{j+1})} u(x_i,t_{j+1})}{\partial t^{\alpha(x_i,t_{j+1})}} &= \frac{1}{\Gamma(1-\alpha(x_i,t_{j+1}))} \sum_{s=0}^j \frac{u_i^{s+1} - u_i^{s-1}}{\phi_2(k)} \int_{(j-s)\phi_2(k)}^{(j-s+1)\phi_2(k)} \frac{d\eta}{\eta^{\alpha(x_i,t_{j+1})}} \\ &= \frac{1}{\Gamma(1-\alpha(x_i,t_{j+1}))} \sum_{n=0}^j \frac{u_i^{j-n+1} - u_i^{j-n}}{\phi_2(k)} \int_{n\phi_2(k)}^{(n+1)\phi_2(k)} \frac{dy}{\eta^{\alpha(x_i,t_{j+1})}}, \end{aligned}$$

then we get

$$\begin{aligned} \frac{\partial^{\alpha(x_i,t_{j+1})} u(x_i,t_{j+1})}{\partial t^{\alpha(x_i,t_{j+1})}} &= \frac{\phi_2(k)^{-\alpha(x_i,t_{j+1})}}{(1-\alpha(x_i,t_{j+1}))\Gamma(1-\alpha(x_i,t_{j+1}))} \times \\ &\quad \sum_{n=0}^j (u_i^{j-n+1} - u_i^{j-n}) [(n+1)^{1-\alpha(x_i,t_{j+1})} - n^{1-\alpha(x_i,t_{j+1})}]. \end{aligned}$$

Let $\eta = t_{j+1} - \xi$ and having in mind that $\Gamma(1+\alpha) = \alpha\Gamma(\alpha)$ and expanding the summation for $n = 0$, we find

$$\begin{aligned} \frac{\partial^{\alpha(x_i,t_{j+1})} u(x_i,t_{j+1})}{\partial t^{\alpha(x_i,t_{j+1})}} &= \frac{\phi_2(k)^{-\alpha(x_i,t_{j+1})}}{\Gamma(2-\alpha(x_i,t_{j+1}))} \left[u_i^{j+1} - u_i^j + \sum_{n=1}^j (u_i^{j-n+1} - u_i^{j-n}) \times \right. \\ &\quad \left. [(n+1)^{1-\alpha(x_i,t_{j+1})} - n^{1-\alpha(x_i,t_{j+1})}] \right], \end{aligned} \quad (5)$$

where $\delta_i^{j+1}(n) = (n+1)^{1-\alpha(x_i, t_{j+1})} - n^{1-\alpha(x_i, t_{j+1})}$, $\forall j = \overline{0, N-1}$. We will use the central difference approximation of space derivative is as follows:

$$\frac{\partial u(x_i, t_{j+1})}{\partial x} = \frac{u_{i+1}^{j+1} - u_{i-1}^{j+1}}{\phi_1(h)} + \Delta(\phi_1(h)). \tag{6}$$

The second-order spatial derivative can be approximated by the following expression:

$$\frac{\partial^2 u(x_i, t_{j+1})}{\partial x^2} = \frac{u_{i+1}^{j+1} - 2u_i^{j+1} + u_{i-1}^{j+1}}{\phi_1^2(h)} + \Delta(\phi_2^2(h)). \tag{7}$$

Using approximations (5), (6) and (7), the semi-linear diffusion equation (1), we obtain

$$\begin{aligned} & \frac{\phi_2(k)^{-\alpha(x_i, t_{j+1})}}{\Gamma(2 - \alpha(x_i, t_{j+1}))} \left[u_i^{j+1} - u_i^j + \sum_{n=1}^j (u_i^{j-n+1} - u_i^{j-n}) \delta_i^{j+1}(n) \right] + a_i^j \frac{u_{i+1}^{j+1} - 2u_i^{j+1} + u_{i-1}^{j+1}}{\phi_1^2(h)} + \\ & + c_i^j \frac{u_{i+1}^{j+1} - u_{i-1}^{j+1}}{\phi_1(h)} = f_i^{j+1}, \quad \forall i = \overline{1, M-1} \text{ and } \forall j = \overline{1, N-1}, \end{aligned} \tag{8}$$

where

$$\begin{aligned} r_i^{j+1} &= a_i^j \frac{\phi_2(k)^{\alpha(x_i, t_{j+1})} \Gamma(2 - \alpha(x_i, t_{j+1}))}{\phi_1^2(h)}, \quad w_i^{j+1} = c_i^j \frac{\phi_2(k)^{\alpha(x_i, t_{j+1})} \Gamma(2 - \alpha(x_i, t_{j+1}))}{\phi_1(h)} \\ \rho_i^{j+1} &= \phi_2(k)^{\alpha(x_i, t_{j+1})} \Gamma(2 - \alpha(x_i, t_{j+1})). \end{aligned}$$

The initial and boundary conditions are $u_0(x_i) = s_i$, $\forall i = \overline{0, M}$, and $u_0^{j+1} = q^{j+1}$, $u_M^{j+1} = p^{j+1}$, $\forall j = \overline{0, N-1}$. We obtain the following approximate scheme for equation (1):

$$\begin{cases} (r_i^{j+1} - w_i^{j+1})u_{i-1}^{j+1} + (1 - 2r_i^{j+1})u_i^{j+1} + (r_i^{j+1} + w_i^{j+1})u_{i+1}^{j+1} \\ \quad = u_i^j - \sum_{n=1}^j (u_i^{j-n+1} - u_i^{j-n}) \delta_i^{j+1}(n) + \rho_i^{j+1} f_i^{j+1}, \quad \forall i = \overline{1, M-1} \text{ and } \forall j = \overline{1, N-1}, \\ u_0^{j+1} = q^{j+1}, \quad u_M^{j+1} = p^{j+1}, \quad \forall j = \overline{0, N-1}, \\ u_i^0 = s_i, \quad \forall i = \overline{0, M}. \end{cases} \tag{9}$$

The coefficients $\delta_i^{j+1}(n)$ ($j = 0, \dots, N-1; i = 0, \dots, M$) satisfy the following properties:

- **P1:** $\delta_i^{j+1}(0) = 1$.
- **P2:** $0 < \delta_i^{j+1}(0) < 1$.

3 Stability of the Approximate Scheme

In this section, we use the method of Fourier analysis to discuss the stability of the approximate scheme (9). Consider the following equation:

$$\begin{cases} (r_i^{j+1} - w_i^{j+1})u_{i-1}^{j+1} + (1 - 2r_i^{j+1})u_i^{j+1} + (r_i^{j+1} + w_i^{j+1})u_{i+1}^{j+1} = \\ \quad u_i^j - \sum_{n=1}^j (u_i^{j-n+1} - u_i^{j-n}) \delta_i^{j+1}(n) + \rho_i^{j+1} f_i^{j+1}, \\ \quad \forall i = \overline{1, M-1} \text{ and } \forall j = \overline{1, N-1}. \end{cases} \tag{10}$$

Now, we define the following function:

$$u^j(x) = \begin{cases} u_i^j, & \text{if } x_{i-\frac{1}{2}} < x < x_{i+\frac{1}{2}}, \quad \forall i = \overline{1, M-1}, \\ 0 & \text{otherwise,} \end{cases}$$

$u^j(x)$ has the Fourier series expansion

$$u^j(x) = \sum_{p=-\infty}^{+\infty} \xi_j(p) e^{\frac{2\pi p}{L}x}, \quad \forall j = \overline{0, N},$$

where

$$\xi_j(p) = \frac{1}{L} \int_0^L u^j(x) e^{-\frac{2\pi p}{L}x} dx.$$

Assume that the solution of the equation (9) has the form

$$v_i^j = \xi_j e^{\mu\theta h i}, \tag{11}$$

where $\theta = \frac{2\pi p}{L}, \mu^2 = -1$. Now, replacing (11) in equation (10), we have

$$\begin{aligned} & \xi_{j+1} (r_i^{j+1} (e^{\mu\theta h} + e^{-\mu\theta h}) + w_i^{j+1} (e^{\mu\theta h} - e^{-\mu\theta h}) + 1 - 2r_i^{j+1}) \\ &= \xi_j - \sum_{n=1}^j (\xi_{j-n+1} - \xi_{j-n}) \delta_i^{j+1}(n), \end{aligned} \tag{12}$$

then we get

$$\xi_{j+1} (1 - 4r_i^{j+1} \sin^2(\frac{\theta h}{2}) + 2\mu w_i^{j+1} \sin(\theta h)) = \xi_j - \sum_{n=1}^j (\xi_{j-n+1} - \xi_{j-n}) \delta_i^{j+1}(n). \tag{13}$$

One can see that equation (13) can be rewritten as

$$\xi_{j+1} = \frac{\xi_j - \sum_{n=1}^j (\xi_{j-n+1} - \xi_{j-n}) \delta_i^{j+1}(n)}{1 - 4r_i^{j+1} \sin^2(\frac{\theta h}{2}) + 2\mu w_i^{j+1} \sin(\theta h)}, \tag{14}$$

then we have the following result.

Theorem 3.1 *The implicit finite difference scheme (9) is unconditionally stable for $0 < \beta < 1$ if*

$$\exists C > 0 \quad \|u^j\|_2 = |\xi_j| \leq C \|u^0\|_2 = C |\xi_0|, \quad j = \overline{1, N}.$$

Proof. We use proof by recurrence for $j = 1$, in view of (14),

$$|\xi_1| = \left| \frac{\xi_0}{1 - 4r_i^1 \sin^2(\frac{\theta h}{2}) + 2\mu w_i^1 \sin(\theta h)} \right| =$$

$$\frac{|\xi_0|}{\sqrt{16[(r_i^1)^2 - (w_i^1)^2] \sin^4(\frac{\theta h}{2}) + 8[2(w_i^1)^2 - r_i^1] \sin^2(\frac{\theta h}{2}) + 1}} = C_i^0 |\xi_0| \leq C |\xi_0|$$

such that $C = \max_{0 \leq i \leq M} C_i^0$. We assume that the following statement is true:

$$|\xi_j| \leq C |\xi_0|, \quad j = 1, 2, \dots, N, \tag{15}$$

and we prove that the following statement is true:

$$|\xi_{j+1}| \leq C|\xi_0|, \quad j = \overline{0, N-1}, \tag{16}$$

we have

$$\begin{aligned} |\xi_{j+1}| &= \left| \frac{\xi_0 - \sum_{n=1}^j (\xi_{j-n+1} - \xi_{j-n}) \delta_i^{j+1}(n)}{1 - 4r_i^{j+1} \sin^2(\frac{\theta h}{2}) + 2\mu w_i^{j+1} \sin(\theta h)} \right| = \\ &= \frac{|\xi_0 - \sum_{n=1}^j (\xi_{j-n+1} - \xi_{j-n}) \delta_i^{j+1}(n)|}{\sqrt{16[(r_i^{j+1})^2 - (w_i^{j+1})^2] \sin^4(\frac{\theta h}{2}) + 8[2(w_i^{j+1})^2 - r_i^{j+1}] \sin^2(\frac{\theta h}{2}) + 1}} \\ &= C_i^j |\xi_0 - \sum_{n=1}^j (\xi_{j-n+1} - \xi_{j-n}) \delta_i^{j+1}(n)| \\ &\leq C^j |\xi_0| + \sum_{n=1}^j (|\xi_{j-n+1}| + |\xi_{j-n}|) |\delta_i^{j+1}(n)| \leq C^j (2N-1) |\xi_0| \leq C |\xi_0| \end{aligned}$$

such that

$$\begin{aligned} C_i^j &= \frac{1}{\sqrt{16[(r_i^{j+1})^2 - (w_i^{j+1})^2] \sin^4(\frac{\theta h}{2}) + 8[2(w_i^{j+1})^2 - r_i^{j+1}] \sin^2(\frac{\theta h}{2}) + 1}}, \\ &\quad \forall i = \overline{0, M} \text{ and } \forall j = \overline{0, N-1}, \\ C^j &= \max_{0 \leq i \leq M} C_i^j, \quad C = (2N-1) \max_{0 \leq i \leq M} C_i^j, \quad \forall j = \overline{0, N-1}. \end{aligned}$$

So we find $|\xi_{j+1}| \leq C|\xi_0|, j = 0, 1, \dots, N-1$. The approximate scheme (9) is unconditionally stable, which concludes the proof of Theorem 3.1.

4 Convergence of the Approximate Scheme

In this section, we use the method of Fourier analysis to discuss the convergence of the approximation error

$$e_i^j = u(x_i, t_j) - u_i^j. \tag{17}$$

Replacing (17) in equation (10), we obtain

$$\begin{aligned} &(r_i^{j+1} - w_i^{j+1})e_{i-1}^{j+1} + (1 - 2r_i^{j+1})e_i^{j+1} + (r_i^{j+1} + w_i^{j+1})e_{i+1}^{j+1} \\ &= e_i^j - \sum_{n=1}^j (e_i^{j-n} - e_i^{j-n-1}) \delta_i^{j+1}(n) + \epsilon_i^j \end{aligned} \tag{18}$$

for all $i = \overline{1, M-1}$ and $j = \overline{1, N-1}$. Then the error e_i^j takes the following form:

$$\epsilon_i^j = \phi_2(k)^{\alpha(x_i, t_{j+1})} \Gamma(2 - \alpha(x_i, t_{j+1})) [\Delta(\phi_2((k)) + \Delta(\phi_1(h))].$$

Now, we define the grid function $e^j(x)$ by

$$e^j(x) = \begin{cases} e_i^j, & \text{if } x_{i-\frac{1}{2}} < x < x_{i+\frac{1}{2}}, \quad \forall i = \overline{1, M-1} \text{ and } \forall j = \overline{1, N-1}, \\ 0, & \text{otherwise,} \end{cases}$$

and

$$e^j(x) = \begin{cases} \epsilon_i^j, & \text{if } x_{i-\frac{1}{2}} < x < x_{i+\frac{1}{2}}, \quad \forall i = \overline{1, M-1} \text{ and } \forall j = \overline{1, N-1}, \\ 0, & \text{otherwise.} \end{cases}$$

Then $e^n(x)$ and $\epsilon^n(x)$ have the Fourier series expansions

$$e^j(x) = \sum_{p=-\infty}^{+\infty} \gamma_j(p)e^{\frac{2\pi p}{L}x}, \quad \epsilon^j(x) = \sum_{p=-\infty}^{+\infty} \lambda_j(p)e^{\frac{2\pi p}{L}x}, \quad \forall j = \overline{0, N}, \tag{19}$$

and

$$\gamma_j(p) = \frac{1}{L} \int_0^L e^j(x)e^{-\frac{2\pi p}{L}x} dx, \quad \lambda_j(p) = \frac{1}{L} \int_0^L \epsilon^j(x)e^{-\frac{2\pi p}{L}x} dx, \tag{20}$$

then

$$\int_0^L |e^j(x)|^2 dx = \sum_{p=-\infty}^{+\infty} |\gamma_j(p)|^2 \quad \text{and} \quad \int_0^L |\epsilon^j(x)|^2 dx = \sum_{p=-\infty}^{+\infty} |\lambda_j(p)|^2, \quad \forall j = \overline{0, N}.$$

Now, we take the norm in the two previous relations, then we get

$$\|e^j\|_2^2 = \sum_{i=1}^{M-1} |\phi_1(h)e_i^j|^2 = \sum_{p=-\infty}^{+\infty} |\gamma_j(p)|^2, \quad \forall j = \overline{0, N}, \tag{21}$$

and

$$\|\epsilon^j\|_2^2 = \sum_{i=1}^{M-1} |h\epsilon_i^j|^2 = \sum_{m=-\infty}^{+\infty} |\lambda_j(p)|^2, \quad \forall j = \overline{0, N}. \tag{22}$$

Now, we suppose

$$e_i^j = \gamma_j e^{\mu\tau hi} \quad \text{and} \quad r_i^j = \lambda_j e^{\mu\tau hi}. \tag{23}$$

Replacing (23) in equation (18), we find

$$\begin{aligned} & \gamma_{j+1}(r_i^{j+1}(e^{\mu\theta h} + e^{-\mu\theta h}) + w_i^{j+1}(e^{\mu\theta h} - e^{-\mu\theta h}) + 1 - 2r_i^{j+1}) \\ &= \gamma_j - \sum_{n=1}^j (\gamma_{j-n+1} - \gamma_{j-n})\delta_i^{j+1}(n) + \lambda_j. \end{aligned} \tag{24}$$

Equation (24) can be rewritten as

$$\gamma_{j+1} = \frac{\gamma_j - \sum_{n=1}^j (\gamma_{j-n+1} - \gamma_{j-n})\delta_i^{j+1}(n) + \lambda_j}{1 - 4r_i^{j+1} \sin^2(\frac{\theta h}{2}) + 2\mu w_i^{j+1} \sin(\theta h)}. \tag{25}$$

Theorem 4.1 *The implicit finite difference scheme (9) is convergent for $0 < \alpha < 1$ if*

$$\|e^j\|_2 = |\gamma_j| \leq C^*(\phi_1(h) + \phi_2(k)), \quad \forall j = \overline{1, N},$$

such that

$$\phi_1(h) + \phi_2(k) \longrightarrow 0 \quad \text{when } (h, k) \rightarrow (0, 0).$$

Proof. We use the proof by recurrence for $j = 1$, we have

$$\begin{aligned}
 |\gamma_1| &= \left| \frac{\gamma_0 + \lambda_0}{1 - 4r_i^{j+1} \sin^2(\frac{\theta h}{2}) + 2\mu w_i^{j+1} \sin(\theta h)} \right| \\
 &= \frac{|\gamma_0 + \lambda_0|}{|1 - 4r_i^{j+1} \sin^2(\frac{\theta h}{2}) + 2\mu w_i^{j+1} \sin(\theta h)|} \\
 &= \frac{|\gamma_0 + \lambda_0|}{\sqrt{16[(r_i^1)^2 - (w_i^1)^2] \sin^4(\frac{\theta h}{2}) + 8[2(w_i^1)^2 - r_i^1] \sin^2(\frac{\theta h}{2}) + 1}} \\
 &\leq \frac{|\gamma_0| + |\lambda_0|}{\sqrt{16[(r_i^1)^2 - (w_i^1)^2] \sin^4(\frac{\theta h}{2}) + 8[2(w_i^1)^2 - r_i^1] \sin^2(\frac{\theta h}{2}) + 1}} \\
 &= \frac{|\lambda_0|}{\sqrt{16[(r_i^1)^2 - (w_i^1)^2] \sin^4(\frac{\theta h}{2}) + 8[2(w_i^1)^2 - r_i^1] \sin^2(\frac{\theta h}{2}) + 1}},
 \end{aligned}$$

we have $\gamma_0 = e_i^0 = u(x_i, 0) - u_i^0 = 0$. By the convergence of the series on the right-hand side of (22), there is a positive constant C_1 such that

$$\exists C_1 > 0 : |\epsilon_i^0| \leq C_1(\phi_1(h) + \phi_2(k)), \quad \forall i = \overline{0, M},$$

then we have

$$\exists C_1 > 0 : \|\epsilon^0\|_2 = |\lambda_0| \leq C_1\sqrt{L}(\phi_1(h) + \phi_2(k)).$$

Subsequently, we obtain

$$\begin{aligned}
 |\gamma_1| &\leq \frac{C_1\sqrt{L}}{\sqrt{16[(r_i^1)^2 - (w_i^1)^2] \sin^4(\frac{\theta h}{2}) + 8[2(w_i^1)^2 - r_i^1] \sin^2(\frac{\theta h}{2}) + 1}}(\phi_1(h) + \phi_2(k)) \\
 &\leq C^*(\phi_1(h) + \phi_2(k)).
 \end{aligned}$$

Let us write

$$C^* = \max_{0 \leq i \leq M} \frac{C_1\sqrt{L}}{\sqrt{16[(r_i^1)^2 - (w_i^1)^2] \sin^4(\frac{\theta h}{2}) + 8[2(w_i^1)^2 - r_i^1] \sin^2(\frac{\theta h}{2}) + 1}}.$$

We assume that the following statement is true:

$$|\gamma_j| \leq C^*(\phi_1(h) + \phi_2(k)), \quad \forall j = \overline{1, N}, \tag{26}$$

and we prove that the following statement is true:

$$|\gamma_{j+1}| \leq C^*(\phi_1(h) + \phi_2(k)), \quad \forall j = \overline{1, N}, \tag{27}$$

then we have

$$\begin{aligned}
 |\gamma_{j+1}| &= \left| \frac{\gamma_j - \sum_{n=1}^j (\gamma_{j-n+1} - \gamma_{j-n}) \delta_i^{j+1}(n) + \lambda_j}{1 - 4r_i^{j+1} \sin^2(\frac{\theta h}{2}) + 2\mu w_i^{j+1} \sin(\theta h)} \right| \\
 &= \frac{|\gamma_j - \sum_{n=1}^j (\gamma_{j-n+1} - \gamma_{j-n}) \delta_i^{j+1}(n) + \lambda_j|}{|1 - 4r_i^{j+1} \sin^2(\frac{\theta h}{2}) + 2\mu w_i^{j+1} \sin(\theta h)|} \\
 &= \frac{|\gamma_j - \sum_{n=1}^j (\gamma_{j-n+1} - \gamma_{j-n}) \delta_i^{j+1}(n) + \lambda_j|}{\sqrt{16[(r_i^{j+1})^2 - (w_i^{j+1})^2] \sin^4(\frac{\theta h}{2}) + 8[2(w_i^{j+1})^2 - r_i^{j+1}] \sin^2(\frac{\theta h}{2}) + 1}} \\
 &\leq \frac{|\gamma_j| + \sum_{n=1}^j (|\gamma_{j-n+1}| + |\gamma_{j-n}|) |\delta_i^{j+1}(n)| + |\lambda_j|}{\sqrt{16[(r_i^{j+1})^2 - (w_i^{j+1})^2] \sin^4(\frac{\theta h}{2}) + 8[2(w_i^{j+1})^2 - r_i^{j+1}] \sin^2(\frac{\theta h}{2}) + 1}} \\
 &\leq \frac{C^*(2N - 1)(\phi_1(h) + \phi_2(k)) + |\lambda_j|}{\sqrt{16[(r_i^{j+1})^2 - (w_i^{j+1})^2] \sin^4(\frac{\theta h}{2}) + 8[2(w_i^{j+1})^2 - r_i^{j+1}] \sin^2(\frac{\theta h}{2}) + 1}}.
 \end{aligned}$$

By the convergence of the series on the right-hand side of (22), there is a positive constant C_1 such that

$$\exists C_1 > 0 : \|\epsilon_i^j\| \leq C_1(\phi_2(k) + \phi_1(h)), \quad \forall i = \overline{0, M} \text{ and } \forall j = \overline{0, N},$$

we obtain

$$\exists C_1 > 0 : \|\epsilon^j\|_2 = |\lambda_j| \leq C_1 \sqrt{L}(\phi_2(k) + \phi_1(h)), \quad \forall j = \overline{0, N}.$$

So

$$\begin{aligned}
 |\gamma_{j+1}| &\leq C_i^j \left((2N - 1)C^* + C_1 \sqrt{L} \right) (\phi_2(k) + \phi_1(h)) \\
 &\leq C \left(C^* + \frac{C_1 \sqrt{L}}{2N - 1} \right) (\phi_2(k) + \phi_1(h)) \\
 &= C^*(\phi_2(k) + \phi_1(h)),
 \end{aligned}$$

then we have

$$\begin{aligned}
 C_i^j &= \frac{1}{\sqrt{16[(r_i^{j+1})^2 - (w_i^{j+1})^2] \sin^4(\frac{\theta h}{2}) + 8[2(w_i^{j+1})^2 - r_i^{j+1}] \sin^2(\frac{\theta h}{2}) + 1}} \\
 &\quad \forall i = \overline{0, M} \text{ and } \forall j = \overline{0, N - 1},
 \end{aligned}$$

where

$$C^j = \max_{0 \leq i < M} C_i^j, \text{ and } C = (2N - 1) \max_{0 \leq i < M} C_i^j, \quad \forall j = \overline{0, N - 1},$$

such that the constant L is given by

$$L = \left(\frac{C^*(1 - C)(2N - 1)}{C_1 C} \right)^2.$$

So we find

$$|\gamma_j| \leq C^*(\phi_1(h) + \phi_2(k)), \quad \forall j = \overline{1, N}. \tag{28}$$

Therefore the implicit finite difference scheme (9) is convergent, which concludes the proof of Theorem 4.1.

5 Solvability of the Approximate Scheme

We have the second result on the solvability of the approximate scheme which is given by Theorem 4.1.

Theorem 5.1 *The approximate scheme (9) is uniquely solvable.*

It can be seen that the corresponding homogeneous linear algebraic equations for the approximate scheme

$$\frac{\phi_2(k)^{-\alpha(x_i, t_{j+1})}}{\Gamma(2 - \alpha(x_i, t_{j+1}))} \left[u_i^{j+1} - u_i^j + \sum_{n=1}^j (u_i^{j-n+1} - u_i^{j-n}) \delta_i^{j+1}(n) \right] + a_i^j \frac{u_{i+1}^{j+1} - 2u_i^{j+1} + u_{i-1}^{j+1}}{\phi_3(h)} + c_i^j \frac{u_{i+1}^{j+1} - u_{i-1}^{j+1}}{\phi_1(h)} = f_i^{j+1},$$

$$\forall i = \overline{1, M-1} \text{ and } \forall j = \overline{1, N-1},$$

where

$$r_i^{j+1} = a_i^j \frac{\phi_2(k)^{\alpha(x_i, t_{j+1})} \Gamma(2 - \alpha(x_i, t_{j+1}))}{\phi_1^2(h)}, w_i^{j+1} = c_i^j \frac{\phi_2(k)^{\alpha(x_i, t_{j+1})} \Gamma(2 - \alpha(x_i, t_{j+1}))}{\phi_1(h)}$$

$$\rho_i^{j+1} = \phi_2(k)^{\alpha(x_i, t_{j+1})} \Gamma(2 - \alpha(x_i, t_{j+1})),$$

are

$$\begin{cases} (r_i^{j+1} - w_i^{j+1})u_{i-1}^{j+1} + (1 - 2r_i^{j+1})u_i^{j+1} + (r_i^{j+1} + w_i^{j+1})u_{i+1}^{j+1} \\ = u_i^j - \sum_{n=1}^j (u_{i+1}^{j-n+1} \\ u_i^{j-n}) \delta_i^{j+1}(n) + \rho_i^{j+1} f_i^{j+1}, \quad \forall i = \overline{1, M-1} \text{ and } \forall j = \overline{1, N-1}, \\ u_0^{j+1} = q^{j+1}, u_M^{j+1} = p^{j+1}, \quad \forall j = \overline{0, N-1}, \\ u_i^0 = s_i, \quad \forall i = \overline{0, M}. \end{cases} \tag{29}$$

Proof. Similar to the proof of Theorem 3.1, we can also verify the solutions of the equations (25) satisfy $\|u^j\|_2 \leq C\|u^0\|, \forall j = \overline{1, N}$, we have $u^0 = 0$, so we get $u^j = 0, \forall j = \overline{1, N}$. This indicates that the equations (29) have only zero solutions, the approximate scheme (9) is uniquely solvable, which concludes the proof of Theorem 5.1.

6 Examples and Numerical Experiments

Here, we present different numerical experiments to support the theoretical and numerical analyses of the previous sections. The following variable-order time-fractional diffusion equation is considered:

$$\begin{cases} \frac{\partial^\alpha u}{\partial t^\alpha} + \frac{\partial^2 u}{\partial x^2}(x, t) + \frac{\partial u}{\partial x} = f(x, t) \quad 0 < x < L, \quad t > 0, \quad 0 < \alpha < 1, \\ u(0, t) = 0, \quad u(1, t) = 0, \\ u(x, 0) = 10x^2(1 - x), \end{cases} \tag{30}$$

where $N=M=N_x=50, 100, 150, 200$, and we have tested our numerical approximations by two values of $\alpha(x, t)$. First, we have $\alpha(x, t) = \frac{\sin(x,t)^2}{4}$. But, in the second part,

$\alpha(x, t) = \frac{\sqrt{(\cos(x.t))^2 + \sqrt{x.t}}}{4}$ and the function $f(x, t)$ are used to test our approaches, where the function $f(x, t)$ is given by

$$f(x, t) = 20x^2(1 - x) \left[\frac{t^{2-\alpha(x,t)}}{\Gamma(3 - \alpha(x, t))} + \frac{t^{1-\alpha(x,t)}}{\Gamma(2 - \alpha(x, t))} \right] + 10(-3x^2 - 4x + 2)(1 + t)^2.$$

The exact solution is given by

$$u(x, t) = 10x^2(1 - x)(t + 1)^2.$$

By the implicit finite-difference scheme discretization method, the derivatives can be approximated as follows.

First, we choose the dominator functions in the following form:

$$\phi_1(h) = h \text{ and } \phi_2(k) = 2(e^k - 1).$$

Let now $[0, 1]$ be the interval of interest we discretise the domain first. We define

$$x_i = i\phi_1(h) \text{ where } i = \overline{0, N_x} \text{ and } t_j = j\phi_2(k) \text{ where } j = \overline{0, N_x},$$

where $\phi_2(k)$ represents the time step size and $\phi_1(h)$ represents the space step length. Let us assume that

$$f(x_i, t_{j+1}) = f_i^{j+1} = 20x_i^2(1 - x_i) \left[\frac{t_{j+1}^{2-\alpha(x_i, t_{j+1})}}{\Gamma(3 - \alpha(x_i, t_{j+1}))} + \frac{t_{j+1}^{1-\alpha(x_i, t_{j+1})}}{\Gamma(2 - \alpha(x_i, t_{j+1}))} \right] + \tag{31}$$

$$+ 10(-3x_i^2 - 4x_i + 2)(1 + t_{j+1})^2,$$

$$q^{j+1} = 0, \tag{32}$$

$$p^{j+1} = 0, \tag{33}$$

where u_i^j is the numerical approximation of $u(x_i, t_j)$ and f_i^j is the numerical approximation of $f(x_i, t_j)$.

We obtain the following approximate scheme for equation (30):

$$\begin{cases} (r_i^{j+1} - w_i^{j+1})u_{i-1}^{j+1} + (1 - 2r_i^{j+1})u_i^{j+1} + (r_i^{j+1} + w_i^{j+1})u_{i+1}^{j+1} \\ = u_i^j - \sum_{n=1}^j (u_{i+1}^{j-n+1} \\ u_i^{j-n-1})\delta_i^{j+1}(n) + \rho_i^{j+1}f_i^{j+1}, \quad \forall i = \overline{1, N_x - 1} \text{ and } \forall j = \overline{1, N_x - 1}, \\ u_0^{j+1} = q^{j+1}, \quad u_{N_x}^{j+1} = p^{j+1}, \quad \forall j = \overline{0, N_x - 1}, \\ u_i^0 = s_i, \quad \forall i = \overline{0, N_x}, \end{cases} \tag{34}$$

where

$$r_i^{j+1} = a_i^j \frac{\phi_2(k)^{\alpha(x_i, t_{j+1})}\Gamma(2 - \alpha(x_i, t_{j+1}))}{\phi_1^2(h)}, w_i^{j+1} = c_i^j \frac{\phi_2(k)^{\alpha(x_i, t_{j+1})}\Gamma(2 - \alpha(x_i, t_{j+1}))}{\phi_1(h)}$$

$$\rho_i^{j+1} = \phi_2(k)^{\alpha(x_i, t_{j+1})}\Gamma(2 - \alpha(x_i, t_{j+1})), \tag{35}$$

and

$$\delta_i^{j+1}(n) = (n + 1)^{1-\alpha(x_i, t_{j+1})} - n^{1-\alpha(x_i, t_{j+1})}, \quad \forall j = \overline{0, N_x - 1}.$$

In this example, we have tested the numerical solution when $N=M=N_x=50, 100, 150, 200$ and $\alpha(x, t) = \frac{\sin(x.t)^2}{4}$. But, in the second part of our test, $\alpha(x, t) = \frac{\sqrt{(\cos(x.t))^2 + \sqrt{x.t}}}{4}$ when $N=M=N_x=50, 100, 150, 200$. Finally, various numerical tests are presented in both one dimension and for general meshes to illustrate the capacity of the schemes and compare theoretical and experimental results.

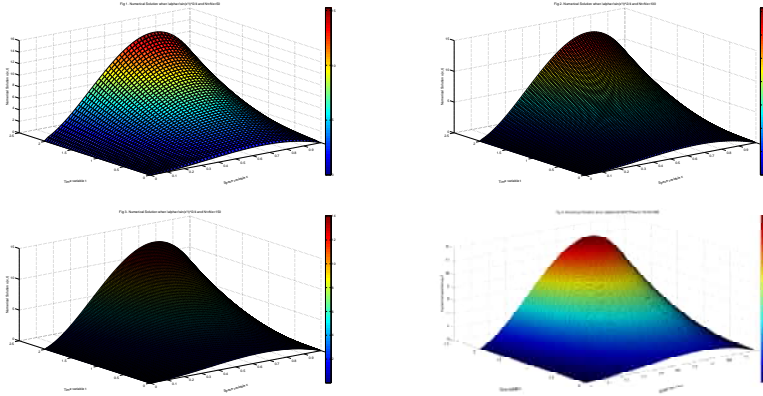


Figure 1: Numerical solution when $N=M=N_x=50,100,150,200$ and $\alpha(x, t) = \frac{\sin(x.t)^2}{4}$.

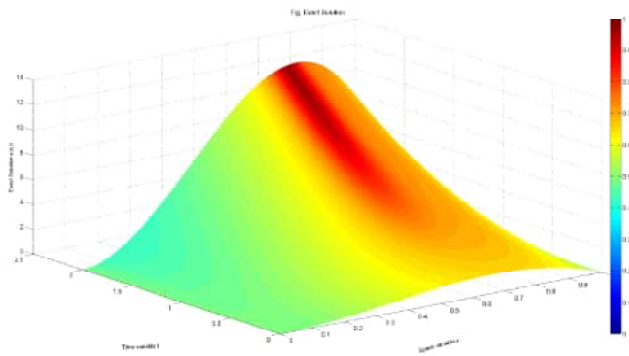


Figure 2: Exact solution when $\alpha(x, t) = \frac{\sin(x.t)^2}{4}$.

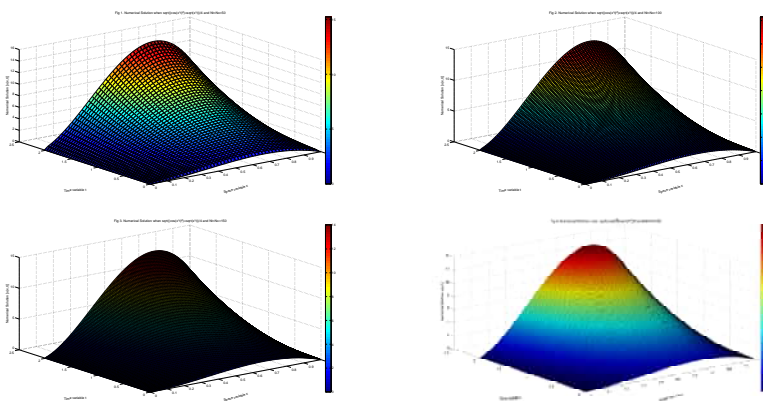


Figure 3: Numerical solution when $N=M=N_x=50,100,150,200$ and $\alpha(x, t) = \frac{\sqrt{\cos(x.t)^2 + \sqrt{x.t}}}{4}$.

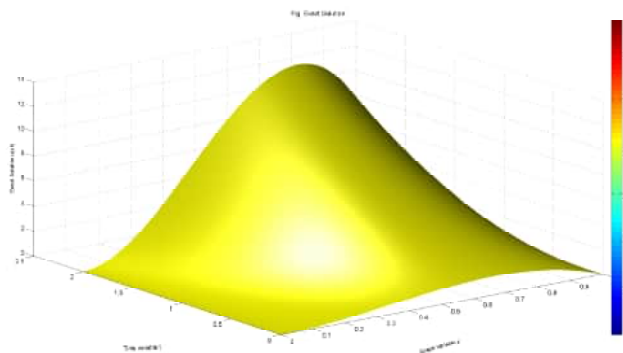


Figure 4: Exact solution when $\alpha(x, t) = \frac{\sqrt{\cos(x.t)^2 + \sqrt{x.t}}}{4}$.

7 Conclusion and Perspectives

In this work, we have discussed implicit discretization techniques by using an approach to forward fractional derivatives and the first-order spatial derivative can be approximated by the forward operator. These are particularly useful whenever the implicit scheme requires a time step. As in the implicit schemes, the values at interior grid points at new time levels cannot be obtained before computing the values at boundaries, an iteration procedure is employed to handle the nonlocal boundary condition. However, the discussion indicates that it is always important to explore the various algorithms when trying to solve a numerical problem and there is a vast literature available to do this. The numerical test applied to these methods gives acceptable results and suggests convergence to the exact solution when h goes to zero, see [6, 8, 12, 18].

References

- [1] A. A. Alikhanov. A new difference scheme for the time fractional diffusion equation. *J. Comput. Phys.* **280** (2015) 424–438.
- [2] B. K. AL-Saltani. Solution of delay fractional differential equations by using linear multistep method. *J. Kerbala Univ.* **5** (4) (2007) 217–222.
- [3] J. J. Benito, F. Urena and L. Gavete. Influence of several factors in the generalized finite difference method. *Appl. Math. Model.* (2001).
- [4] V. Daftardar-Gejji, Y. Sukale and S. Bhalekar. Solving fractional delay differential equations: A new approach. *Fract. Calcul. Appl. Anal.* **18** (2015) 400–418.
- [5] V. Daftardar-Gejji and H. Jafari. An iterative method for solving non linear functional equations. *J. Math. Anal. Appl.* **316** (2006) 753–763.
- [6] M. Djaghout, A. Chaoui and Kh. Zennir. On Discretization of the Evolution p-Bi-Laplace Equation. *Numer. Anal. Appl.* **15** (2022) 303–315.
- [7] K. Diethelm. An improvement of a nonclassical numerical method for the computation of fractional derivatives. *J. Vibr. Acoust.* **131** (1) (2009) Article ID 014502.
- [8] M. D. Johansyah, I. Sumiati, E. Rusyaman, Sukono, M. Muslikh, M. A. Mohamed and A. Sambas, Numerical Solution of the Black-Scholes Partial Differential Equation for the Option Pricing Model Using the ADM-Kamal Method. *Nonl. Dynam. Sys. Theory* **23** (3) (2023) 295–309.

- [9] L. Galeone and R. Garrappa. Explicit methods for fractional differential equations and their stability properties. *J. Comput. Appl. Math.* **228** (2) (2009) 548–560.
- [10] M. M. Khader and A. S. Hendy. The approximate and exact solutions of the fractional-order delay differential equations using Legendre pseudospectral method. *Inter. J. Pure and Appl. Math.* **74** (3) (2012) 287–297.
- [11] A. A. Kilbas, H. M. Srivastava and J. J. Trujillo. *Theory and Application of Fractional Differential Equation*. Oxford, New York, 2006.
- [12] M. Labid and N. Hamri. Chaos Anti-Synchronization between Fractional-Order Lesser Date Moth Chaotic System and Integer-Order Chaotic System by Nonlinear Control. *Nonl. Dynam. Sys. Theory* **23** (2) (2023) 207–213.
- [13] F. Mainardi. *Fractional Calculus and Waves in Linear Visco-elasticity: An Introduction to Mathematical Models*. Imperial College Press, London, 2010.
- [14] B. P. Moghaddam and Z. S. Mostaghim. A numerical method based on finite difference for solving fractional delay differential equations. *J. Taibah Univ. Sci.* **7** (3) (2013) 120–127.
- [15] B. P. Moghaddam and Z. S. Mostaghim. Modified finite difference method for solving fractional delay differential equations. *Boletim da Sociedade Paranaense de Matematica* **35** (2017) 49–58.
- [16] A. Piskarev. Fractional equations and difference schemes. In: *Proc. Int. Conference : Computational Methods in Applied Mathematics*. Javaskyla, Finland, 2016.
- [17] T. Young and M. J. Mohlenkamp. *Introduction to Numerical Methods and Matlab Programming for Engineers*, 2011.
- [18] A. Zarour and M. Dalah. Analysis and Numerical Approximation of the Variable-Order Time-Fractional Equation. *Nonl. Dynam. Sys. Theory* **24** (2) (2024) 205–216.



Application of Discrete Event Simulation and System Dynamics Modeling in Optimizing the Performance of OutPatient Department

Amina Boukoftane^{1*}, Muhammad Ahmed Kalwar², Nadia Oukid¹,
Khaled Zennir³, Muhammad Saad Memon⁴ and Muhammad Ali Khan⁴

¹ *Department of Mathematics, University of Blida 1, B.P. 270, LAMDA-RO Laboratory, Blida, Algeria.*

² *Department of Industrial Engineering and Management, Mehran UET, Jamshoro, Sindh, Pakistan.*

³ *Department of Mathematics, College of Sciences, Qassim University, Saudi Arabia*

⁴ *Department of Industrial Engineering and Management, Mehran UET, Hyderabad, Sindh, Pakistan*

Received: January 31, 2024; Revised: May 31, 2024

Abstract: This research is aimed to optimize the length of queues and the waiting time of patients at the general OutPatient Department (OPD). A Discrete Event Simulation (DES) model was developed to model the queuing system of OPD and a system dynamics (SD) model was developed to conduct the cost calculations of the OPD. Both models were constructed by using the same data. Since the association of variables, waiting time, number of patients, number of servers at various service channels and opportunity cost, with one another is non-linear, this was the reason the authors used the SD approach for calculations. The present research is a reflection of how the performance of OPDs can be optimized by using the DES and SD modelling techniques. The present research contributes to giving a direction to hospitals to optimize their performance by using the DES and SD modelling and simulation techniques.

Keywords: *queuing system; nonlinear systems; outpatient department; waiting time; length of the queue; Nash equilibrium.*

Mathematics Subject Classification (2010): 81T80, 93C10, 93C65.

* Corresponding author: <mailto:boukoftaneam@yahoo.fr>

1 Introduction

Hospitals are described as complicated systems with certain benefits that are expensive for the general public [1]. Patient overcrowding in waiting areas, emergency rooms, intensive care units, and outpatient departments (OPDs) is presently one of the hospital's biggest concerns [2]. This is due to the absence of end-to-end queuing system administration in numerous hospital departments [2]. The main issue is the queue, which is unquestionably caused by improper administration of queuing systems [1]. When the number of servers is less than the number of entities to be served in the system, then a queue is formed [3]. Addressing issues regarding health care including resource utilization, epidemiologic concerns, patient flows, and allocation of resources, in DES, has proven to be a reliable tool for healthcare systems [4].

The SD modeling approach is used to model the variables that are non-linearly correlated with one another. Numerous authors have worked on the DES modeling approach and studied patient flows in the clinical setting. Torri et al. [5] studied activities workflow at the Department of Laboratory Medicine of the "San Paolo" Hospital in Naples. Williams et al. [6] used a DES modeling approach for the determination of bed requirements at the critical care unit in the United Kingdom. Melman et al. [7] utilized the DES modeling approach to define the patient flows in emergency surgery and elective surgery during the COVID-19 pandemic. Numerous authors have worked on the optimal allocation of resources in healthcare settings by using DES modeling and simulation; they have worked on the minimization of waiting time [8,9]. Whereas in the present research, the DES and SD modeling approaches were used to evaluate and analyze the current queuing system of the OPD.

In the present research, a queuing system of the OPD of an anonymous hospital was studied and the number of required resources was suggested accordingly to the congestion at the various service channels. Moreover, the Nash equilibrium was used to decide the best scenario analyzed by the DES and SD modeling approaches.

2 Research Methodology

2.1 Data collection

Data collection was the first step of the present research; it included the arrival rate of patients at the OPD and their service rate at the reception and triage; furthermore, the service rate of patients by various doctors available at the OPD was also collected. The second step was the model development in Anylogic software, it was conducted using the DES modeling (see Figure 4) and SD modeling techniques.

The arrival rate of patients was collected as the number of patients who arrived at the OPD per hour. The arrival rate of patients was then put into the custom distribution function of Anylogic software. The service rate of patients at the reception was collected as the time to serve one patient, the service rate was also put into the custom distribution function for various stages of service. Some distribution functions are given below.

Resource pools were used to include the set of resources (receptionists, nurses, various types of doctors) and the parameters were used to initialize the number of the various resources (see Figure 3).

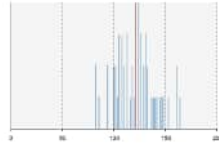


Figure 1: The arrival rate of the patients at the clinic.

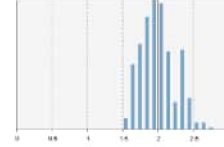


Figure 2: Service rate of patients at reception.

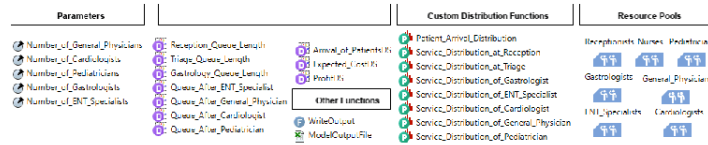


Figure 3: Parameters, datasets, custom distribution functions, and resource pools as used during the model development.

2.2 Model development

2.2.1 Development of DES model

In the gravity of consideration to the discussion in the process workflow of the OPD, the flow of patients, the DES model was developed (see Figure 4). Several elements from the process modeling library were in the model given in Figure 4. The ‘*Source*’ was used for the arrival of patients, and the number of patients arriving at the OPD per hour was already put in the custom distribution function; therefore, the input of the *source* in the model was put to be the ‘*Patient_Arrival_Distribution*’. After the entrance of the patients into the OPD, their entrance time was noted by using the ‘*time measure start*’ from the process modeling library of Anylogic.

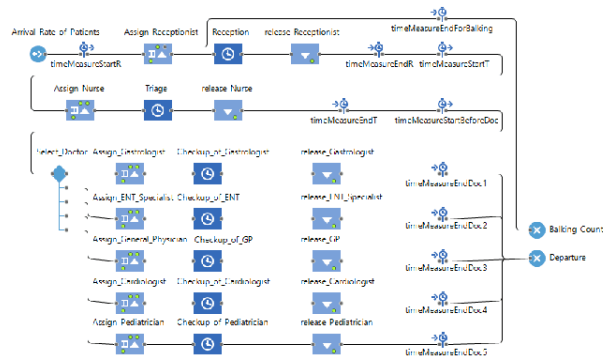


Figure 4: The discrete event simulation model designed in Anylogic.

The receptionist from the resource pool (*Receptionists*) was then seized (*Assign_Receptionist*) at the reception and the queue is formed; the condition was applied to the queue that if the waiting time of the patient in the reception queue exceeds 60 minutes, then he/she balks. The ‘*Delay*’ function (*Reception*) was used to serve the patients at the reception and the service distribution of patients was put to be the ‘*Ser-*

vice_Distribution_At_Reception' (see Figures 2-3). The total time spent by the patients at the reception (waiting time + reception service time) was calculated by the *'time measure end'* function from the process modeling library. Similarly to reception, the time spent by the patients at various service channels (triage, gastrologists, ENT specialists, cardiologists, pediatricians, and general physicians) was calculated using the *'time measure end'* function. After the patients are served at the reception, then the nurses are seized at triage to serve the patients. As per the data collection, 36.68% of patients visited the OPD for health issues related to gastrology, 12.47% of the patients because of ENT issues, 27.68% of the patients visited the OPD because of issues associated with cardiology, 13.95% of patients visit the OPD because of issues associated with their children; moreover, 9.23% visit the OPD to consult general physicians. After the patients were served from the triage, they were sent to a specific type of doctor as per the nature of their health issue. The decision of sending a particular patient to a specific type of doctor was made based on the above-discussed percentages. At the end of the queuing system, the time spent by the patients in the queue to consult the doctor and the consultation time of patients were recorded. When a patient is served from all the service channels, he/she departed from the OPD.

2.2.2 Development of system dynamics model

The system dynamics model was also developed in the present research. The stock and flow diagram was developed (see Figure 5) using the flow of patients through various service channels. Various distributions used in the DES model were put in the flows of the system dynamics model. The input in the Arrival rate flow was put to be the Patient arrival distribution, the flow, i.e., the service rate at reception was initialized with the distribution function of the service Distribution at reception, the service rate at triage was initialized with the service distribution at triage. The Service distributions of patients by various types of doctors were also put in the same way.

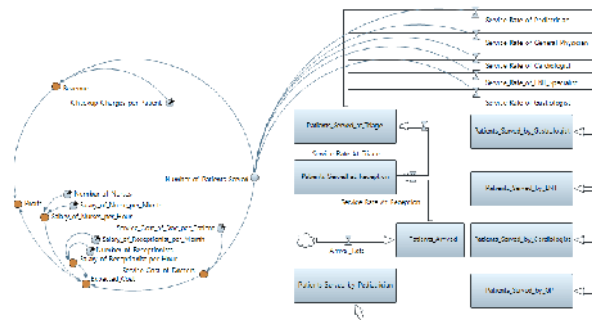


Figure 5: The system dynamics model synchronized with the discrete event model.

The set of equations represents the various stocks used in Figure 5.

$$P_a(t) = \int_{t_0}^t \varphi_{ar} dt + P_a(t_0), \tag{1}$$

$$P_{sr}(t) = \int_{t_0}^t [\varphi_{ar} - \varphi_{srr}] dt + P_{sr}(t_0), \tag{2}$$

$$P_{st}(t) = \int_{t_0}^t [\varphi_{srr} - \varphi_{srt}] dt + P_{st}(t_0), \quad (3)$$

$$P_{sg}(t) = \int_{t_0}^t [\varphi_{srt} - \varphi_{srg}] dt + P_{sg}(t_0), \quad (4)$$

$$P_{sent}(t) = \int_{t_0}^t [\varphi_{srt} - \varphi_{srent}] dt + P_{sent}(t_0), \quad (5)$$

$$P_{sc}(t) = \int_{t_0}^t [\varphi_{srt} - \varphi_{src}] dt + P_{sc}(t_0), \quad (6)$$

$$P_{sgp}(t) = \int_{t_0}^t [\varphi_{srt} - \varphi_{srgp}] dt + P_{sgp}(t_0), \quad (7)$$

$$P_{sp}(t) = \int_{t_0}^t [\varphi_{srt} - \varphi_{srp}] dt + P_{sp}(t_0). \quad (8)$$

The total number of patients served at the OPD was calculated by (9), the cost of receptionists per hour was calculated by (10), (11) was for the calculation of the cost of nurses per hour, the service cost of doctors was calculated by using (12), the total expected cost was calculated by using (13), (14) was for the calculation of revenue, and (15) was for the calculation of profit.

$$N_{ps} = \varphi_{srg} + \varphi_{srent} + \varphi_{src} + \varphi_{srgp} + \varphi_{srp} \quad (9)$$

$$C_{rph} = \frac{C_{rpm}}{D_w T_h} N_{recep}, \quad (10)$$

$$C_{nph} = \frac{C_{nurpm}}{D_w T_h} N_{nur}, \quad (11)$$

$$C_{sd} = N_{ps} C_{sdocpp}, \quad (12)$$

$$C_{ex} = C_{rph} + C_{nph} + C_{sd}, \quad (13)$$

$$R = N_{ps} C_{check}, \quad (14)$$

$$P = (R - C_{ex}). \quad (15)$$

2.3 Model initialization

The DES model was initialized in two scenarios as given in Figure 6. Scenario 1 represents the present situation of the OPD and Scenario 2 is the suggested situation for the OPD.

Since the performance of the OPD was based on the number of resources and length of the queue after each human resource (receptionist, nurse, gastrologist, ENT specialist, cardiologist, pediatrician, and general physician), it was dependent on the availability of the number of human resources. The discussion model initialization was applied to both models because they are integrated.

3 Results and Discussions

Under this heading, the results of the present situation of the OPD were discussed and after increasing the number of several resources, the queue length and various other parameters were discussed in detail.

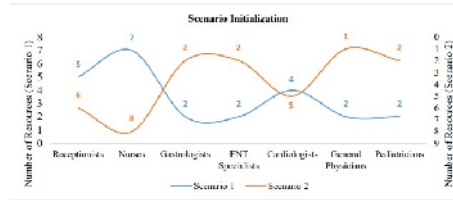


Figure 6: Initialization of the DES model.

3.1 Arrival rate of patients

The arrival rate of patients as indicated by Figure 7 was taken from the output of the flow, i.e., the ‘Arrival_Rate’ of the system dynamics model given in Figure 5. A look at Figure 7 indicates that the arrival rate of patients at the OPD was between 80 to 165 patients per hour, which means that this number of patients arrives at the reception and passed through all the service channels. Note: the x-axis of the figure indicates the model

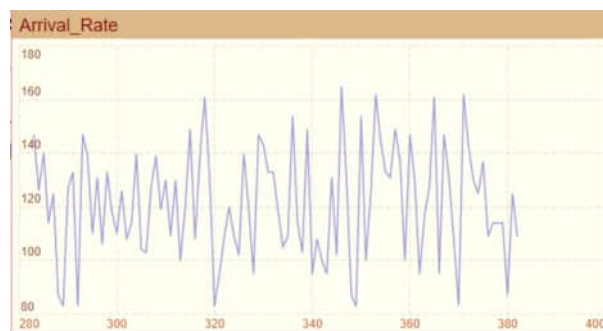


Figure 7: The arrival rate of patients obtained after simulating the SD model.

time in hours and the y-axis indicates the number of patients arriving at the OPD.

3.1.1 Results of Scenario 1

The main problem at the OPD was the congestion of the patients at every service channel. At the reception, even after the availability of 5 receptionists, the queue length of the patients mostly fluctuates between 5 to 10 patients; at one point, the queue length at reception reached 18 patients as indicated by Figure 8. According to the simulation results from Anylogic software, the patients spent an average time of 0.053 hours at the reception including waiting time in the queue and service time of the receptionist. Furthermore, the minimum and maximum time of patients at the reception was taken out to be 0.196 hours and 0.026 hours, respectively. In the existing scenario (Scenario 1), the headcount of nurses was 7 and the queue length of triage indicates that around 10 to 20 patients were in the queue in 382 simulated hours of the OPD, and sometimes even more patients wait in the queue; at one point, the simulation results (see Figure 8) indicate around 45 people in the queue of triage. Furthermore, according to the simulation results, the patients spent an average time of 0.089 hours at the triage including waiting time in the queue and service time of the nurse. The minimum and maximum time of patients

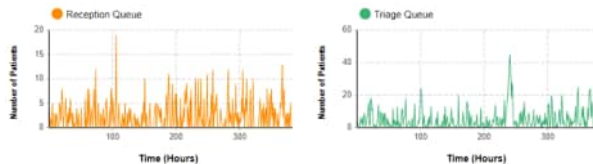


Figure 8: Length of queue at reception and triage.

at the triage was 0.402 hours and 0.035 hours respectively.

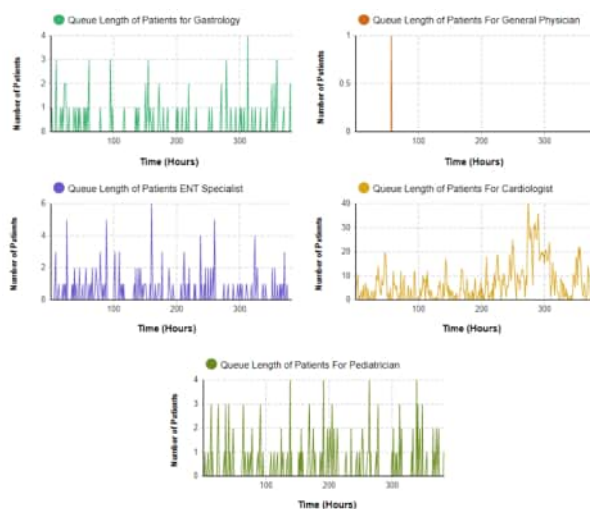


Figure 9: Length of the queue for various types of doctors.

Five types of doctors were available at the OPD. In the existing scenario (Scenario 1), the queue of patients who came to consult gastrologists contained 3 patients on average throughout the simulation time. Similarly, the queues for the ENT specialists and pediatricians are short, which indicates that enough doctors (gastrologists, ENT Specialists, and pediatricians) were there to provide the consultation to the patients. The patients spent an average of 0.032 hours, a maximum time of 0.124 hours, and a minimum of 0.02 hours only to consult a gastrologist; the time spent by the patients to consult an ENT specialist (average = 0.1 hours, minimum = 0.063 hours, and maximum = 0.436 hours) and pediatrician (average = 0.092 hours, minimum = 0.052 hours, and maximum = 0.386 hours) was quite less; this is the reason the queue length for the mentioned doctors was significantly short as given in Figure 9

The queue length for general physicians indicated that as per the flow of patients arriving at the OPD to consult general physicians, the availability of doctors was larger than the requirement. The patients spent an average of 0.036 hours. The time of patients (waiting time in the queue to see a general physician plus the consultation time) indicates that the patients got free quickly from the cabins of general physicians. In this regard, the authors suggested decreasing the number of general physicians as per the current workload. Furthermore, the queue length for cardiologists indicates that the availability of doctors was less than the requirement as per the flow of patients arriving at the OPD

to consult cardiologists; this is the reason the queue gets long and patients wait longer to see the doctor. The patients spent 0.29 hours on average, 0.083 hours minimally, and 1.197 hours maximally consulting the cardiologists. The waiting time of patients in the queue and the doctors consultation time were significantly greater as compared to those for the rest of the doctors, this is the reason for the long queue after cardiologists.



Figure 10: The expected cost, revenues, and profits of the OPD in Scenario 1.

With 5 receptionists, 7 nurses, and 12 doctors, the expected cost, revenues, and profits can be noticed as given in Figure 10. The average expected cost (calculated from the downloaded data into Microsoft Excel), revenue, and profit were calculated to be PKR 61.06.71, PKR 7479.68, and PKR 1362.86, respectively. Moreover, the waiting cost of patients was calculated to be PKR 77.96.

3.2 Results of Scenario 2

The queue length at reception and triage was found to be greater in Scenario 1 as indicated by Figure 14. The authors suggested an increase in the number of receptionists and nurses. In this regard, the numbers of one receptionist and one nurse were increased in Scenario 2 and the DES model was simulated; the results of the simulation are presented in Figure 11 in terms of the queue length at reception and triage.

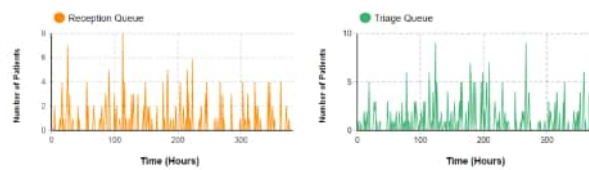


Figure 11: Length of queue at reception and triage.

The length of the queue at reception decreased from 10 to 15 patients to 4 to 6 patients (see Figure 11). Moreover, the patients spent 0.038 hours on average, their minimum time was 0.026 hours, and their maximum time was 0.105 hours. The average time of patients spent at reception decreased from 0.053 hours (Scenario 1) to 0.038 hours (Scenario 2). The length of the queue at triage decreased from 10 to 20 patients to 5 to 9 patients (see Figure 11). Moreover, the patients spent 0.057 hours on average, their minimum time was 0.035 hours, and their maximum time was 0.162 hours. The average

time of patients spent at triage decreased from 0.089 hours (Scenario 1) to 0.057 hours (Scenario 2). The maximum time of patients at triage also decreased significantly from 0.402 hours (Scenario 1) to 0.162 hours (Scenario 2). Increasing of the numbers of one receptionist and one nurse increased the service rate of both service channels significantly. The number of general physicians decreased from 2 to 1 and the number of cardiologists increased from 4 to 5 in Scenario 2; this suggestion was made considering the length of the queue for both types of doctors. The queue length for the general physicians was very short, therefore, the number of doctors was reduced and the number of cardiologists was increased because of the greater length of the queue of patients. In Scenario 2, there are some patients in the queue (see Figure 12), whereas, in Scenario 1, the queue length was either 0 or 1, which means the general physicians were under-utilized. The patient's time incurred in the queue for general physicians and the time incurred in the consultation increased (average = 0.047 hours, minimum = 0.026 hours, and maximum = 0.214 hours) as compared to Scenario 1.

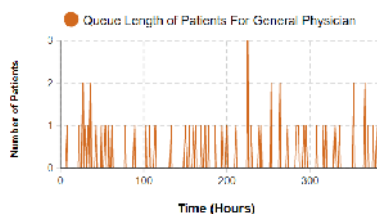


Figure 12: Length of the queue for general physicians after decreasing by one doctor.

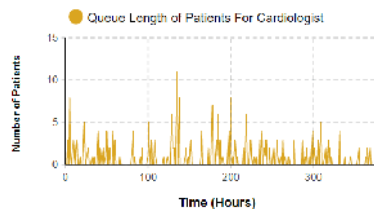


Figure 13: Length of the queue for cardiologists after increasing the number of one doctor.

The length of the queue for cardiologists decreased from 10 to 20 patients to 4 to 10 patients (see Figure 13). Since the number of doctors increased, the system time of patients at the service channel decreased significantly. The patients spent 0.123 hours (instead of 0.29 hours) on average, their minimum time was 0.083 hours, and their maximum time was 0.365 hours (instead of 1.197 hours). The average time of patients spent seeing a cardiologist decreased by 57.58% in Scenario 2 just by increasing the number of one cardiologist.



Figure 14: The expected cost, revenues, and profits of the OPD in Scenario 2.

The variation in the expected cost, revenues, and profits were noticed as given in Figure 14. The average expected cost (calculated from the downloaded data into Microsoft Excel), revenue, and profit were calculated to be PKR 6350.60, PKR 7454.67, and PKR 1123.88, respectively. The average opportunity cost of a patient in Scenario 2 was calculated to be PKR 39.90.

4 Calculation of Nash Equilibrium

We summarize the possible metaphorical or analogical transpositions from game theory to the strategic OPD model from the five fundamental concepts of game theory (see Table 4). Player strategies are defined based on payment functions. It is from the expected

Concept of game theory	Useful transposition to the strategic OPD model
strategy	Scenarios 1 and 2
decision tree	Concept of bifurcation
players	Patients
payment functions	Taking into account the advantages of other patients
Equilibrium	the notion of indeterminacy causing instability. the result of the strategy is random

Table 3: Concepts of Game Theory.

gains, and taking into account the expected gains of other players. The player examines the consequences attached to the system of possibilities, consequences that do not depend solely on his own decisions. The equilibrium is a situation where everyone’s expectations are realized [10].

4.1 Discussion of equilibrium in the OPD model

Let us discuss the Nash equilibrium for 2 patients and which will be generalized for n patients, we will study the Nash equilibrium according to the cost and waiting time, it is in our interest to minimize it, according to Scenario 1 (S_1) and Scenario 2 (S_2) described in this paper. For Scenario 2 (suggested situation of the OPD), the cost of service increases, but the waiting time of the patients decreases and this is the major interest of patients. According to the cost, we have $C_2 > C_1$, where C_i is the patient service cost according to the scenario i ; $i = 1, 2$, the different situations are given in Table 4. The Nash equilibrium i is (C_1, C_1) , it is clear that if, for example, patient

		patient2	patient2
		S_1	S_2
Patient 1	S_1	(C_1, C_1)	(C_1, C_2)
Patient 1	S_2	(C_2, C_1)	(C_2, C_2)

Table 4: Cost matrix of both scenarios.

1 follows the scenario S_2 and patient 2 follows S_1 , patient 1 can follow S_1 in order to minimize the service cost, so (C_2, C_1) is not a Nash equilibrium.

If we consider now the waiting time of patients $T_i, i = 1, 2, T_2 < T_1$, we obtain the following. By the same methodology, the Nash equilibrium is (T_2, T_2) , we conclude that

		patient2	patient2
		S_1	S_2
patient 1	S_1	(T_1, T_1)	(T_1, T_2)
patient 1	S_2	(T_2, T_1)	(T_2, T_2)

Table 5: Waiting time matrix of both scenarios.

the Nash equilibrium confirms the results of the two scenarios and we can generalize it for n patients.

4.2 Price of anarchy

The price of anarchy is a concept in algorithmic game theory that measures how far a system where all agents act to optimize their interests can be from an optimal situation from the global point of view. We define in our model a set of n patients, two strategies (2 scenarios), and utilities $U_i : S \rightarrow \mathbb{R}$, where $S = S_1 \times S_2$. We can define a measure of the efficiency of each outcome which we call a welfare function $W : S \rightarrow \mathbb{R}$, $W(s) = \sum_{i \in N} U_i(S)$. We can define a subset $Equil \subseteq S$ to be the set of strategies in equilibrium. If, instead of a welfare which we want to maximize, the function measure of efficiency is a cost function $Cost : S \rightarrow \mathbb{R}$ which we want to minimize, then

$$P_0A = \frac{\max_{s \in Equil} Cost(s)}{\min_{s \in S} Cost(s)}. \quad (16)$$

According to the table of costs defined above, the cost function is

$$C(S_1, S_2) = u_1(S_1, S_2) + u_2(S_1, S_2). \quad (17)$$

The worst (and the only) Nash equilibrium will be when both patients follow S_2 and the resulting cost is $C_{equil} = 2C_2$ as calculated by (18). However, the highest social welfare occurs when both patients follow S_1 , in this case, the cost is $C_{min} = 2C_1$. Thus the P_0A in this situation will be

$$C_{Equil}/C_{min} = C_2/C_1. \quad (18)$$

If, instead of a welfare which we want to maximize, the function measure of efficiency is a waiting time function $T : S \rightarrow \mathbb{R}$ which we want to minimize, the worst Nash equilibrium will be when both patients follow S_1 and the result is $T_{equil} = 2C_1$. In this case, $P_0A = C_1/C_2$. We have studied an OPD situation with two scenarios for which we calculated the equilibrium and the price of anarchy for the two scenarios and for two patients, something that can be generalized for n patients.

5 Conclusion

At the selected OPD, the queue used to be longer at the reception and triage and cardiologists, whereas it was shorter for the general physicians. Due to the long queues, the system time of patients was longer and they led the OPD to be congested with patients. In this regard, the numbers of one receptionist, one nurse, and one cardiologist were suggested to be increased. Furthermore, due to the short queue of patients to general physicians, one general physician was reduced. The results of the simulation indicated a significant drop in the waiting time of patients in the system and optimization of the length of the queues at the various service channels of the OPD by using the DES. The SD and DES techniques helped researchers to conduct an in-depth analysis of OPD's current situation and the way it can be optimised at a quite reasonable cost. The present research contributes to providing substantial guidelines to hospital management to optimize OPD's performance.

Appendix $P_a(t)$ = Patients Arrived, $P_{sr}(t)$ = Patients Served at Reception, $P_{st}(t)$ = Patients Served at Triage, $P_{sg}(t)$ = Patients Served by Gastrologis, $P_{sent}(t)$ = Patients Served by EN, $P_{sc}(t)$ = Patients Served by Cardiologist, $P_{sgp}(t)$ = Patients Served

by General Physician, $P_{sp}(t)$ = Patients Served by Pediatrician. φ_{ar} = Arrival Rate, φ_{srr} = Service Rate at reception, φ_{srt} = Service Rate at Triage, φ_{srg} = Service Rate of Gastrologist, φ_{srent} = Service Rate of ENT Specialist, φ_{src} = Service Rate of Cardiologist, φ_{srgp} = Service Rate of General Physician, φ_{srp} = Service Rate of Pediatrician. N_{ps} = Number of Patients Served, C_{rph} = Salary of Receptionist per Hour, C_{nph} = Salary of Nurse per Hour, C_{sd} = Service Cost of Doctors, C_{ex} = Expected Cost, R = Revenue, P = Profit. N_{recep} = Number of Receptionists, N_{nur} = Number of Nurses, C_{rpm} = Salary of Receptionist per Month, C_{nurpm} = Salary of Nurse per Month, C_{sdocpp} = Service Cost of Doctor per Patient, C_{check} = Checkup Charges per Patient. D_w = Working Days, T_h = Working Hours.

References

- [1] M. A. Khan, S. A. Khaskheli, H. A. Kalwar, M. A. Kalwar, H. B. Marri and M. Nebhwani. Improving the Performance of Reception and OPD by Using Multi-Server Queuing Model in Covid-19 Pandemic. *Int. J. Sci. Eng. Investig.* **10** (11) (2021) 20–21.
- [2] M. A. Kalwar, H. B. Marri, M. A. Khan and S. A. Khaskheli. Applications of Queuing Theory and Discrete Event Simulation in Health Care Units of Pakistan. *Int. J. Sci. Eng. Investig.* **10** (2021) 6–18.
- [3] T. Ikwunne and M. Onyesolu. Optimality Test for Multi-Sever Queuing Model with Homogenous Server in the Out-Patient Department (OPD) of Nigeria Teaching Hospitals. *Comput. Sci.* **4** (2016) 9–17.
- [4] H. Hvitfeldt-Forsberg, P. Mazzocato, D. Glaser, C. Keller and M. Unbeck. Staffs and managers perceptions. *BMJ Open* **7** (2) (2016) 1–63.
- [5] A. Torri, O. Tamburis, T. Abbate and A. Pepino. New Perspectives for Workflow Analysis in the Health Italian Sector through Discrete Event Simulation: The Case of a Department of Laboratory Medicine. *Intell. Inf. Manag.* **7** (3) (2015) 93–106.
- [6] E. Williams, T. Szakmany, I. Spernaes, B. Muthuswamy and P. Holborn. Discrete-Event Simulation Modeling of Critical Care Flow: New Hospital, Old Challenges. *Crit. Care Explor* **2**(9) (2020) e0174.
- [7] G. J. Melman, A. K. Parlikad and E. A. Cameron. Balancing scarce hospital resources during the COVID-19 pandemic using discrete-event simulation. *Health Care Manag. Sci.* **24** (2021) 356–374.
- [8] I. P. Lade, S. Choriwar and P. B. Sawaitul. Simulation of Queuing Analysis in Hospital. *Int. J. Mech. Eng. Robot. Res.* **2** (3) (2013) 122–128.
- [9] C. Kittipittayakorn, K. C. Ying. Using the integration of discrete event and agent-based simulation to enhance outpatient service quality in an orthopedic department. *J. Healthc. Eng.* **8** (2016) 1–9.
- [10] I. Ekeland. Agreeing on strategies. *Nature* **400** (1999) 623–624.



Sharing Keys Using Some Toeplitz Matrices and Logistic Maps

Benzeghli Brahim* and Adoui Salah

University of Batna 2, Batna, Algeria.

Received: February 12, 2024; Revised: June 21, 2024

Abstract: In symmetric cryptosystems, we use the same keys to encrypt and decrypt data, our question is how to share this common keys? Using the commutativity of the multiplication of circular matrices and sensibility to initial conditions in chaotic logistic maps through two different channels, we give some new techniques for creating and sharing two keys and use them to increase the level of security during the encryption and decryption of texts or digital images.

Keywords: *Toeplitz matrices; circular matrices; logistic maps; chaos; cryptography; BB84 protocol; Diffie-Hellman protocol.*

Mathematics Subject Classification (2010): 70K55, 37D45.

1 Introduction

The main goal of this work is the creation of two keys through two different channels. For the first key, based on the same techniques as in our previous work [1], we set a $t \in [-1, 1]$ and we create a circular matrix generated by the vector $(a(t), b(t), c(t))$ such that $a = t^2 + 1$, $b = t$ and $c = -t$. This choice is made so that the trace and the determinant of the generated circular matrix are strictly positive, which allows us to calculate the initial parameters of a logistic sequence as follows:

$$\mu = \frac{\det \mathcal{T}}{\det \mathcal{T} + 1} + 3 \quad \text{and} \quad x_0 = \frac{\text{tr} \mathcal{T}}{\text{tr} \mathcal{T} + 1}. \quad (1)$$

This choice checks the chaotic case because $\mu \in]3, 4[$ and $x_0 \in]0, 1[$. These two parameters will be shared through a quantum channel by the exchange protocol BB84.

* Corresponding author: <mailto:b.benzeghli@univ-batna2.dz>

So, the key K created will be the circular matrix generated by the vector $V(y_1, \dots, y_n)$, where

$$\forall i \in \mathbb{N}, \quad y_i = [10^{15}x_i] \pmod{p} \in (\mathbb{Z}/p\mathbb{Z})^*;$$

p is a prime number such that $\forall i \in \mathbb{N}, \quad p > y_i$ and x_i are the terms of the logistic sequence

$$\forall n \in \mathbb{N}, \quad x_{n+1} = \mu x_n(1 - x_n).$$

Then $K = \langle y_1, y_2, \dots, y_n \rangle$.

The creation of the second key will be done using the first key K and based on the commutativity of the multiplication of circular matrices.

These two keys K and C will be used for the encryption and decryption of digital images.

2 Toeplitz Matrices of Order 3

In 1911, *Otto Toeplitz* introduced the *Toeplitz matrices* after the study of the quadratic forms $\sum \varphi_{i,j}x_iy_j$, for which the coefficients of these forms verify the particular property $\varphi_{i,j} = \varphi_{i-j}$, and thus obtained associated matrices $\mathcal{T} = (\varphi_{i,j})_{i,j}$ on diagonal and on-diagonal and sub-diagonal constants that are now called the Toeplitz matrices [3,4]. More recently, the particular structure with diagonals and on-diagonals and/or sub-diagonals constants of the Toeplitz matrices appears in various problems as a result of the different methods of resolution used or by the methods of raising data at regular time interval or space which will make appear systems with diagonal matrices and on-constant diagonals and sub-constant diagonals.

Definition 2.1 We call the Toeplitz matrix, any matrix $\mathcal{T} \in \mathcal{M}_n(\mathbb{R})$ with diagonal and on-diagonal and sub-diagonal constants, that is to say, any matrix of the form

$$\mathcal{T} = \begin{bmatrix} t_0 & t_1 & \cdots & t_{-(n-1)} \\ t_1 & t_0 & \ddots & \vdots \\ \vdots & \ddots & \ddots & t_{-1} \\ t_{n-1} & \cdots & t_1 & t_0 \end{bmatrix}, \text{ where } t_i \in \mathbb{R} \text{ for all } i \in \{-(n-1), \dots, n-1\}.$$

We can distinguish two particular cases in the following remark.

Remark 2.1

1. If $t_{n-j} = t_{-j}$ for $j \in \{0, \dots, n\}$, the matrix \mathcal{T} is said to be a circular matrix.
2. If $t_{n-j} = -t_{-j}$ for $j \in \{0, \dots, n\}$, so we are talking about an anti-circular matrix.

The particular case of circular and anti-circular matrices is interesting in the context of diagonalization. Indeed, these matrices with a particular structure can be diagonalized using the *FFT (Fast Fourier Transform)* with a lower complexity than any matrix without a particular structure.

The shape of a circular matrix is given in the following definition.

Definition 2.2 A circular matrix is a Toeplitz matrix given by

$$\mathcal{C}_n = \mathcal{C}_n(c_1, \dots, c_n) = \begin{bmatrix} c_1 & c_2 & \cdots & c_n \\ c_n & c_1 & \ddots & \vdots \\ \vdots & \ddots & \ddots & c_2 \\ c_2 & \cdots & c_n & c_1 \end{bmatrix} \in \mathcal{M}_n(\mathbb{R}).$$

3 The Abelian Group of *Circular Matrices* of Order 3 with Some Conditions

The aim of this section is to create an abelian group of circular matrices of order 3 with matricial composition, we denote it by $\mathbf{C}_3(I)$, where $I \subset \mathbb{R}$ such that the elements of \mathbf{C}_3 are invertible, see [7, 9].

Definition 3.1 A square matrix C of order 3 is said to be circular if and only if it is generated by one vector $V(a, b, c)$. Such a matrix is of the form

$$C = \langle V \rangle = \langle a, b, c \rangle = \begin{pmatrix} a & b & c \\ c & a & b \\ b & c & a \end{pmatrix}. \quad (2)$$

We know that an abelian group must verify the commutativity, the associativity, the existence of a neutral element and the invertibility of all elements.

Theorem 3.1 (Commutativity in \mathbf{C}_3) For any $A, B \in \mathbf{C}_3$, we have $AB = BA$.

Proof. By definition, A and $B \in \mathbf{C}_3$ means that there exist $V(a, b, c)$ and $V'(a', b', c')$ such that

$$A = \begin{pmatrix} a & b & c \\ c & a & b \\ b & c & a \end{pmatrix} \quad \text{and} \quad B = \begin{pmatrix} a' & b' & c' \\ c' & a' & b' \\ b' & c' & a' \end{pmatrix}.$$

We have

$$\begin{aligned} AB &= \begin{pmatrix} a & b & c \\ c & a & b \\ b & c & a \end{pmatrix} \begin{pmatrix} a' & b' & c' \\ c' & a' & b' \\ b' & c' & a' \end{pmatrix} \\ &= \begin{pmatrix} aa' + bc' + cb' & ab' + ba' + cc' & ac' + bb' + ca' \\ ca' + ac' + bb' & cb' + aa' + bc' & cc' + ab' + ba' \\ ba' + cc' + ab' & bb' + ca' + ac' & bc' + cb' + aa' \end{pmatrix} \\ &\quad (\text{addition and multiplication are commutatives in } \mathbb{R}) \\ &= \begin{pmatrix} a'a + c'b + b'c & b'a + a'b + c'c & c'a + b'b + a'c \\ a'c + c'a + b'b & b'c + a'a + c'b & c'c + b'a + a'b \\ a'b + c'c + b'a & b'b + a'c + c'a & c'b + b'c + a'a \end{pmatrix} \\ &= \begin{pmatrix} a' & b' & c' \\ c' & a' & b' \\ b' & c' & a' \end{pmatrix} \begin{pmatrix} a & b & c \\ c & a & b \\ b & c & a \end{pmatrix} \\ &= BA. \end{aligned}$$

Theorem 3.2 (Associativity in \mathbf{C}_3) For any A, B and $C \in \mathbf{C}_3$ we have

$$A(BC) = (AB)C = ABC.$$

It is easy to verify the equality with a useful calculus.

Theorem 3.3 *The identity matrix I_3 is the neutral element in \mathbf{C}_3 for matrix multiplication.*

We know that the Toeplitz matrices are not always invertible, and to have the invertibility, we must impose some conditions on its terms.

For a matrix to be invertible, it is necessary and sufficient that its determinant is not null.

We choose the vector $V = (a, b, -b)$, where $a = t^2 + 1$ and $b = t$. The matrix becomes

$$\mathcal{T} = \begin{pmatrix} a & b & -b \\ -b & a & b \\ b & -b & a \end{pmatrix} = \begin{pmatrix} t^2 + 1 & t & -t \\ -t & t^2 + 1 & t \\ t & -t & t^2 + 1 \end{pmatrix}. \tag{3}$$

Then, the determinant of \mathcal{T} is

$$\begin{aligned} \det(\mathcal{T}) &= a^3 + b^3 + c^3 - 3abc \\ &= t^6 + 6t^4 + 6t^2 + 1. \end{aligned}$$

We can see that $\det(\mathcal{T})$ is a function of t .

Proposition 3.1 *The function*

$$\begin{aligned} f: \mathbb{R} &\rightarrow \mathbb{R} \\ t &\mapsto f(t) = \det(\mathcal{T}) = t^6 + 6t^4 + 6t^2 + 1 \end{aligned}$$

is strictly positive ($f > 0$).

Proof. By plotting the function f with *GeoGebra*, we get the following graph (Figure 1).

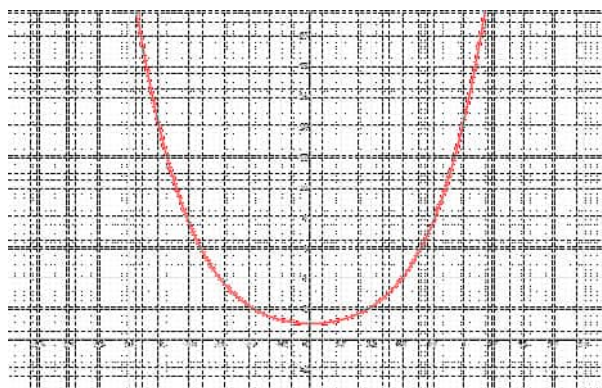


Figure 1: The graph of $f(t) = \det(\mathcal{T})$ on \mathbb{R} .

We observe that the curve of the function f is always on the x -axis, which shows that f is strictly positive.

Theorem 3.4 *The matrix \mathcal{T} in (3) is invertible and the inverse \mathcal{T}^{-1} is given by*

$$\mathcal{T}^{-1} = \frac{1}{t^6 + 6t^4 + 6t^2 + 1} \begin{pmatrix} t^4 + 3t^2 + 1 & -t^3 + t^2 - t & t^3 + t^2 + t \\ t^3 + t^2 + t & t^4 + 3t^2 + 1 & -t^3 + t^2 - t \\ -t^3 + t^2 - t & t^3 + t^2 + t & t^4 + 3t^2 + 1 \end{pmatrix}. \quad (4)$$

Proof. The existence of the inverse matrix is ensured by Proposition 3.1.

To calculate it, we use the formula $\mathcal{T}^{-1} = \frac{1}{\det \mathcal{T}} \text{Com}({}^t\mathcal{T})$, the desired result is obtained.

Theorem 3.5 *The set \mathbf{C}_3 menu by the law of matrix composition forms an abelian group.*

Proof. The demonstration is immediate according to Theorems 3.1, 3.2, 3.3 and 3.4.

4 Logistic Maps

In mathematics, a logistic map is a real simple sequence, but its recurrence is not linear, see [2, 10, 11].

Definition 4.1 A logistics map $(x_n)_{n \in \mathbb{N}}$ is a non-linear real sequence defined by its first term $x_0 \in [0, 1]$ and the following recurring formula:

$$\begin{aligned} x_n : \mathbb{N} &\rightarrow \mathbb{R} \\ n &\mapsto x_{n+1} = \mu x_n(1 - x_n), \quad \mu \in [0, 4]. \end{aligned} \quad (5)$$

Depending on the value of the parameter $\mu \in [0, 4]$, to ensure that the values of X remain in $[0, 1]$, it generates either a convergent sequence, a series subjected to oscillations, or a chaotic sequence.

4.1 The chaotic case ($\mu \in [3.57, 4]$)

We are interested in the chaotic case, where $\mu \in [3.57, 4]$.

Most values above 3.57 have a chaotic character, but there are some isolated values of μ with a behaviour that is not. For example, from $1 + \sqrt{8}$ (about 3.82), a small range of μ values has an oscillation between three values and for a slightly larger μ , between six values, then twelve, etc. Other ranges offer oscillations between 5 values, etc. All periods of oscillation are present, again independently of the initial population.

The horizontal axis bears the values of the parameter μ (noted r), while the vertical axis shows the possible adhesion values.

4.2 Sensitivity to the initial conditions

The most important property of the logistic maps is sensitivity to the initial conditions. This results in a radical change in the sequence behaviour as soon as there is a very small change in the initial value x_0 .

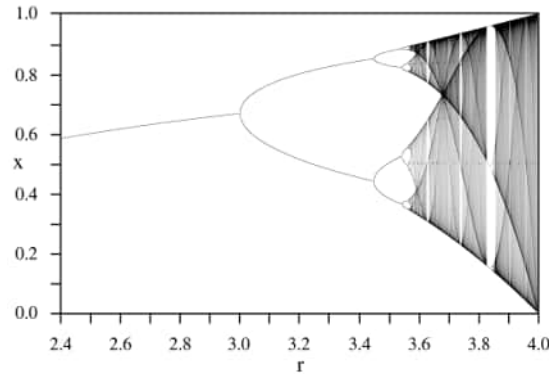


Figure 2: A bifurcation diagram of a logistic map.

5 Application in Cryptography

In general, cryptography is a writing technique where an encrypted message is written using secret codes or encryption keys. Cryptography is primarily used to protect a message considered confidential. This method is used in many areas such as the secret army, information technology, privacy, etc. There are many cryptographic algorithms that can be used to encrypt (and decrypt for the recipient) the message, see [8, 14].

Definition 5.1 [Cryptosystem] A cryptosystem is a term used in cryptography to refer to a set of cryptographic algorithms and all possible plain texts, encrypted texts and keys.

Definition 5.2 [Components of a cryptosystem] A basic cryptosystem consists of the following variants:

1. **Plain text:** This is the data (text or images) that we want to protect during transmission.
2. **Encryption Algorithm:** This is a mathematical process that produces encryption for all data in clear and key encryption. It is a cryptographic algorithm that takes the plain text and an encryption key as an input and produces an encrypted text.
3. **Encrypted text:** This is the scrambled version of the plain text produced by the encryption algorithm using a specific encryption key. The encrypted text is not protected. It circulates on a public channel. It can be intercepted or compromised by anyone with access to the communication channel.
4. **Decryption algorithm:** This is a mathematical process, which produces a single clear text for any given digit and decryption key. It is a cryptographic algorithm that takes a number and a decryption key as an entry, and produces a plain text. The decryption algorithm essentially reverses the encryption algorithm and is therefore closely related to it.

5. **Encryption key:** This is a value known to the sender. The sender enters the encryption key into the encryption algorithm with the plain text to calculate the encrypted text.
6. **Decryption key:** This is a known value of the receiver. The decryption key is linked to the encryption key, but it is not always identical. The receiver enters the decryption key into the decryption algorithm with encryption to calculate the plain text.

5.1 Asymmetric and symmetric cryptograpy

Definition 5.3 [Asymmetric cryptography] In the case of asymmetric encryption, each user has two keys:

- The private key, which must be kept secret;
- The public key, which is available to all other users.

These two keys are mathematically linked.

Definition 5.4 [Symmetric cryptography] It is about multiple people using the same key to encrypt and decrypt messages.

The main problem of this system is the exchange of a single key between different people. So we must ask the question: How can this unique key be shared, allowing each person to encrypt and decrypt safely?

5.2 Key exchange protocols

Definition 5.5 A key exchange protocol (or key negotiation, or key establishment, or key distribution) is a mechanism through which multiple participants agree on a cryptographic key.

The invention of public key cryptography in the 1970's produced the first key exchange protocol that can be demonstrated to be secure, even when communications are made over an unprotected channel, without the use of trusted third parties. One of the first protocols of this type, due to *Whitfield Diffie* and *Martin Hellman*, is now the most used on the *Internet*, see [5, 12].

5.3 Diffie and Hellman key exchange protocol

Diffie and Hellman proposed in 1976 a completely secure key exchange protocol. The problem was as follows.

Two persons want to exchange an encrypted message using an algorithm requiring a key K . They want to exchange this key, but they do not have a secure channel for it. Diffie and Hellman's key exchange protocol addresses this problem when K is an integer. The idea of Diffie and Hellman is based on modular arithmetic, and on the following postulate

Being given integers p , a and x with p prime and $0 < a < p$, in $(\mathbb{Z}/p\mathbb{Z})^*$, it is easy to calculate the integer $y = a^x \pmod{p}$. But, if we know $y = a^x \pmod{p}$, a and p , it is very difficult to find x since p is big enough. This problem is called the discrete logarithm problem on $(\mathbb{Z}/p\mathbb{Z})^*$.

5.4 Steps of the key exchange protocol

We resume five steps of the key exchange protocol in the following table.

	Salah	Brahim
Step 1	Salah and Brahim choose together a sufficiently large prime number p and an integer $1 \leq a \leq p - 1$. This exchange does not need to be secured.	
Step 2	Salah secretly chooses x_1	Brahim secretly chooses x_2
Step 3	Salah calculates $y_1 = a^{x_1} \text{ mod } (p)$	Brahim calculates $y_2 = a^{x_2} \text{ mod } (p)$
Step 4	Salah and Brahim exchange the values of y_1 and y_2 . This exchange does not need to be secured.	
Step 5	Salah calculates $y_2^{x_1} = (a^{x_2})^{x_1} \text{ mod } (p) = a^{x_1 x_2} \text{ mod } (p)$ and calls this number K , the secret key to shared with Brahim.	Brahim calculates $y_1^{x_2} = (a^{x_1})^{x_2} \text{ mod } (p) = a^{x_1 x_2} \text{ mod } (p)$ and calls this number K , the secret key to shared with Salah.

Figure 3: Steps of the key exchange protocol

5.5 Our contribution

In Subsection 5.3, we saw that in the *Diffie-Hellman key exchange protocol*, the integer a was public and our variables were integers that belong to the commutative group $(\mathbb{Z}/p\mathbb{Z})^*$.

According to the same techniques as in our last paper [1], we propose to work in the set of the circular matrices and more. The integer a will be replaced by a secrete matrix built with a safe exchange of parameters using a quantum protocol *BB84* and also using logistic maps.

Our new technique will be given through the following steps.

Two persons Salah and Brahim want to create a common secrete key.

Step 1: Creating the first common secrete key

- Using the famous exchange quantum protocol *BB84* through the quantum channel, Salah and Brahim share two parameters: $t \in [-1, 1]$ and $p \in \mathbb{N}$ (p prime), see [6,13].

1. Each one calculates

$$a = t^2 + 1, \quad b = t \quad \text{and} \quad c = -t. \tag{6}$$

2. Creates the circulate matrix \mathcal{T} of order 3 generated by the vector $V = (a, b, c)$. So,

$$\mathcal{T} = \begin{pmatrix} a & b & c \\ c & a & b \\ b & c & a \end{pmatrix}, \quad \text{with} \quad \forall t \in [-1, 1], \quad \det(\mathcal{T}) > 0. \tag{7}$$

- Using the famous logistic maps

$$x_{n+1} = \mu x_n(1 - x_n), \quad 3 < \mu < 4 \quad \text{and} \quad 0 < x_0 < 1. \tag{8}$$

Proposition 5.1 *We can choose*

$$\mu = \frac{\det(\mathcal{T})}{\det(\mathcal{T}) + 1} + 3 \quad \text{and} \quad x_0 = \frac{\text{tr}(\mathcal{T})}{\text{tr}(\mathcal{T}) + 1}.$$

Proof.

– From Section 3, we have $\det(\mathcal{T}) > 0$, so, $\det(\mathcal{T}) < \det(\mathcal{T}) + 1$, then

$$0 < \frac{\det(\mathcal{T})}{\det(\mathcal{T}) + 1} < 1.$$

by adding 3 to all terms of the inequality, we get

$$3 < \frac{\det(\mathcal{T})}{\det(\mathcal{T}) + 1} + 3 < 4,$$

so, the choice of μ is good.

– We have

$$\text{tr}(\mathcal{T}) = 3a = 3t^2 + 3 > 0,$$

then

$$0 < \frac{\text{tr}(\mathcal{T})}{\text{tr}(\mathcal{T}) + 1} < 1,$$

so, the choice of x_0 is good too.

The first key K created will be the circular matrix generated by the vector $V(y_1, \dots, y_n)$, where

$$\forall i \in \mathbb{N}, \quad y_i = [10^{15} x_i] \pmod{p} \in (\mathbb{Z}/p\mathbb{Z})^*;$$

p is a prime number such that $\forall i \in \mathbb{N}, \quad p > y_i$ and x_i are the terms of the logistic sequence

$$\forall n \in \mathbb{N}, \quad x_{n+1} = \mu x_n (1 - x_n).$$

Now Salah and Brahim can build the following circular matrix of order n using the terms of the previous logistic map.

We denote by K the first shared key

$$K = \langle y_1, y_2, \dots, y_n \rangle = \begin{pmatrix} y_1 & y_2 & \cdots & y_n \\ y_n & y_1 & \cdots & y_{n-1} \\ \vdots & \vdots & \ddots & \vdots \\ y_2 & y_3 & \cdots & y_1 \end{pmatrix}.$$

Step 2: Creating the second common secrete key

We take the first shared key K created in the first step, then

- Salah chooses twice private circular matrices (M_1, M_2) , calculates and sends to Brahim the cipher

$$K_A = M_1 K M_2.$$

- Likewise, Brahim chooses twice private circular matrices (M_3, M_4) , calculates and sends to Salah the cipher

$$K_B = M_3KM_4.$$

- Salah receives K_B and calculates

$$C_A = M_1K_BM_2.$$

- Also, Brahim receives K_A and calculates

$$C_B = M_3K_AM_4.$$

Proposition 5.2 *We have*

$$C_A = C_B := C \quad \text{Same key shared.}$$

Proof. By construction, we have

$$\begin{aligned} C_A &= M_1K_BM_2 \\ &= M_1M_3KM_4M_2 \quad , \text{ because } K_B = M_3KM_4 \\ &= M_3M_1KM_2M_4 \quad , \text{ by commutativity} \\ &= M_3K_AM_4 \quad , \text{ because } K_A = M_1KM_2 \\ &= C_B. \end{aligned}$$

So, we have managed to build a matrix C which will be the secret common key between two interlocutors. It will also be used to encrypt and decrypt a text or image.

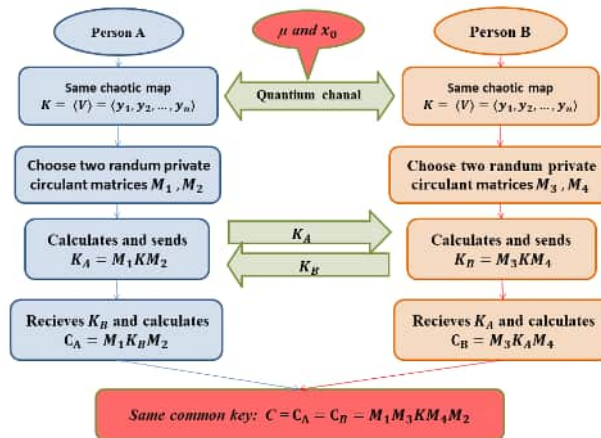


Figure 4: Diagram explaining the mechanism of creating a common key C .

In the following table (see Table 1), we show the time required to run the key K , using *Matlab R 2018a (9.4.0.813654) 64-bit (Win64) on PC Intel(R) Core(TM) i5-6400 CPU @ 2.70GHz 2.71 GHz RAM 12Go*.

For $\mu = 3.61$ and $x_0 = 0.73$, we get the following results.

Size of the key K	64×64	128×128	256×256	512×512	1024×1024
Time required (second)	0.000042	0.000147	0.000697	0.003108	0.024277

Table 1: Execution time of the proposed method to generate the key K .

In the following table (see Table 2), we show the time required to run the key C , using *Matlab R 2018a (9.4.0.813654) 64-bit (Win64) on PC Intel(R) Core(TM) i5-6400 CPU @ 2.70GHz 2.71 GHz RAM 12Go*.

For this, we use three logistic maps with the parameters $(\mu = 3.61, x_0 = 0.73)$, $(\mu' = 3.65, X'_0 = 0.77)$ and $(\mu'' = 3.67, X''_0 = 0.82)$, we get the following results.

Size of the key C	64×64	128×128	256×256	512×512	1024×1024
Time required (second)	0.000286	0.001477	0.005092	0.031820	0.186870

Table 2: Execution time of the proposed method to generate the key C .

6 Encryption and Decryption of Some Digital Images Using Our Method

In this paragraph, we test our method on some images of different sizes, using the key created in Section 5.1, see [1, 8, 14].

Salah wants to send Brahim an image m of size $n \times n$. To encrypt and decrypt this image, they must proceed as follows.

- Salah converts the image m to a matrix M of the same size as m .
- **Image Encryption:**

Salah encrypts the image M to the matrix H as follows:

$$CMK = H,$$

where K and C are the common keys created in the previous Section 5.1 (K , C and H have the same size). Then he sends H to Brahim.

- **Image Decryption:**

Brahim receives H and deciphers it as follows:

$$C^{-1}HK^{-1} = M$$

because

$$C^{-1}HK^{-1} = C^{-1}CMKK^{-1} = M.$$

- Brahim converts the matrix M into an image, it gets the initial image.

To study the effectiveness of our image encryption, we analyse its security. The proposed method should withstand several types of attacks, as it is symmetrical, the keys that would be used during encryption and decryption must be transmitted through the secured and other unsecured channels. For the implementation of the proposed scheme, we choose $n \in \{64, 128, 256, 512, 1024\}$.

7 Performance and Safety Analysis

7.1 The key space

The secret key K is probabilistic because the transmitter and receiver use any circular matrices (C_1 and C_2) to obtain a common key K .

If we use the proposed key generation method with ($n = 256$), $x_i \in \{0, \dots, 255\}$, this provides 256^{256} possible keys (the elements used are not null) for the C_1 key, we have 256^{256} possible keys for the key C_2 , as well as we have 15^{60} possible keys to get the key K (with fifteen decimal digits after the comma), the one-dimensional logistic map used has interesting properties such as periodicity and significant dependence on initial values, but it has low security, to overcome the inconvenience of its small key space, we must use several logistic maps to generate the K key in the first phase. The proposed schema key space size is greater than $256^{256} \times 256^{256} \times 15^{60}$ and the key space is large enough for a brute force attack or comprehensive attack is not possible.

7.2 Statistical analysis

The proposed image encryption scheme is examined using different statistical measures. These measures involve histogram, information entropy analysis and correlation analysis.

Each of these measures is described in detail in the subsections.

We use five test images: Pict6464.jpg, Pict128128.jpg, Pict256256.jpg, Pict512512.jpg and Pict10241024.jpg.

Histogram

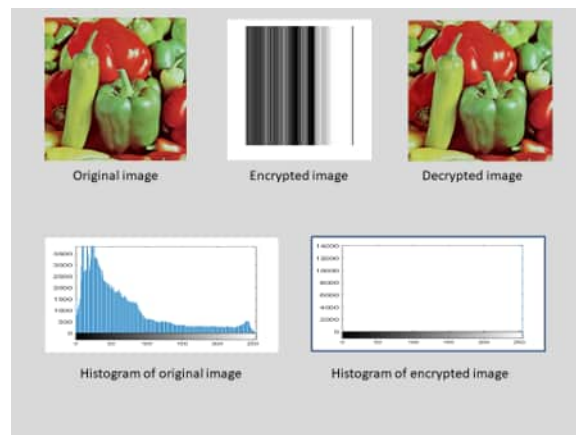


Figure 5: Encrypted and decrypted Pict256256.jpg images and their histograms.

In image processing, the histogram of an image normally represents a histogram of the pixel intensity values. This is a graph showing the pixel variety in an image at each other intensity value in that image.

For an 8-bit gray-scale image, there are 256 different possible extremes, so the histogram will graphically display 256 numbers showing the distribution of pixels among these gray-scale values.

The histogram of the encryption system image must be uniform as it shows in our encryption diagram in Figure 5. The histogram of our encrypted images is almost uniform and significantly different from the histogram of simple images that makes statistical attacks difficult.

Information Entropy Analysis

Entropy is one of the best functions for calculating and measuring the random character of the encrypted image. Ideally, the information entropy should be $8 - bits$ for gray-scale images. If an encryption generates an output digit image with lower entropy at $8 - bits$, then there would be a possibility of predictability, which could threaten its security. The entropy of the information is calculated using the previous equation.

Simulation results for entropy analysis for the images used are presented in the table.






Encrypted image	Size	(μ, x_0)	(μ', x'_0)	(μ'', x''_0)	Entropy
	64×64	$(3.61, 0.73)$	$(3.65, 0.77)$	$(3.67, 0.82)$	7.2955
	128×128	$(3.61, 0.73)$	$(3.65, 0.77)$	$(3.67, 0.82)$	7.7326
	200×200	$(3.61, 0.73)$	$(3.65, 0.77)$	$(3.67, 0.82)$	7.8159
	256×256	$(3.61, 0.73)$	$(3.65, 0.77)$	$(3.67, 0.82)$	7.7050
	300×300	$(3.61, 0.73)$	$(3.65, 0.77)$	$(3.67, 0.82)$	7.2768

Table 3: Entropy results for some encrypted images.

Correlation analysis of two adjacent pixels

Correlation determines the connection between two variables. In other terms, correlation is a measure that determines the level of similarity between two variables. The correlation coefficient is a useful evaluation to judge the encryption quality of any cryptosystem. Any image cryptosystem is said to be good if the encryption method hides all attributes and features of a plain text image, and the encrypted image is totally random and extremely uncorrelated.

For a regular image, each pixel is highly associated with its nearby pixels. An ideal encryption technique should generate the cipher images with no such correlation in the adjacent pixels. We have examined the correlation of two adjacent pixels in the original image and encrypted image in several images like Pict6464.jpg, Pict128128.jpg, Pict256256.jpg, Pict512512.jpg and Pict10241024.jpg. We find their correlation very close to 1, we mean there is a perfect match between the original and decrypted images.

8 Concluding Remarks

This paper deals with clear image encryption and decryption techniques. A new technique has been proposed using logistic maps.

We merged between the creation of circulant matrices of order n generated by a vector in the components being the first n elements of a logistic map taken in order from a given rank.

Two parameters in (1) of our logistic map will be generated also by a circulant matrix of order 3 whose components are parametric curves of order 3 chosen in a way that insures the invertibility, so the existence of a non-zero determinant that insures that μ and x_0 in (1) satisfy $\mu \in]3, 4[$ and $x_0 \in]0, 1[$ for any $t \in]-1, 1[$.

These choices assure us that the chaotic case of our system mentioned earlier is very sensitive to changes in the initial value x_0 or the parameter μ that, in our work, change mutually for each $t \in]-1, 1[$ without losing stability.

References

- [1] S. Adoui, B. Benzeghli and L. Noui. Sharing Keys Using Circular Matrices and Logistic Maps Through Quantum Channel. *Advances in Mathematics: Scientific Journal CCS '12* (2022) 1361–1378.
- [2] M. Ausloos. *The Logistic Map and the Route to Chaos: From the Beginnings to Modern Applications*. Springer, 2006.
- [3] B. Silbermann, A. Böttcher, I. Gohberg and P. Junghanns. *Toeplitz Matrices and Singular Integral Equations: The Bernd Silbermann Anniversary Volume*. Birkhäuser Basel, 2012.
- [4] A. Böttcher and B. Silbermann. *Introduction to Large Truncated Toeplitz Matrices*. Springer, New York, 2012.
- [5] C. Boyd and A. Mathuria. *Protocols for Authentication and Key Establishment*. Allemagne: Springer, Berlin, Heidelberg, 2013.
- [6] C. Kollmitzer and M. Pivk. *Applied Quantum Cryptography*. Springer, 2010.
- [7] P. J. Davis. *Circulant Matrices*. Wiley, 1979.
- [8] H. Delfs and H. Knebl. *Introduction to Cryptography: Principles and Applications*. Allemagne: Springer, Berlin, Heidelberg, 2012.
- [9] R. M. Gray. *Toeplitz and Circulant Matrices: A Review*. Pays-Bas: Now Publishers, 2006.
- [10] K. D. R. Dewi, K. Fahim and S. Subchan. Application of Model Predictive Control (MPC) to Longitudinal Motion of the Aircraft Using Polynomial Chaos. *Nonlinear Dynamics and Systems Theory* **23** (5) (2023) 487–498.
- [11] K. M. Hosny. *Multimedia Security Using Chaotic Maps: Principles and Methodologies*. Studies in Computational Intelligence, **884**. Springer International Publishing, 2020.
- [12] A. Mahalanobis. *Diffie-Hellman Key Exchange Protocol, Its Generalization and Nilpotent Groups*. (n.p.): Florida Atlantic University, 2005.
- [13] D. F. Urrego González. *Implementation of the protocol BB84 for encryption of a message*. Colombie: Uniandes, 2014.
- [14] M. Veni. *Encryption and Watermarking for Digital Images*. Japon: Mohd Abdul Sattar, 2023.
- [15] W. S. Mada Sanjaya, A. Roziqin, A. W. Temiesela, M. Fauzi Badru Zaman, A. D. Wibik-sana and D. Anggraeni. *Moore-Spiegel Chaotic Encryption for Digital Images and Voices*. *Nonlinear Dynamics and Systems Theory*. **23** (5) (2023) 445–460.



Analysis and Existence of Rumor Spreading with Campaign and Punishment Control

Irma Fitria¹, Subchan Subchan^{2*}, Dinda Anisa Maulina² and
Alvian Alif Hidayatullah²

¹ *Study Program of Statistics, Department of Mathematics and Information Technology,
Institut Teknologi Kalimantan, Balikpapan, Indonesia.*

² *Department of Mathematics, Faculty of Science and Data Analytics, Institut Teknologi
Sepuluh Nopember.*

Received: November 29, 2023; Revised: June 9, 2024

Abstract: Rumors are pieces of unverified information that are spread from individual to individual. The spread of rumors that are not controlled can impact human life in many ways, one of which is that people start to worry about information that is not necessarily true. As such, efforts have been made to curb the spread of gossip through campaigns and punishment to reduce the number of gossip spreaders. This paper proposes the analysis and existence of a rumor-spreading model with campaigns and punishment control. The positivity, uniqueness, and existence of optimal control in the problem are analyzed and proven. In this paper, positivity and uniqueness are employed to validate the control and the unique solution of the rumor spreading model. Furthermore, based on the positivity and uniqueness of the rumor spreading model with control, the existence of optimal control in the model can be solved.

Keywords: *rumors; optimal control; positivity; uniqueness.*

Mathematics Subject Classification (2010): 49Jxx, 49Kxx, 49Lxx, 93Cxx.

* Corresponding author: <mailto:subchan@matematika.its.ad.id>

1 Introduction

The rapid development of technology has made things easily accessible to many people. Nowadays, humans do everything digitally, one example is obtaining or disseminating information through social media platforms such as Twitter and Instagram. Based on the Katadata Insight Center (KIC) survey, 76% of Indonesians get information from social media [1]. The information obtained or disseminated through this medium can be in the form of rumors. Rumors are still being confirmed and can negatively impact if the information is false [2]. According to the results of a digital literacy survey conducted by the Katadata Insight Center (KIC), this ease of dissemination of information has a huge impact on the community. In the survey, almost 60 % of Indonesians obtained information through rumors or hoaxes when accessing social media [3]. The spread of rumors that are out of control can have an impact on human life, one of which is that people are starting to worry about information that is not necessarily true. Special handling is certainly needed to control the spread of rumors. For example, punishment can be imposed on those who spread rumors, or some kind of campaign can be carried out among people who are vulnerable to information. Handling this kind of problem is very important because rumors can damage people's trust in social media and are difficult to control because they spread quickly.

The concept of optimization can assist in decision-making on achieving a goal and one of the alternatives in determining the optimal control of a problem [4–8]. Modeling of the spread of rumors has been studied by several researchers, such as Daley and Kendall [9], discussing the model of spreading rumors which has similarities with the construction of epidemic models of disease spread. The compartments used are Susceptible (a population that does not yet know rumors), Infected (a population that spreads rumors), and Recovered (a population that does not spread rumors anymore). This model does not consider the time it takes for a rumor to be received or even spread. Mathematical modeling of rumor spread has been further developed by several people such as Dahl et al. [10] in 2016. Efforts to control the spread of rumors entail the addition of control variables to the rumor-spreading model formed. As such, the value of the control variable is immediately given. In 2023, the model introduced by Dhar et al. [10] was used by Jain et al. [11] for control by adding the assumption that there is a delay for thinkers to spread the news. In the research, the implementation of delay for thinkers to spread the news has primary challenge in the attempt to control the spread of rumors. The model constructed by Jain is certainly valid. It has been shown in the model that the constructed model satisfies the positively invariant set property so that the model has a positive, bounded, and unique solution.

Time delays may be a useful tool in controlling the spread of rumor, but the truth is that people's confidence in the information they get is still very strong. This highlights the complexity of human behavior within digital networks and the desire for a more comprehensive strategy to manage the spread of rumors in our rapidly changing digital era. Therefore, based on the description above and several previous studies on the rumor spread mode, in this paper, a model for spreading rumors is constructed with control in the form of campaign and punishment. The campaign is carried out in an effort to impart knowledge to individual who obtains the rumor, and who is exposed, about the importance of information validation and the dangers of rumor propagation. This control mechanism aims to reduce the number of individuals exposed to rumors, and who subsequently spread them, thereby decreasing the count of infected individuals.

However, punishment control is carried out to provide a deterrent effect on individuals who spread rumors so that the individual will not spread rumors or can be said to be cured. Throughout this paper, we propose and construct a nonlinear dynamic model for rumor spreading, expanding on the previous models by Jain et al. [11]. In this paper, the positivity, uniqueness, and existence of optimal control over the problem are analyzed and proven. Positivity and uniqueness are employed to validate the control and unique solution of the rumor spreading model. Furthermore, based on the positivity and uniqueness of the rumor spreading model with control, the existence of optimal control in the model can be solved.

2 Mathematical Model

Rumors are pieces of unverified information passed from individual to individual. Information spreads on social networks quickly due to their increasing popularity. Individuals disseminate information in seconds without verifying its validity. Therefore, the spread of rumors among social media users can cause unnecessary panic [12]. Before modern communication gadgets such as smartphones existed, rumors were spread by word of mouth, so the spread of information was limited by the length of time it required. Therefore, with the development of technology today, rumors can spread faster than before [13].

Rumor-spreading problems can be formulated as a mathematical model. For example, Jain et al. [11] have described the optimal control of rumor spreading model on homogeneous social network with the consideration of influence of delay on thinkers [11] and Liu et al. [14] have described and analyzed a model of spreading rumors on heterogeneous network. In addition, Liu et al. [15] describe the rumor spreading model in complex social networks with hesitating mechanism. In this paper, the entire population is grouped into four compartments: Susceptible (S), individuals who are not aware of rumors but are vulnerable to knowing rumors; Exposed (E), individuals who know about rumors and have the possibility to spread them; Infected (I), individuals who spread rumors; and Recovered (R), individuals who have stopped spreading rumors. N denotes the total individual population and satisfies $N(t) = S(t) + E(t) + I(t) + R(t)$. The relationship between populations in the rumor-spreading model can be expressed in the following mathematical model:

$$\begin{aligned}\frac{dS}{dt} &= \theta N - \alpha\beta SI - \mu S, \\ \frac{dE}{dt} &= \alpha\beta SI - \sigma E + \gamma m I - \mu E, \\ \frac{dI}{dt} &= \sigma h E - \gamma I - \mu I, \\ \frac{dR}{dt} &= \sigma(1-h)E + \gamma(1-m)I - \mu R\end{aligned}\tag{1}$$

with

θ : Susceptible individual growth rate,

μ : Natural death rate,

α : The rate of change from *Susceptible* individuals to *Exposed* individuals,

β : The rate of interaction between *Susceptible* individuals and *Infected* individuals,

σ : The rate of individuals leaving the exposed class (*Exposed*),

γ : The rate of individuals leaving the class of Infected (*Infected*),

m : Proportion of Infected individuals to Exposed individuals,

h : Proportion of Exposed individuals to Infected individuals,

and the initial conditions

$$S(0) = S_0, \quad E(0) = E_0, \quad I(0) = I_0, \quad R(0) = R_0.$$

The spread of rumors is getting more and more worrying day by day. There is a lot of fake news or information that is conveyed interestingly and continuously, causing many people to believe it. A rumor is a public communication obtained from a person’s hypothesis about an incident with accusations based on non-existent evidence. Rumors from reliable sources tend to be believed by many people [16]. Therefore, action must be taken to reduce the spread of these rumors. This paper proposes two controllers: a campaign for individuals who knew there were rumors and punishment for those who spread rumors. We assume that everyone concerned shares a very high level of confidence in the information they are given. From the assumption, the campaign is carried out in an effort to impart knowledge to individual who obtains the rumor, and is exposed, about the importance of information validation and the dangers of rumor propagation. This control mechanism aims to reduce the number of individuals exposed to rumors and who subsequently spread them, thereby decreasing the count of infected individuals. However, punishment control is carried out to provide a deterrent effect on individuals who spread rumors so that the individual will not spread rumors or can be said to be cured.

The mathematical model of controlled spread of rumors can be expressed as follows:

$$\begin{aligned} \frac{dS}{dt} &= \theta N - \alpha\beta SI - \mu S, \\ \frac{dE}{dt} &= \alpha\beta SI - \sigma E + \gamma m I - \mu E - u_1 E, \\ \frac{dI}{dt} &= \sigma h E - \gamma I - \mu I - u_2 I, \\ \frac{dR}{dt} &= \sigma(1-h)E + \gamma(1-m)I - \mu R + u_1 E + u_2 I, \end{aligned} \tag{2}$$

with u_1 and u_2 representing an effort to prevent the spread of rumors through a campaign to individuals who know there are rumors and efforts to impose sanctions on individuals who spread rumors, respectively. The objective function can be defined as follows:

$$J(u_1, u_2) = \min \int_{t_0}^{t_f} \left[a_1 I + \frac{1}{2} (b_1 u_1^2(t) + b_2 u_2^2(t)) \right] dt. \tag{3}$$

3 Positivity and Uniqueness

A model must be valid with existing conditions. This means that in this case, the solution given must be positive. This indicates that the population of each individual in model (2) always exists. Thus, if the initial population of S, E, I and R is positive, then the population at time t must also have a positive value.

We introduce the concept of a positive invariant set to solve the problem. This set is based on the initial solution and the solution of the system. More details can be given as in the following definition.

Definition 3.1 (Positively invariant set). Given $\dot{\mathbf{x}} = \mathbf{f}(t, \mathbf{x})$ is a dynamic system, with the initial conditions $\mathbf{x}_0 = \mathbf{x}(t_0)$. Given Ω is a subset of \mathbb{R}^n . Then Ω is said to be a positive invariant set if for $\mathbf{x}_0 \in \Omega$, it implies $\mathbf{x}(t, x_0) \in \Omega$ for every $t \geq t_0$.

Now, for $N(t) = S(t) + E(t) + I(t) + R(t)$, we suppose $\mathbf{x}(t) = (S(t), E(t), I(t), R(t))$, and the initial condition $\mathbf{x}(t_0) = (S(t_0), E(t_0), I(t_0), R(t_0))$, define $\omega = \max\{1, e^{(\theta-\mu)t_f}\}$ and set

$$\Omega_{\mathbf{x}(t_0)} := \{\mathbf{x}(t) \mid t_0 \leq t \leq t_f, \mathbf{x}(t) \geq \mathbf{0}, N(t) \leq N(0) \cdot \omega\}. \quad (4)$$

The fact that (4) is a positive invariant set can be proven in the following theorem.

Theorem 3.1 Let $\omega = \max\{1, e^{(\theta-\mu)t_f}\}$ and

$$\Omega_{\mathbf{x}(t_0)} := \{\mathbf{x}(t) \mid t_0 \leq t \leq t_f, \mathbf{x}(t) \geq \mathbf{0}, N(t) \leq N(0) \cdot \omega\}$$

be the subset all solutions of model (2) with the initial condition $\mathbf{x}(t_0)$. Then $\Omega_{\mathbf{x}(t_0)}$ is a positively invariant set.

Proof. We can divide the proof into several cases as follows.

1. First, we prove that the total population N is bounded. Based on the dynamic equation (2), note that

$$\begin{aligned} \frac{dS}{dt} + \frac{dE}{dt} + \frac{dI}{dt} + \frac{dR}{dt} &= \theta N - \mu(S + E + I + R), \\ (\Rightarrow) \quad \frac{dN}{dt} &= \theta N - \mu N, \\ (\Rightarrow) \quad \frac{dN}{dt} &= (\theta - \mu)N, \end{aligned}$$

with the solution $N(t) = N(0)e^{(\theta-\mu)t}$. From this, it is clear that if $\theta - \mu \leq 0$, then $0 < N(t) \leq N(0)$ and if $0 < \theta - \mu$, then $0 < N(t) \leq N(0)e^{(\theta-\mu)t_f}$. Then it follows that $N(t) \leq N(0) \cdot \omega$ for every time $0 \leq t \leq t_f$. Thus, this proves that the total population N is bounded at all times.

2. We know that N is positive and bounded for every time t . Then we can use it to prove S is positive. From the dynamic equation (2), we assume that there is $t \in (0, t_f]$ and $S(t) \leq 0$. Suppose $S_* = \{t \in (0, t_f] \mid S(t) \leq 0\}$ and take $t^* = \inf S_*$. It is clear that $t^* \neq 0$ so $S(t) > 0, \forall t \in [0, t^*)$. Then we know that I is a continuous function on $[0, t_f]$, so there is $M \in \mathbb{R}$ and $I(t) < M$ for every $t \in [0, t_f]$. As a result,

$$\begin{aligned} \frac{dS}{dt} &= \theta N - \alpha\beta SI - \mu S, \\ (\Rightarrow) \quad \frac{dS}{dt} &> -\alpha\beta MS - \mu S, \quad \forall t \in [0, t_f]. \end{aligned}$$

We can solve the above inequality and obtain that

$$S(t^*) > S(0) e^{-(\alpha\beta M + \mu)t^*}. \quad (5)$$

From equation (5), we obtain that $S(t^*) > S(0) e^{-(\alpha\beta M + \mu)t^*} > 0$. However, this contradicts the statement $S(t^*) \leq 0$, so from this, it follows that $S(t) > 0$ for every time $t \in [0, t_f]$.

3. By evaluating equation (2), we assume that there is $t \in (0, t_f]$ and $E(t) \leq 0$ or $I(t) \leq 0$. First, assume that $E(t) \leq 0$. Suppose $E_* = \{t \in (0, t_f] \mid E(t) \leq 0\}$ and take $t^* = \inf E_*$. It can be easily seen that $t^* \neq 0$, so $E(t) > 0, \forall t \in [0, t^*)$ and

$$\begin{aligned} \frac{dI}{dt} &= \sigma hE - \gamma I - \mu I - u_2 I, \\ (\Rightarrow) \quad \frac{dI}{dt} &> -\gamma I - \mu I - u_2 I, \quad \forall t \in [0, t_f), \\ (\Rightarrow) \quad \frac{dI}{dt} + \gamma I + \mu I + u_2 I &> 0. \end{aligned}$$

Assuming that there is $t \in (0, t^*)$ and $I(t) \leq 0$, suppose $I_* = \{t \in (0, t^*) \mid I(t) \leq 0\}$ and take $t_I^* = \inf I_*$. It can be easily seen that $t_I^* \neq 0$, so $I(t) > 0, \forall t \in [0, t_I^*)$ and

$$\frac{dI}{dt} + \gamma I + \mu I + I \geq \frac{dI}{dt} + \gamma I + \mu I + u_2 I > 0, \quad \forall t \in [0, t_I^*).$$

By solving the above inequality, it is obtained that

$$I(t_I^*) > I(0) e^{-(\gamma+\mu+1)t_I^*}.$$

From this, we obtain that $I(t_I^*) > I(0) e^{-(\gamma+\mu+1)t_I^*} > 0$. However, this contradicts the statement $I(t_I^*) \leq 0$, and we obtain that $I(t) > 0$ for every time $t \in [0, t^*)$. From this, we obtain

$$\begin{aligned} \frac{dE}{dt} &= \alpha\beta SI - \sigma E + \gamma mI - \mu E - u_1 E, \\ (\Rightarrow) \quad \frac{dE}{dt} &> -\sigma E - \mu E - u_1 E, \quad \forall t \in [0, t^*), \\ (\Rightarrow) \quad \frac{dE}{dt} + \sigma E + \mu E + u_1 E &> 0, \\ (\Rightarrow) \quad \frac{dE}{dt} + \sigma E + \mu E + E &> \frac{dE}{dt} + \sigma + \mu + u_1 E > 0. \end{aligned}$$

Furthermore, by solving the above problems, it is obtained that

$$E(t^*) > E(0) e^{-(\sigma+\mu+1)t^*}$$

and $E(t^*) > E(0) e^{-(\sigma+\mu+1)t^*} > 0$. However, this contradicts the statement $E(t^*) \leq 0$, and we obtain $E(t) > 0$ for every time $t \in [0, t_f]$. Furthermore, in the same way, for the assumption that there is t such that $I(t) \leq 0$, the assumption given is also wrong. So it follows that $I(t) > 0$ for every time $t \in [0, t_f]$.

4. From the dynamic model system (2), we assume that there is $t \in (0, t_f]$ and $R(t) \leq 0$. Suppose $R_* = \{t \in (0, t_f] \mid R(t) \leq 0\}$ and we take $t^* = \inf R_*$. It can be easily seen that $t^* \neq 0$, so $R(t) > 0, \forall t \in [0, t^*)$ and

$$\begin{aligned} \frac{dR}{dt} &= \sigma(1-h)E + \gamma(1-m)I - \mu R + u_1 E + u_2 I, \\ (\Rightarrow) \quad \frac{dR}{dt} &> -\mu R, \quad \forall t \in [0, t^*), \\ (\Rightarrow) \quad \frac{dR}{dt} + \mu R &> 0. \end{aligned}$$

From this, we obtain that $R(t^*) > R(0) e^{-\mu t^*} > 0$. However, this contradicts the statement $R(t^*) \leq 0$, so it follows that $R(t) > 0$ for every time $t \in [0, t_f]$.

From the above proof, we obtain that M is a *positively invariant set*; as such, the dynamic model system (2) is valid. We have proven that the set defined in (4) is a positively invariant set. This results in the fact that if the initial conditions in the rumor spreading model (2) with control are positive, then the solution of the model is positive for each time interval. However, this model does not guarantee that a single solution is given for an initial condition; so, we have to show whether the rumor spread model (2) with control has a single solution or not.

Now, to guarantee that the model (2) is existent and unique, we can use the concept of the Lipschitz condition in model (2) [17]. For that, we prove that model (2) satisfies the Lipschitz condition as given in the following theorem.

Theorem 3.2 *The rumor-spreading model with control (2) that satisfies a given initial condition $S(t_0), E(t_0), I(t_0), R(t_0) > 0$ has a unique solution.*

Proof. Let $X = (S, E, I, R)$ and

$$\varphi(X) = \begin{bmatrix} \frac{dS}{dt} \\ \frac{dE}{dt} \\ \frac{dI}{dt} \\ \frac{dR}{dt} \end{bmatrix}.$$

We can write the rumor-spreading model with control (2) as

$$\varphi(X) = \begin{bmatrix} \theta N - \alpha\beta SI - \mu S \\ \alpha\beta SI - \sigma E + \gamma m I - \mu E - u_1 E \\ \sigma h E - \gamma I - \mu I - u_2 I \\ \sigma(1-h)E + \gamma(1-m)I - \mu R + u_1 E + u_2 I \end{bmatrix}$$

and we show that $\varphi(X)$ has a unique solution with the initial condition $(S(0), E(0), I(0), R(0)) > 0$. Note that

$$\varphi(X_1) - \varphi(X_2) = \begin{bmatrix} \theta(N_1 - N_2) - \alpha\beta(S_1 I_1 - S_2 I_2) - \mu(S_1 - S_2) \\ \alpha\beta(S_1 I_1 - S_2 I_2) - \sigma(E_1 - E_2) + \gamma m(I_1 - I_2) - \mu(E_1 - E_2) - u_1(E_1 - E_2) \\ \sigma h(E_1 - E_2) - \gamma(I_1 - I_2) - \mu(I_1 - I_2) - u_2(I_1 - I_2) \\ (\sigma(1-h) + u_1)(E_1 - E_2) + (\gamma(1-m) + u_2)(I_1 - I_2) - \mu(R_1 - R_2) \end{bmatrix}. \quad (6)$$

We know that S and I represent the positive continuous function at $[0, t_f]$ so that S and I are the bounded functions at $[0, t_f]$. Since N is bounded for every initial condition $(S(0), E(0), I(0), R(0))$, there exist M and K such that

$$-M(S_1(t) - S_2(t)) \leq -\alpha\beta(S_1(t) I_1(t) - S_2(t) I_2(t)) \leq M(S_1(t) - S_2(t))$$

and

$$-K(I_1(t) - I_2(t)) \leq \alpha\beta(S_1(t) I_1(t) - S_2(t) I_2(t)) \leq K(I_1(t) - I_2(t))$$

for every solution X_1 and X_2 with the initial condition being $X_1(0)$ and $X_2(0)$. Then, from (6), we have

$$-A(X_1 - X_2) \leq \varphi(X_1) - \varphi(X_2) \leq A(X_1 - X_2)$$

with

$$A = \begin{bmatrix} \theta + M - \mu & \theta & \theta & 0 \\ 0 & -\sigma - \mu - u_1 & K + \gamma m & 0 \\ 0 & \sigma h & -\gamma - \mu - u_2 & 0 \\ 0 & -h + u_1 & \sigma + \gamma - m + u_2 & -\mu \end{bmatrix}.$$

We easily show that

$$\|\varphi(X_1) - \varphi(X_2)\|_2 \leq \|A(X_1 - X_2)\|_2 \leq \|A\| \|X_1 - X_2\|_2$$

with $\|X\|_2$ being the Euclidean norm in \mathbb{R}^4 and $\|A\| = \sqrt{\text{tr}(A^T A)}$; so, we obtain that the function $\varphi(X)$ is uniformly Lipschitz continuous. From this,

$$X(t) = X(t_0) + \int_{t_0}^t \varphi(X) dt$$

so that X has a unique solution for the initial condition $S(t_0), E(t_0), I(t_0), R(t_0) > 0$.

4 The Existence of Optimal Control

We have shown in Section 3 that the rumor-spreading model with controls (2) has a single and positive solution. From this, we will then determine whether or not the rumor-spreading model with controls (2) has optimal control. Using a result by Fleming and Rishel [18], we can prove the existence of the optimal control checking the following points:

1. The set U defined as

$$U = \{(u_1, u_2) \mid 0 \leq u_1(t), u_2(t) \leq 1, \forall t \in [0, t_f]\}$$

is a nonempty set.

This can be seen from Theorem (3.1) and Theorem (3.2), where every control $u \in U$ has a unique and positive solution and is not an empty set.

2. The set U , which is defined as

$$U = \{(u_1, u_2) \mid 0 \leq u_1(t), u_2(t) \leq 1, \forall t \in [0, t_f]\},$$

is a closed convex set.

To show that U is a closed convex set, let $v_1 = (u_{11}, u_{21}), v_2 = (u_{12}, u_{22}) \in U$. It can be easily seen that $0 \leq u_{11}(t), u_{21}(t), u_{12}(t), u_{22}(t) \leq 1$ for $t \in [0, t_f]$; so, with every $\lambda \in [0, 1]$, we obtain

$$0 \leq \lambda u_{11}(t) + (1 - \lambda) u_{21}(t) \leq 1$$

and

$$0 \leq \lambda u_{12}(t) + (1 - \lambda) u_{22}(t) \leq 1$$

for $t \in [0, t_f]$. From this, we have

$$(1 - \lambda)v_1 + \lambda v_2 = \begin{bmatrix} \lambda u_{11}(t) + (1 - \lambda)u_{21}(t) \\ \lambda u_{12}(t) + (1 - \lambda)u_{22}(t) \end{bmatrix} \in U.$$

As such, we obtain that U is a convex set. To show that U is a closed set, it is enough to show that for every convergent sequence $(u_n) = (u_{1n}, u_{2n}) \subseteq U$, one has $\lim_{n \rightarrow \infty} u_n \in U$. This statement is equivalent to u_{1n} and u_{2n} is a convergent sequence with $(x, y) = (\lim_{n \rightarrow \infty} u_{1n}, \lim_{n \rightarrow \infty} u_{2n}) \in U$. Now we define

$$\|u - v\| := \sup\{|u(t) - v(t)| \mid t \in [0, 1]\}.$$

Then we know that u_{1n} and u_{2n} is a convergent sequence such that for every $\varepsilon > 0$, there exists $K(\varepsilon) \in \mathbb{N}$ that satisfies

$$\|u_{1n} - x\| < \varepsilon$$

and

$$\|u_{2n} - y\| < \varepsilon$$

for every $n \geq K(\varepsilon)$. From this, we obtain

$$\|u_{1n} - x\| < \varepsilon,$$

$$\begin{aligned} (\Rightarrow) \quad & |u_{1n}(t) - x(t)| < \sup\{|u_{1n}(t) - x(t)| \mid t \in [0, t_f]\} < \varepsilon, \\ (\Rightarrow) \quad & -\varepsilon < x(1) - u_{1n}(t) < \varepsilon, \\ (\Rightarrow) \quad & -\varepsilon \leq u_{1n}(t) - \varepsilon < x(1) < \varepsilon + u_{1n}(t) \leq \varepsilon + 1, \\ (\Rightarrow) \quad & -\varepsilon < x(t) < 1 + \varepsilon, \end{aligned}$$

and

$$\|u_{2n} - y\| < \varepsilon,$$

$$\begin{aligned} (\Rightarrow) \quad & |u_{2n}(t) - y(t)| < \sup\{|u_{2n}(t) - y(t)| \mid t \in [0, t_f]\} < \varepsilon, \\ (\Rightarrow) \quad & -\varepsilon < y(1) - u_{2n}(t) < \varepsilon, \\ (\Rightarrow) \quad & -\varepsilon \leq u_{2n}(t) - \varepsilon < y(1) < \varepsilon + u_{2n}(t) \leq \varepsilon + 1, \\ (\Rightarrow) \quad & -\varepsilon < y(t) < 1 + \varepsilon. \end{aligned}$$

Since it is satisfied for every $\varepsilon > 0$, we obtain $0 \leq x(t), y(t) \leq 1$ and $(x, y) \in U$. Consequently, we show that U is a closed set. Furthermore, it can be proven that U is a closed convex set.

3. The function $\mathbb{J} : U \rightarrow \mathbb{R}$, which is defined as

$$\mathbb{J}(u_1, u_2) = a_1 I + \frac{1}{2} (b_1 u_1^2(t) + b_2 u_2^2(t)) dt,$$

is a bounded convex function on U .

To prove that \mathbb{J} is a bounded convex function, first, note that I is a continuous function at $[0, t_f]$, so that there exist I_{\min} and I_{\max} such that $I_{\min} \leq I(t) \leq I_{\max}$ and we know $0 \leq u_1(t) \leq 1$ and $0 \leq u_2(t) \leq 1$ so that

$$a_1 I_{\min} \leq \mathbb{J}((u_1, u_2)) \leq a_1 I_{\max} + \frac{1}{2}(b_1 + b_2).$$

From this, we can say that \mathbb{J} is a bounded function. Then, suppose

$$g(u_1, u_2) = \frac{1}{2}b_1u_1^2 + \frac{1}{2}b_2u_2^2$$

and the Hessian matrix of g is

$$H = \begin{bmatrix} \frac{\partial^2 g}{\partial u_1^2} & \frac{\partial^2 g}{\partial u_1 \partial u_2} \\ \frac{\partial^2 g}{\partial u_2 \partial u_1} & \frac{\partial^2 g}{\partial u_2^2} \end{bmatrix} = \begin{bmatrix} 2b_1 & 0 \\ 0 & 2b_2 \end{bmatrix}.$$

We can prove that H is semidefinite positive so g is a convex function. From this, we obtain that g and a_1I are convex functions on U . Also,

$$\mathbb{J}(u_1, u_2) = a_1I + \frac{1}{2}(b_1u_1^2(t) + b_2u_2^2(t)) dt$$

is a convex function on U . Then, we have established that \mathbb{J} is a bounded convex function.

4. We know that $S(t), E(t), I(t)$ and $R(t)$ is a continuous function on $[0, t_f]$ so $S(t), E(t), I(t)$ and $R(t)$ is a bounded function with

$$0 < S(t) \leq S_{max}, 0 < E(t) \leq E_{max}, 0 < I(t) \leq I_{max}, 0 < R(t) \leq R_{max}$$

for every $t \in [0, t_f]$. From this, we obtain

- (a) $\frac{dS}{dt} = \theta N - \alpha\beta SI - \mu S < \theta(S_{max} + E_{max} + I_{max} + R_{max}),$
- (b) $\frac{dE}{dt} = \alpha\beta SI - \sigma E + \gamma m I - \mu E - u_1 E < \alpha\beta S_{max} I_{max} + \gamma m I_{max},$
- (c) $\frac{dI}{dt} = \sigma h E - \gamma I - \mu I - u_2 I < \sigma h E_{max},$
- (d) $\frac{dR}{dt} = \sigma(1-h)E + \gamma(1-m)I - \mu R + u_1 E + u_2 I < (\sigma(1-h) + 1)E_{max} + (\gamma(1-m) + 1)I_{max},$

so that the right-hand side equation of the rumor-spreading model with control (2) is bounded. We also know that the control system (2) can be represented as

$$\begin{aligned} \frac{dS}{dt} &= f_1(S, E, I, R) + u_1g_1(S, E, I, R) + u_2h_1(S, E, I, R), \\ \frac{dE}{dt} &= f_2(S, E, I, R) + u_1g_2(S, E, I, R) + u_2h_2(S, E, I, R), \\ \frac{dI}{dt} &= f_3(S, E, I, R) + u_1g_3(S, E, I, R) + u_2h_3(S, E, I, R), \\ \frac{dR}{dt} &= f_4(S, E, I, R) + u_1g_4(S, E, I, R) + u_2h_4(S, E, I, R). \end{aligned}$$

From this, we can say that the control system can be represented as the linear function below u_1 and u_2 . So we obtain that the control system is linearly bounded below u_1 and u_2 .

5 Conclusion

The nonlinear dynamic model of rumor spreading with control constructed in this paper is based on the very high level of public vulnerability in receiving information. Therefore, the model in this paper applies two controls, a campaign (u_1) for the Exposed population and a punishment (u_2) for the Infected population. By analysis, the constructed model is valid and has a unique solution. This is shown based on the concept of a positively invariant set and reviewing that the model is Lipschitz. The positivity of the resulting solution indicates that the population in the model, namely, Susceptible, Exposed, Infected and Recovered, always exists. The expectation is that although the rumor spreaders (Infected) and the susceptible (Exposed) exist at all times, at least an optimal control is needed to suppress the rate of rumor spread and increase the population of rumor-free people (Recovered). This is in accordance with the existence concept of optimal control as proven in this paper.

Acknowledgements

The authors gratefully acknowledge the Institut Teknologi Sepuluh Nopember for financial support to this work, within the 2023 Publication Writing and IPR Incentive Program (PPHKI) project programme.

References

- [1] Y. Pusparisa. Masyarakat paling banyak mengakses informasi dari media sosial. <https://databoks.katadata.co.id/datapublish/2020/11/23/masyarakat-paling-banyak-mengakses-informasi-dari-media-sosial>. Accessed: 2022-12-08.
- [2] N. Song and L. Huo. Dynamical interplay between the dissemination of scientific knowledge and rumor spreading in emergency. *Physica A: Statistical Mechanics and its Applications* **461** 73–84.
- [3] I.R. Cahyadi. Survei kic: Hampir 60% orang indonesia terpapar hoax saat mengakses internet. <https://www.beritasatu.com/digital/700917/survei-kic-hampir-60-orang-indonesia-terpapar-hoax-saat-mengakses-internet>. Accessed: 2022-12-08.
- [4] S. Hota, F. Agosto, H.R. Joshi, and S. Lenhart. Optimal control and stability analysis of an epidemic model with education campaign and treatment. *Dynamical Systems, Differential Equations and Applications AIMS Proceedings* (2015) 621–634.
- [5] Martin Bohner, Cosme Duque and Hugo Leiva. Controllability of Dynamic Equations with Memory. *Nonlinear Dyn. Syst. Theory* **22** (5) (2022) 489–502.
- [6] A. Morsli, A. Tlemcani and H. Nouri. Control of a Shunt Active Power Filter by the Synchronous Referential Method Connected with a Photovoltaic Solar Energy. *Nonlinear Dyn. Syst. Theory* **22** (4) (2022) 424–431.
- [7] S. Subchan and R. Zbikowski. Computational optimal control of the terminal bunt manoeuvre—part 1: Minimum altitude case. *Optimal Control Applications and Methods* **28** (5) (2007) 311–353.
- [8] K.D.R. Dewi, K. Fahim and S. Subchan. Application of Model Predictive Control (MPC) to Longitudinal Motion of the Aircraft Using Polynomial Chaos. *Nonlinear Dyn. Syst. Theory* **23** (5) (2023) 487–498.

- [9] D.J. Daley and D.G. Kendall. Stochastic Rumours. *IMA Journal of Applied Mathematics* **1** (1) (1965) 42–55.
- [10] J. Dhar, A. Jain and V.K. Gupta. A mathematical model of news propagation on online social network and a control strategy for rumor spreading. *Social Network Analysis and Mining* **6** (2016) 1–9.
- [11] A. Jain, J. Dhar and V.K. Gupta. Optimal control of rumor spreading model on homogeneous social network with consideration of influence delay of thinkers. *Differential Equations and Dynamical Systems* **31** (2023) 113–134.
- [12] R. Krithika and A.K. Mohan. Inspecting Irresponsible Hypes: Rumors in Social Media Networks. *International Journal on Computer Science and Engineering* **09** (5) (2017) 333–337.
- [13] L. Zhao, X. Wang, X. Qiu and J. Wang. A model for the spread of rumors in Bar-rat–Barthelemy–Vespignani (BBV) networks. *Physica A: Statistical Mechanics and its Applications* **392** (21) (2013) 5542–5551.
- [14] Q. Liu, T. Li and M. Sun. The analysis of an SEIR rumor propagation model on heterogeneous network. *Physica A: Statistical Mechanics and its Applications* **469** (2017) 372–380.
- [15] X. Liu, T. Li and M. Tian. Rumor spreading of a seir model in complex social networks with hesitating mechanism. *Advances in Difference Equations* **1** 1 (2018) 1–24.
- [16] R.L. Rosnow. Rumor as communication: A contextualist approach. *Journal of Communication* **38** (1) (1998) 12–28.
- [17] X. Chen and B. Liu. Existence and uniqueness theorem for uncertain differential equations. *Fuzzy Optimization and Decision Making* **9** (2010) 69–81.
- [18] W.H. Fleming and R.W. Rishel. *Deterministic and Stochastic Optimal Control*. Springer Science & Business Media, 1975.



Square Root Ensemble Kalman Filter for Forefinger Motion Estimation as Post-Stroke Patients' Medical Rehabilitation

T. Herlambang¹, F. A. Susanto¹, H. Nurhadi², K. Oktafianto³, H. Arof⁴
and R. S. Marjianto^{5*}

¹ Department of Information Systems, Universitas Nahdlatul Ulama Surabaya, Indonesia.

² Department of Industrial Mechanical Engineering, Sepuluh Nopember Institute of Technology, Indonesia.

³ Department of Mathematics, University of PGRI Ronggolawe, Indonesia.

⁴ Department of Electrical Engineering, University of Malaya, Malaysia.

^{5*} Department of Engineering, Faculty of Vocational Studies, University of Airlangga, Surabaya, Indonesia.

Received: August 18, 2023; Revised: June 17, 2024

Abstract: Hemiparesis is a medical term to describe a condition of weakness on one side of the body or the inability to move a limb on one side. The term comes from the word 'hemi' meaning half or one side and "paresis" meaning weakness. Hemiparesis patients are still able to move the affected side of the body and are not completely paralyzed. It is just that the side of the body experiencing the disorder is so weak and powerless, the movements that arise are also very little. Current robotics technology has developed rapidly along with advances in science and technology to assist medical rehabilitation, one of which is a post-stroke rehabilitation, especially the rehabilitation of finger movement. One technology useful to develop is the finger motion estimation of the Finger Prosthetic Robotic Arm for patients with upper extremity paresis. Finger motion estimation is one of the important aspects in the development of such technology because it is designed to determine the accuracy and effectiveness of the robot in providing motion assistance to hands affected by paresis. The study in this paper used the Square Root Kalman Filter method to estimate the motion of the index finger robot by generating 250 ensembles, 500 ensembles and 750 ensembles. The simulation results with 750 ensembles have the best accuracy of around 97-98%.

Keywords: *hemiparesis, finger prosthetic robotic arm; EnKF; SR-EnKF; forefinger motion estimation.*

Mathematics Subject Classification (2010): 93E10, 62F10.

* Corresponding author: <mailto:rachmansinatriya@vokasi.unair.ac.id>

1 Introduction

According to the data from the World Health Organization (WHO), in 2016, the recorded stroke cases ranked second as a non-communicable disease that causes death and third as the main cause of disability worldwide. A stroke can cause weakness in one part or side of the body (hemiparesis), and stroke patients will have difficulty moving and using one side of their body. The affected limbs are usually the facial muscles, respiratory muscles of the chest, arms, hands, or lower limbs on one side. It can occur on the right or left side only and if it occurs on both sides, it is called total or bilateral paresis [1].

Stroke is the medical term for a condition under which blood cannot flow to the brain normally due to the blockage (Ischemic Stroke) or rupture of blood vessels (Hemorrhagic Stroke). A stroke can cause disability on one side of the body, including the upper limbs such as fingers being difficult to move. So, rehabilitation is needed to restore the function of the fingers [2]. Hands and fingers are the most important and complex parts of the human. The muscles in them can perform any movement as the human brain commands, without having to control them one by one.

Robotics technology is currently developing rapidly along with advances in science and technology to assist medical rehabilitation, one of which is a post-stroke rehabilitation, especially the rehabilitation of finger movement. This is also due to the human desire to help each other in accelerating the recovery of post-stroke patients. For example, the way humans walk, hold objects and others. The goal of medical rehabilitation is to maximize the functional independence and ability of patients to resume their way of life or role as before the illness and to improve the quality of life [3].

Fingers are one part of the human body playing an important role in human movement to perform various activities [4]. Humans have a total of ten fingers that function to hold objects. From the working principle of human fingers, it is then used as the basis for the development of finger robots designed to hold objects. Finger robots are one solution to help accelerate the rehabilitation process, specifically for finger movements. One of the efforts for the development of finger robots is finger motion estimation.

One of the main challenges in the development of a Finger Prosthetic Robotics Arm is how to estimate finger motion accurately. One of the estimation methods having a small error is the Ensemble Kalman Filter Square Root method, which is very reliable for both linear and nonlinear models with the addition of square root in the correction stage. The EnKF-SR method is frequently used for motion and position estimation of AUVs [5], [6], [7], ASVs [8], missiles [9] and mobile robots [10]. And for this paper, the finger motion estimation was carried out, especially for the index finger on the left hand, by using the Square Root EnKF (SR-EnKF) method, and the accuracy of the simulation results was compared when generating 250 ensembles, 500 ensembles and 750 ensembles.

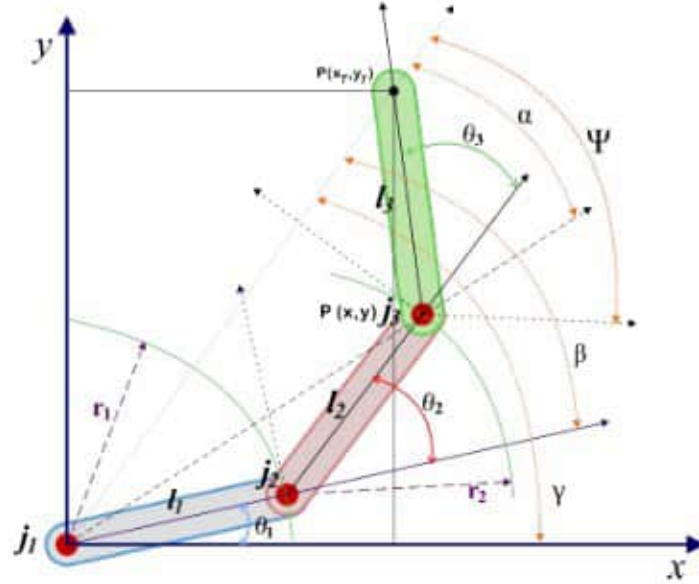
2 Finger Arm Robot Model

Here is the analysis of the 3-joint finger arm robot. Figure 1 shows a 3-joint finger arm robot using forward kinematics in x and y coordinates as its equation analysis [5].

The angle Ψ is the angle of the facing direction of the third arm with respect to the X-axis, as in equation (1).

$$\Psi = (\theta_1 + \theta_2 + \theta_3). \quad (1)$$

And for the angle equation, θ_1 and θ_2 as well as Ψ are as follows:



Gambar 2.14 Konfigurasi robot lengan 3 sendi

Figure 1: Configuration of the 3-joint finger arm robot [4].

$$\begin{aligned}
 \theta_2 &= \cos^{-1} \left(\frac{x^2 + y^2 - l_1^2 - l_2^2}{2l_1l_2} \right) \\
 \theta_1 &= \tan^{-1} \left(\frac{y(l_1 + l_2 \cos \theta_2) - xl_2 \sin \theta_2}{x(l_1 + l_2 \cos \theta_2) + yl_2 \sin \theta_2} \right) \\
 \Psi &= \theta_1 + \theta_2 + \theta_3 \\
 &= \sin^{-1} \left(\frac{l_1(\cos \theta_1 - \sin \theta_1) + l_2(\cos(\theta_1 + \theta_2) - \sin(\theta_1 + \theta_2))}{2l_3} \right). \quad (2)
 \end{aligned}$$

The image of the finger arm robot is shown in Figure 2.

3 Square Root Ensemble Kalman Filter

The following is the flow of applying the mathematical model of the forefinger arm robot to the ENKF-SR algorithm, see Figure 3.

4 Simulation Results

This study was started with the aim of helping the recovery process of post-stroke patients, especially for the fingers, and more specifically, the index finger. To help improve the quality of life of patients with upper extremity paresis, this paper tries to initiate developing finger technology using a mathematical model of a finger prosthetic arm robot that has 3 joints as a motion system platform adapted to the structure of human fingers,



Figure 2: Image of a finger arm robot.

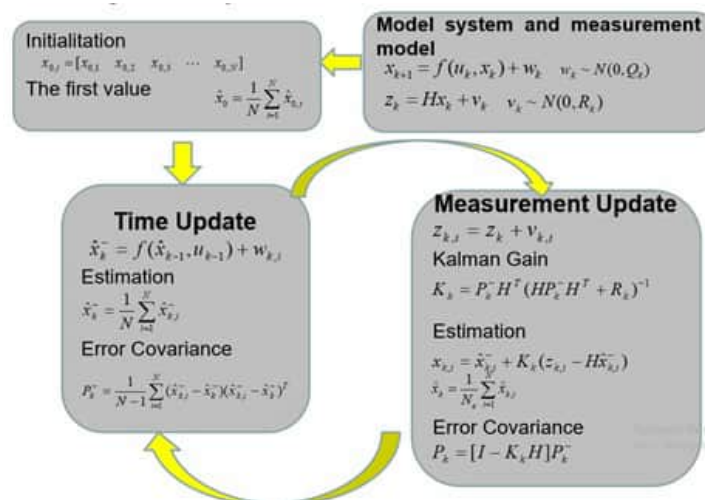


Figure 3: Ensemble Kalman Filter Square Root Algorithm [11,12,13].

especially Surabaya residents in the Republic of Indonesia, who have a ring finger length of about 7.9 - 8.2 cm. In this paper, the trajectory of the index finger movement is determined in the form of a semicircular motion, which with a movement of about 180 degrees can train the finger to improve its function and recover as before. The study in this paper implemented the Kalman Filter Square Root Ensemble method for index finger motion estimation, and for the simulation results, the accuracy comparison was made when generating 250 ensembles, 500 ensembles and 750 ensembles as shown in

Figures 4-7.

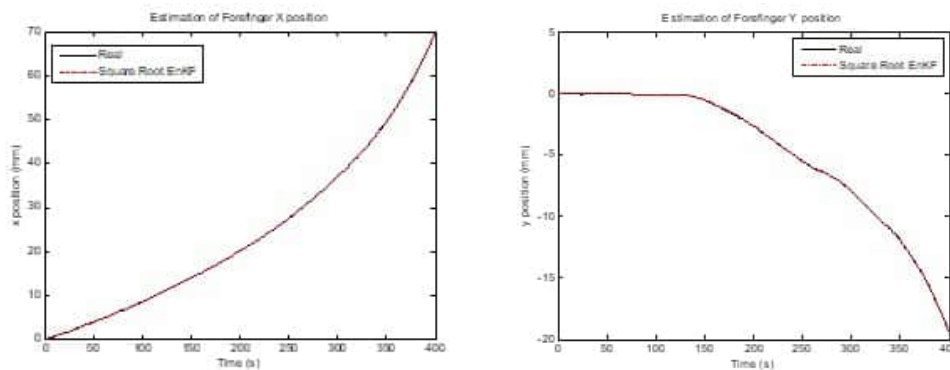


Figure 4: Motion estimation of a finger arm robot, especially the index finger, using 250 ensembles on the X-plane and Y-plane.

In Figure 4, it can be seen that the motion of the index finger in the 2-dimensional movement in the X and Y planes takes 400 seconds. From Figure 4, it can be seen that the EnKF-SR method has high accuracy with an error of about 1-2%.

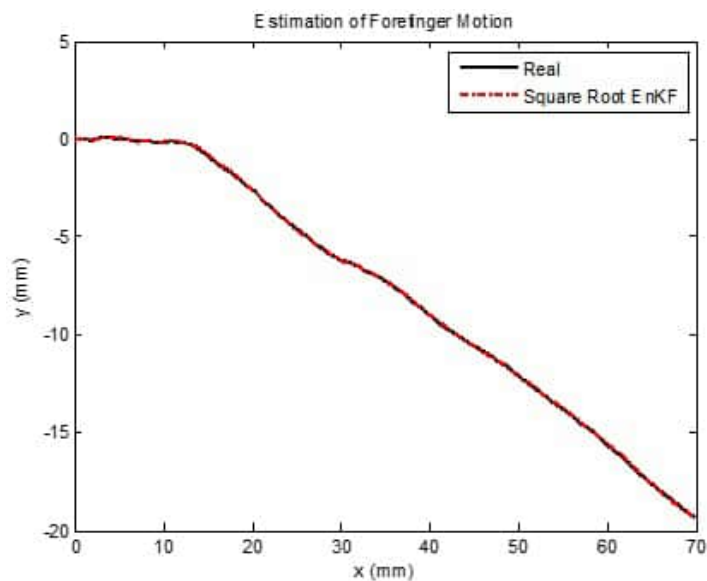


Figure 5: Motion estimation of a finger arm robot, especially the index finger, using 250 ensembles.

Figure 5 shows a semicircular motion in the XY plane, and it can be seen that the EnKF-SR method has a fairly small error. Figure 5 is the simulation result by generating 250 ensembles. The movement of the index finger that resembles a semicircle as in Figure 5 is compared to the motion of a semicircle with a diameter of about 7.9 cm, whereas in

Figure 4, it is obtained that its diameter is

$$\sqrt{7^2 + 2^2} = \sqrt{49 + 4} = \sqrt{53} = 7.3 \text{ cm}$$

so that overall, when viewed from the diameter of about 7.9 - 8.2 cm, it has an error of about 7.5%. The second and third simulations are shown in Figures 6 and 7. In the second

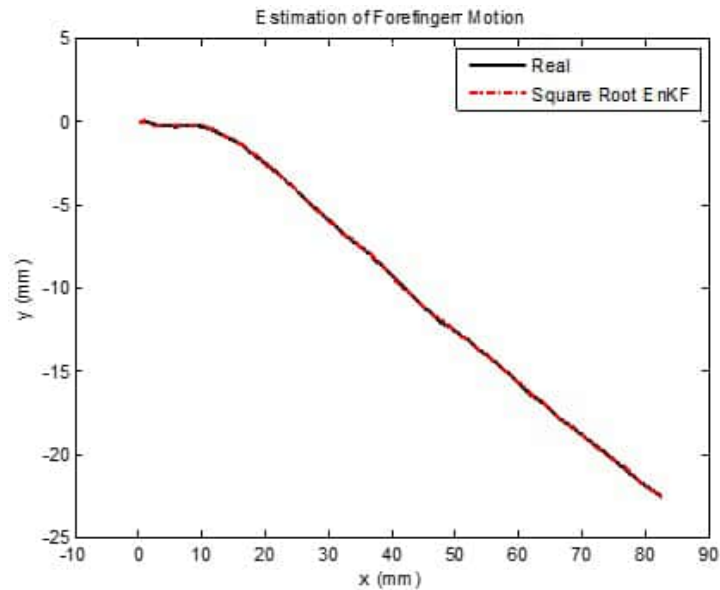


Figure 6: Motion estimation of a finger arm robot, especially the index finger, using 500 ensembles.

simulation by generating 500 ensembles, this paper displays the results of the simulations in the XY plane only as shown in Figure 6, which gives the results of simulations using the Square Root EnKF method by generating 500 ensembles resulting in movements that resemble a semicircle with a diameter of $\sqrt{8.1^2 + 2.3^2} = \sqrt{65.61 + 5.29} = \sqrt{70.9} = 8.42$ cm, so that overall, if viewed from a diameter of about 7.8 cm - 8.3 cm, then using 500 ensembles has an error of about 2.68%, in other words, it has an accuracy of about 97.32%. So, the EnKF-SR method can be effectively used to estimate the motion of the finger arm robot, especially the index finger.

Figure 7 shows a semicircular motion in the XY plane, where it can be seen that the Square Root EnKF method has a fairly small error. Figure 7 is the simulation result by generating 750 ensembles. The movement of the index finger that resembles a semicircle as in Figure 7 is compared with the motion in a semicircle with a diameter of 7.9 - 8.2 cm, where in Figure 7 the obtained diameter is $\sqrt{8.05^2 + 2.3^2} = \sqrt{64.8025 + 5.29} = \sqrt{70.0925} = 8.37$, so that overall, when viewed from a diameter of about 7.9 - 8.2 cm, it has an error of about 2.07%.

Table 1 shows that the simulation with 750 ensembles has a smaller error than those using 250 and 500 ensembles. The three simulation results are compared for the size of the index finger of the Surabaya community in Indonesia with an average length of about 7.9 - 8.2 cm, which performs a semicircular motion. So, in view of the three simulations

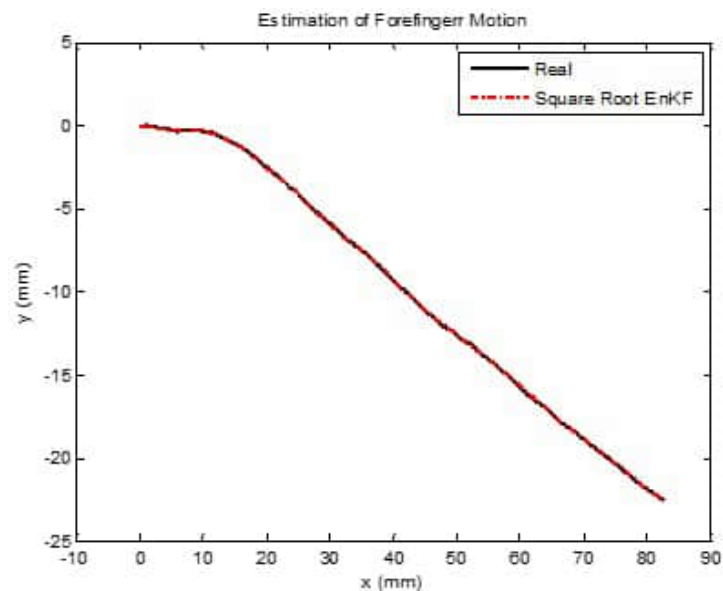


Figure 7: Motion estimation of a finger arm robot, especially the index finger, using 750 ensembles.

	250 ensembles	500 ensembles	750 ensembles
XY Motion	7.5%	2.8%	2.07%
Simulation Time	5.9 s	9.85 s	12.9 s

Table 1: Comparison of error values based on the generation of different number of ensembles by the Square Root EnKF method

above, the Square Root EnKF method can be used as a reliable estimation method in estimating the finger arm robot, having an error of not more than 8%.

5 Conclusion

Based on the analysis of the results of three simulations, comparing the simulations based on the generation of different number of ensembles, it can be concluded that the Square Root EnKF method can be used as a reliable estimation method to estimate the motion of the finger arm robot showing an error of not more than 2-3% range for the simulations generating 500 and 750 ensembles, while the simulation with 250 ensembles produces an error of 7.5% or, in other words, it has an accuracy of 92.5%. Overall, the 750 ensemble simulation has the highest accuracy as compared to those using 250 and 500 ensembles.

Acknowledgment

We gratefully acknowledge the support from LPPM - Universitas Nahdlatul Ulama Surabaya (UNUSA).

References

- [1] T. Herlambang, H. Nurhadi, A. Muhith, D. Rahmalia and P.B. Tomosouw. Estimation of Third Finger Motion Using Ensemble Kalman Filter. *BAREKENG: Journal of Mathematics and Its Application* **16** (3) (2022) 1079–1086.
- [2] T. Herlambang, H. Nurhadi, A. Muhith, A. Suryowinoto and K. Oktafianto. Estimation of Forefinger Motion with Multi-DOF Using Advanced Kalman Filter. *Nonlinear Dynamics and Systems Theory* **23** (1) (2023) 24–33.
- [3] O. S. Purwanti and A. Maliya. Rehabilitasi Klien Pasca Stroke. *Berita Ilmu Keperawatan* **1** (1) (2008) 43–46.
- [4] E. S. Ningrun, B. Sumantri, B. Wijayanto, C. Yanuar and M. I. Riansyath. Optimasi Pergerakan Robot Planar 3 Sendi Pada Robot Penggenggam Menggunakan Metode Pemrograman Genetika. *Jurnal Inovtek* **3** (1) (2013) 20–25.
- [5] T. Herlambang, E. B. Djatmiko, H. Nurhadi. Ensemble Kalman Filter with a Square Root Scheme (EnKF-SR) for Trajectory Estimation of AUV SEGOROGENI ITS. *International Review of Mechanical Engineering IREME Journal* **9** (6) (2015) 553–560.
- [6] S. Subchan, T. Herlambang and H. Nurhadi. UNUSAITs AUV Navigation and Guidance System with Nonlinear Modeling Motion Using Ensemble Kalman Filter. In: *Proc. International Conference on Advanced Mechatronics, Intelligent Manufacture, and Industrial Automation (ICAMIMIA)* Malang, Indonesia, 2019.
- [7] T. Herlambang, S. Subchan and H. Nurhadi. Navigation and Guidance Control System of UNUSAITs AUV Based on Dynamical System Using Ensemble Kalman Filter Square Root. In: *Proc. the Third International Conference on Combinatorics, Graph Theory and Network Topology* Jember, Indonesia, 2019.
- [8] H. Nurhadi, T. Herlambang and D. Adzkiya. Trajectory Estimation of Autonomous Surface Vehicle Using Square Root Ensemble Kalman Filter. In: *Proc. International Conference on Advanced Mechatronics, Intelligent Manufacture, and Industrial Automation (ICAMIMIA)* Malang, Indonesia, 2019.
- [9] T. Herlambang. Design of a Navigation and Guidance System of Missile with Trajectory Estimation Using Ensemble Kalman Filter Square Root (EnKF-SR). In: *Proc. International Conference on Computer Applications and Information Processing Technology (CAIPT)* Bali, Indonesia, 2019. 8–10.
- [10] T. Herlambang, F. A. Susanto, D. Adzkiya, A. Suryowinoto, and K. Oktafianto. Design of Navigation and Guidance Control System of Mobile Robot with Position Estimation Using Ensemble Kalman Filter (EnKF) and Square Root Ensemble Kalman Filter (SR-EnKF). *Nonlinear Dynamics and Systems Theory*. **22** (4) (2022) 390–399.
- [11] T. Herlambang, A. Muhith, D. Rahmalia, H. Nurhadi. Motion Optimization using Modified Kalman Filter for Invers-Kinematics based Multi DOF Arm Robot. *International Journal of Control and Automation*. **13** (2) (2020) 66–71.
- [12] D. F. Karya, K. Puspandam and T. Herlambang. Stock Price Estimation Using Ensemble Kalman Filter Square Root Methods. *The First International Conference on Combinatorics, Graph Theory and Network Topology, University of Jember-Indonesia*. (2017) 25–26.
- [13] A. Muhith, T. Herlambang, D. Rahmalia, I. Irhamah and D. F. Karya. Estimation of Thrombocyte Concentrate (TC) in PMI Gresik using unscented and square root Ensemble Kalman Filter. *The 5th International Conference of Combinatorics, Graph Theory, and Network Topology (ICCGANT)*, 2021.



On the Synchronization of a Novel Chaotic System with Two Control Methods

Lakehal Nadjet¹ and Fareh Hannachi^{2*}

¹ *Laboratory of Mathematics, Informatics and Systems (LAMIS), Echahid Cheikh Larbi
Tebessi University - Tebessa, Algeria.*

² *Echahid Cheikh Larbi Tebessi University - Tebessa, Algeria.*

Received: January 14, 2024; Revised: July 17, 2024

Abstract: This paper reports a new chaotic system and its synchronization via active and adaptive control methods. The novel system is presented and its chaoticity is confirmed using the Lyapunov exponents tool. Furthermore, it is demonstrated that the new system possesses the property of co-existing attractors. Moreover, two control methods are employed: active control and adaptive control. By designing appropriate controllers and estimation laws based on the stability theory of integer-order systems, we achieve synchronization between chaotic systems. Finally, numerical simulations are implemented to demonstrate the effectiveness and flexibility of the synchronization controllers and the estimation laws for the two methods.

Keywords: *chaotic system; strange attractor; Lyapunov exponent; Lyapunov stability theory; adaptive control; synchronization.*

Mathematics Subject Classification (2010): 34D08, 34C28, 37B55, 37B25, 37D45, 70K20, 93D05, 93D21.

1 Introduction

The chaos theory deals with the dynamical behavior of nonlinear dynamical systems which are highly sensitive to initial conditions and system parameters. Recently, chaos theory has achieved great development and has been successfully applied in many fields such as electronic engineering [1], computer science [2], communication systems [3, 4], medical image processing [1,2], complex networks [5], chemical engineering [6], investigation of HIV virus [28] and economic models [7]. By now, numerous chaotic systems with different types of attractors have been proposed and studied, for example those with

* Corresponding author: <mailto:fareh.hannachi@univ-tebessa.dz>

self-excited attractors [8,9], hidden attractors [10,11,12], coexisting attractors [13,14], infinitely many shifted attractors [15,16], multi scroll attractors [17,18], memristor attractors [19,20] and chaotic systems with fractional orders [11,21]. In the past few decades, chaos synchronization has received great attention owing to its applications in designing secure communication system. Synchronization of chaotic systems is a topic of interest in the field of nonlinear dynamics. It involves the design of control strategies that can make two or more chaotic systems behave identically or follow a certain pattern over time. Some of the methods used for chaotic synchronization include active control, adaptive control, fuzzy sliding mode control, sliding mode controller [22-25], backstepping neural network method [26], observer-based synchronization [27] and so on. This paper is organized as follows. Section 2 describes the new chaotic system, its phase plots and equilibrium points. Section 3 describes the dynamic analysis of the new chaotic system including multistability and coexisting attractors. Moreover, the synchronization of the chaotic system with two control methods is realized by designing appropriate active and adaptive controllers and estimation laws using the stability theory of integer-order systems in Section 4. In Section 5, numerical simulations are implemented to demonstrate the effectiveness and flexibility of the synchronization controllers and the estimation laws for the two methods. The conclusion is given in the last section.

2 Description and Analysis of System

The new chaotic system has three positive parameters, cosine and nonlinear terms described by

$$\begin{cases} \dot{x}_1 = a(-x_1 \cos(x_2) + x_2), \\ \dot{x}_2 = -bx_1 - x_3, \\ \dot{x}_3 = -x_1(1 - x_2^2) + cx_3, \end{cases} \quad (1)$$

where $X = (x_1, x_2, x_3)^T$ are the states and a, b, c are the positive constants.

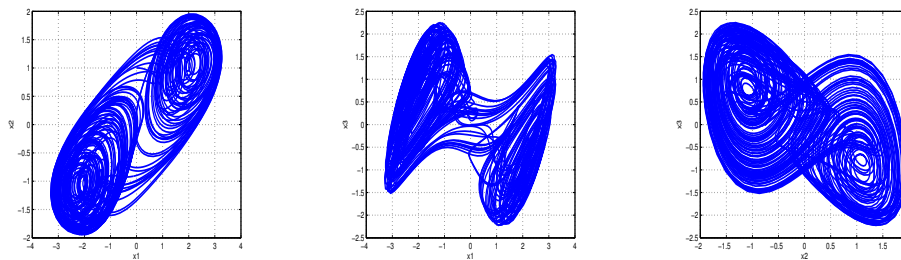


Figure 1: Strange Attractor of New Hyperchaotic System.

2.1 Equilibrium points

Putting equations of the system (1) equal to zero, i.e.,

$$\begin{cases} a(-x_1 \cos(x_2) + x_2) = 0, \\ -bx_1 - x_3 = 0, \\ -x_1(1 - x_2^2) + cx_3 = 0, \end{cases} \quad (2)$$

then we can verify the following:

- If $1 + bc \leq 0$, the system (1) has only one equilibrium point $p_0 = (0, 0, 0)$,
- If $1 + bc > 0$ and $1 + bc \neq \left(k\frac{\pi}{2}\right)^2$, $k \in \mathbb{Z}^*$, the system (1) has three equilibrium points:

$$\begin{cases} P_0 = (0, 0, 0), \\ P_1 = \left(\frac{\sqrt{1+bc}}{\cos(\sqrt{1+bc})}, \sqrt{1+bc}, -\frac{b\sqrt{1+bc}}{\cos(\sqrt{1+bc})}\right), \\ P_2 = \left(-\frac{\sqrt{1+bc}}{\cos(\sqrt{1+bc})}, -\sqrt{1+bc}, \frac{b\sqrt{1+bc}}{\cos(\sqrt{1+bc})}\right). \end{cases} \quad (3)$$

In order to check the stability of the equilibrium points, we derive the Jacobian matrix at a point $p(x_1, x_2, x_3)$ of the system (1).

$$J(p) = \begin{pmatrix} -a\cos(x_2) & ax_1\sin(x_2) + a & 0 \\ -b & 0 & -1 \\ -1 + x_2^2 & 2x_1x_2 & c \end{pmatrix}. \quad (4)$$

Therefore, the characteristic equation of J is obtained as

$$\lambda^3 + \eta_1\lambda^2 + \eta_2\lambda + \eta_3 = 0. \quad (5)$$

Based on the Routh-Hurwitz theorem, p is a stable point if the following conditions are satisfied:

$$\begin{cases} \eta_1 > 0, \eta_2 > 0, \\ \eta_1\eta_2 > \eta_3. \end{cases} \quad (6)$$

When $a = 1.2, b = c = 0.46$, system (1) has the following equilibria:

$$\begin{cases} p_0 = (0, 0, 0), \\ p_1 = (1.1007, 1.1007, 0.5063), \\ p_2 = (-1.1007, -1.1007, 0.5063). \end{cases} \quad (7)$$

The corresponding eigenvalues and their stability are given in the following table.

Equilibrium points	Eigenvalues	stability
p_0	$\lambda_{1,2} = -0.83620 \pm 0.92742i, \lambda_3 = 0.93240$	unstable foci point
$p_{1,2}$	$\lambda_{1,2} = 0.15272 \pm 1.8336i, \lambda_3 = -0.38900$	unstable foci points

3 Dynamic Analysis of the New Chaotic System (1)

3.1 Lyapunov-exponent and Kaplan-York dimension

In this section, we will prove that the new system (1) is chaotic by calculating the Lyapunov exponents using the Wolf-Swift algorithm [29]. Simulation in Matlab gives us the following Lyapunov exponents:

$$L_1 = 0.153564, L_2 = 0, L_3 = -0.378558. \quad (8)$$

Also, the Kaplan-York dimension of system (1) is given by

$$D_L = 2 + \frac{1}{|L_3|} \sum_{i=1}^2 L_i = 2.40565. \quad (9)$$

Since L_1, L_2 are positive Lyapunov exponents and $\sum_{i=1}^3 L_i < 0$, the novel system (1) is a chaotic dissipative system with fractal dimension.

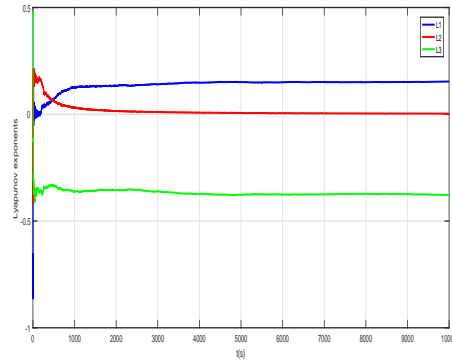


Figure 2: Lyapunov exponent spectrum.

3.2 Multistability in the new 3-D chaotic system (1)

Multistability in chaotic systems refers to a phenomenon where a system can exhibit multiple stable states, or attractors, under certain conditions. This means that the system can evolve into different, distinct chaotic behaviors depending on its initial conditions or external parameters. In order to study the coexistence attractors and other characteristics of the system better, it is necessary to give some disturbance to the initial conditions under the condition of keeping the system parameters constant. The proposed 3D chaotic system (1) has symmetrical attractors with respect to the origine (equilibrium point $(0, 0, 0)$) because it is invariant under the coordinate transformation

$$(x_1, x_2, x_3) \longrightarrow (-x_1, -x_2, -x_3). \tag{10}$$

Fig.3 shows the dynamic behavior with coexistence chaotic attractors with different initial conditions.

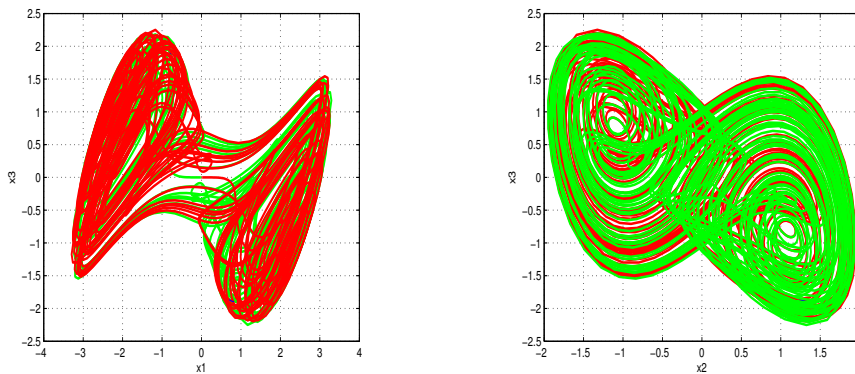


Figure 3: Coexistence of two attractors with different initial values and parameters.

4 Identical Synchronization with Two Method

The synchronization error state is define by

$$e(t) = Y(t) - X(t),$$

where $Y(t) = (y_1, y_2, y_3)$ and $X(t) = (x_1, x_2, x_3)$, $e(t) = (e_1, e_2, e_3)$. The error dynamics is obtained as

$$\dot{e}(t) = \dot{Y}(t) - \dot{X}(t).$$

The drive system is described by

$$\begin{cases} \dot{x}_1 = a(-x_1 \cos(x_2) + x_2), \\ \dot{x}_2 = -bx_1 - x_3, \\ \dot{x}_3 = -x_1(1 - x_2^2) + cx_3. \end{cases} \quad (11)$$

The response system is

$$\begin{cases} \dot{y}_1 = a(-y_1 \cos(y_2) + y_2) + u_1, \\ \dot{y}_2 = -by_1 - y_3 + u_2, \\ \dot{y}_3 = -y_1(1 - y_2^2) + cy_3 + u_3, \end{cases} \quad (12)$$

where $U(t) = (u_1, u_2, u_3)^T$ is the controller.

The synchronization error of system (11) and (12) is described as follows:

$$\begin{cases} \dot{e}_1 = ae_2 + a(x_1 \cos(x_2) - y_1 \cos(y_2)) + u_1, \\ \dot{e}_2 = -be_1 - e_3 + u_2, \\ \dot{e}_3 = -e_1 + ce_3 + y_1 y_2^2 - x_1 x_2^2 + u_3. \end{cases} \quad (13)$$

4.1 Active Control Method

The controller system is constructed as follows:

$$\begin{cases} u_1 = -ae_2 - a(x_1 \cos(x_2) - y_1 \cos(y_2)) - \dot{e}_1, \\ u_2 = be_1 + e_3 - \dot{e}_2, \\ u_3 = e_1 - ce_3 - y_1 y_2^2 + x_1 x_2^2 - \dot{e}_3, \end{cases}$$

where

$$\begin{cases} \dot{e}_1 = -k_1 e_1, \\ \dot{e}_2 = -k_2 e_2, \\ \dot{e}_3 = -k_3 e_3, \end{cases}$$

with $k_i > 0$, $i = 1, 2, 3$, being the constant gains. The controller system is

$$\begin{cases} u_1 = ae_2 - a(x_1 \cos(x_2) - y_1 \cos(y_2)) - k_1 e_1, \\ u_2 = be_1 + e_3 - k_2 e_2, \\ u_3 = e_1 - ce_3 - y_1 y_2^2 + x_1 x_2^2 - k_3 e_3. \end{cases} \quad (14)$$

Substituting (14) into (13), we can obtain

$$\begin{cases} \dot{e}_1 = -k_1 e_1, \\ \dot{e}_2 = -k_2 e_2, \\ \dot{e}_3 = -k_3 e_3. \end{cases} \quad (15)$$

It is clear from (15) that the eigenvalues of the Jacobian matrix of the error system are negative, thus the zero solution of the errors systems is asymptotically stable, i.e., $\lim_{t \rightarrow \infty} |e(t)| = 0$. Hence the synchronization using active control between systems (11) and (12) is achieved.

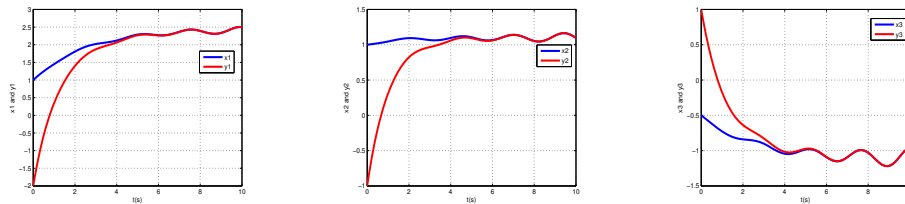


Figure 4: Synchronization between $x_i, y_i, i = 1, 2, 3$, using active control.

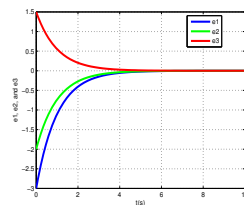


Figure 5: The time-history of the synchronization errors $e_1(t), e_2(t), e_3(t)$ using active control.

4.2 Adaptive control method

We choose system (11) as the driver system and (12) as the response system; similarly, the synchronization error is defined as $\dot{e}(t) = \dot{Y}(t) - \dot{X}(t)$, then system (13) is the synchronization error system. The controller system is constructed as follows:

$$\begin{cases} u_1 = -\hat{a}e_2 - \hat{a}(x_1 \cos(x_2) - y_1 \cos(y_2)) - \dot{e}_1, \\ u_2 = \hat{b}e_1 + e_3 - \dot{e}_2, \\ u_3 = e_1 - \hat{c}e_3 - y_1 y_2^2 + x_1 x_2^2 - \dot{e}_3. \end{cases} \quad (16)$$

Substituting (16) into (13), we obtain the error dynamics

$$\begin{cases} \dot{e}_1 = (a - \hat{a})e_2 + (a - \hat{a})(x_1 \cos(x_2) - y_1 \cos(y_2)) - k_1 e_1, \\ \dot{e}_2 = (b - \hat{b})e_1 - e_3 - k_2 e_2, \\ \dot{e}_3 = -e_1 + (c - \hat{c})e_3 + y_1 y_2^2 - x_1 x_2^2 - k_3 e_3. \end{cases} \quad (17)$$

Let us now define the parameter estimation error as $e_a = a - \hat{a}$, $e_b = b - \hat{b}$, $e_c = c - \hat{c}$. The error dynamics simplifies to

$$\begin{cases} \dot{e}_1 = e_a e_2 + e_a(x_1 \cos(x_2) - y_1 \cos(y_2)) - k_1 e_1, \\ \dot{e}_2 = -e_b e_1 - k_2 e_2, \\ \dot{e}_3 = e_c e_3 - k_3 e_3. \end{cases} \quad (18)$$

Now, consider the Lyapunov stability function V given by

$$V = \frac{1}{2}(e_1^2 + e_2^2 + e_3^2 + e_a^2 + e_b^2 + e_c^2), \quad (19)$$

then

$$\dot{V} = (e_1 \dot{e}_1 + e_2 \dot{e}_2 + e_3 \dot{e}_3 + \dot{e}_a e_a + \dot{e}_b e_b + \dot{e}_c e_c) \quad (20)$$

with

$$\dot{e}_a = -\hat{a}, \dot{e}_b = -\hat{b}, \dot{e}_c = -\hat{c}. \quad (21)$$

In view of Eq. (20), the parameter update law can be chosen as

$$\begin{cases} \dot{\hat{a}} = e_1 e_2 + e_1(x_1 \cos(x_2) - y_1 \cos(y_2)) + k_4 e_a, \\ \dot{\hat{b}} = -e_1 e_2 + k_5 e_b, \\ \dot{\hat{c}} = e_c e_3 + k_6 e_c. \end{cases} \quad (22)$$

Consequently,

$$\dot{V} = -k_1 e_1^2 - k_2 e_2^2 - k_3 e_3^2 - k_4 e_a^2 - k_5 e_b^2 - k_6 e_c^2 < 0, \quad (23)$$

which is a negative definite function. Using the Lyapunov stability theory [30], we conclude that the closed-loop system (18) is globally asymptotically stable for all initial values of the error signals e_1, e_2, e_3 by using the adaptive controller (16) and the update parameter law (22). It proves that the adaptive synchronization between the drive and response system is achieved.

5 Numerical Simulation

In order to verify our results, we applied the fourth order Runge-Kutta method in Matlab with the step size $h = 10^{-6}$ to solve the systems of differential equations (11), (12) and (13) for the active control method with the initial conditions $X_0(1, 1, -0.5), Y_0(-2, -1, 1), e_0(-3, -2, 1.5)$ and the systems of differential equations (11), (12), (17) and (22) for the adaptive control method with the initial conditions $X_0(0.1, 0.2, -0.5), Y_0(-0.5, -0.2, 0.1), e_0(-0.6, -0.4, 0.6), (a_0, b_0, c_0) = (1, 0.5, 0.5), k_1 = k_2 = k_3 = 1$. The parameter values of systems are taken as in the chaotic case $a = 1.2, b = 0.46, c = 0.46$. In Figs.4, 6, the synchronization between the states x_i and $y_i, i = 1, 3$, is depicted. In Figs.5, 7, the time-history of the synchronization errors $e_1(t), e_2(t), e_3(t)$ is depicted for the two used control methods, respectively.

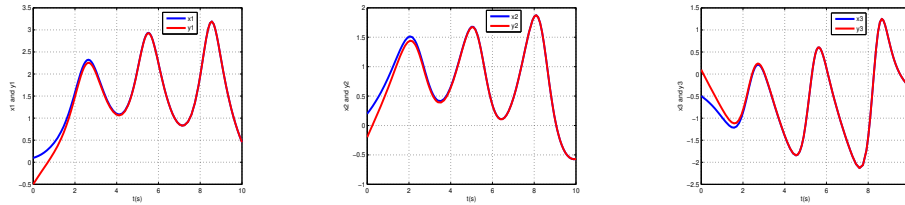


Figure 6: Synchronization between $x_i, y_i, i = 1, 2, 3$, using adaptive control.

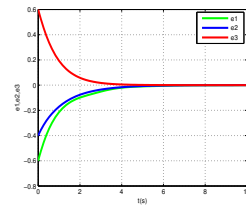


Figure 7: The time-history of the synchronization errors $e_1(t), e_2(t), e_3(t)$ using adaptive control.

6 Conclusion

This paper introduces a new chaotic system and proposes two control methods, active control and adaptive control, for synchronization using this system. We confirm the chaotic nature of the system using the Lyapunov exponents and demonstrate the coexistence of attractors. For active control, we design a controller based on the stability theory of integer-order systems to achieve synchronization. For adaptive control, we develop an estimation law to estimate the unknown parameters of the system and achieve synchronization. Numerical simulations are conducted to demonstrate the effectiveness and flexibility of both control methods.

The main important points in this work are:

- A novel chaotic system is presented and its chaoticity is confirmed using the Lyapunov exponents.
- The synchronization between identical 3-D chaotic systems using two different control methods is achieved by designing appropriate active and adaptive controllers and estimation laws using the stability theory of integer-order systems.

The results achieved through the study of the novel chaotic system and the proposed control methods can be applied to various fields that involve chaotic systems, for example secure communication systems and encryption and decryption algorithms, Biological modeling and simulation of chaos-based robotics, making further research of the system particularly relevant. As such, they will be given due consideration in future work.

Acknowledgment

The author would like to thank the editor-in-chief and the referees for their valuable suggestions and comments.

References

- [1] J. H. B. Deane and D. C. Hamill. Instability, Subharmonics, and Chaos in Power Electronic Systems. *IEEE Transactions on Power Electronics* **5** (3) (1990) 260–268.
- [2] T. Munakata, S. Sinha and W. L. Ditto. Chaos computing: implementation of fundamental logical gates by chaotic elements. *IEEE Transactions on Circuits and Systems I: Fundamental Theory and Applications* **49** (11) (2002) 1629–1633.
- [3] L. Xiong, Z. Liu, X. Zhang. Dynamical Analysis, Synchronization, Circuit Design, and Secure Communication of a Novel Hyperchaotic System. *Complexity* **2017** (1) (2017) 4962739.
- [4] J. Sun, Y. Shen, Q. Yin and C. Xu. Compound synchronization of four memristor chaotic oscillator systems and secure communication. *Chaos: An Interdisciplinary Journal of Nonlinear Science* **23** (1) 2013.
- [5] J. Lu and G. Chen. A time-varying complex dynamical network model and its controlled synchronization criteria. *Institute of Electrical and Electronics Engineers Transactions on Automatic Control* **50** (6) (2005) 841–846.
- [6] S. Vaidyanathan. Adaptive synchronization of chemical chaotic reactors. *International Journal of ChemTech Research* **8** (2) (2015) 612–621.
- [7] Y. Okuyama and S. E. Chang. Modeling spatial and economic impacts of disasters. In: Springer Science and Business Media, 2013.
- [8] G. Xu, Y. Shekofteh, A. Akgül, et al. A new chaotic system with a self-excited attractor: Entropy measurement, signal encryption, and parameter estimation. *Entropy* **20** (2) (2018) 86.
- [9] Z. Faghani, F. Nazarimehr, S. Jafari, et al. Simple chaotic systems with specific analytical solutions. *International Journal of Bifurcation and Chaos* **29** (09) (2019) 1950116.
- [10] V.T. Pham, C. Volos, S. Jafari, et al. A chaotic system with different families of hidden attractors. *International Journal of Bifurcation and Chaos* **26** (08) (2016) 1650139.
- [11] A. Ouannas, A.A. Khennaoui, S. Momani, et al. Hidden attractors in a new fractional–order discrete system: Chaos, complexity, entropy, and control. *Chinese Physics B* **29** (5) (2020) 050504.
- [12] R. Rameshbabu, K. Kavitha, P. S. Gomathi and K. Kalaichelvi. A New Hidden Attractor Hyperchaotic System and Its Circuit Implementation, Adaptive Synchronization and FPGA Implementation. *Nonlinear Dynamics and Systems Theory* **23** (2) (2023) 214–2264.
- [13] Q. Lai, Z. Wan, P.D.K. Kuate, et al. Coexisting attractors, circuit implementation and synchronization control of a new chaotic system evolved from the simplest memristor chaotic circuit. *Communications in Nonlinear Science and Numerical Simulation* **89** (2020) 105341.
- [14] Q. Lai, Z. Wan and P.D.K. Kuate. Modelling and circuit realisation of a new no-equilibrium chaotic system with hidden attractor and coexisting attractors. *Electronics Letters* **56** (20) (2020) 1044–1046.
- [15] Q. Lai, P.D.K. Kuate, H. Pei, et al. Infinitely many coexisting attractors in no-equilibrium chaotic system. *Complexity* **2020** (1) (2020) 8175639.
- [16] J. Wen and J. Wang. A chaotic system with infinite attractors based on memristor. *Frontiers in Physics* **10** (2022) 902500.

- [17] K. Sugandha and P.P. Singh. Generation of a multi-scroll chaotic system via smooth state transformation. *Journal of Computational Electronics* **21** (4) (2022) 781–791.
- [18] S. Liu, Y. Wei, J. Liu, et al. Multi-scroll chaotic system model and its cryptographic application. *International Journal of Bifurcation and Chaos* **30** (13) (2020) Article ID 2050186.
- [19] D. Yan, L. Wang, S. Duan, et al. Chaotic attractors generated by a memristor-based chaotic system and Julia fractal. *Chaos, Solitons and Fractals* **146** (2021) 110773.
- [20] J. Sun, X. Zhao, J. Fang, et al. Autonomous memristor chaotic systems of infinite chaotic attractors and circuitry realization. *Nonlinear Dynamics* **94** (2018) 2879–2887.
- [21] A. Rami and H. Fareh. A novel Fractional-order chaotic system and its synchronization via adaptive control method. *Nonlinear Dynamics and Systems Theory* **23** (4) (2023) 359–366.
- [22] S. Vaidyanathan. Sliding mode controller design for the global stabilization of chaotic systems and its application to Vaidyanathan jerk system. *Advances and Applications in Chaotic Systems*. Springer (2016) 537–552.
- [23] J. Mostafaei, S. Mobayen, B. Vaseghi, et al. Finite-time synchronization of a new five-dimensional hyper-chaotic system via terminal sliding mode control. *Scientia Iranica* **30** (1) (2021) 167–182.
- [24] S. Vaidyanathan, V.T. Pham and C.K. Volos. Adaptive backstepping control, synchronization and circuit simulation of a novel jerk chaotic system with a quartic nonlinearity. *Advances and Applications in Chaotic Systems*. Springer (2016) 109–135.
- [25] T. Niknam and M.H. Khooban. Fuzzy sliding mode control scheme for a class of non-linear uncertain chaotic systems. *IET Science, Measurement and Technology* **7**(5) (2013) 249–255.
- [26] G. Ma, C. Chen, Y. Lyu and Y. Guo. Adaptive backstepping-based neural network control for hypersonic reentry vehicle with input constraints. *IEEE Access* **6** (2017) 1954–1966.
- [27] J. Kabziński and P. Mosiolek. Adaptive, observer-based synchronization of different chaotic systems. *Applied Sciences* **12**(7) (2022) 3394.
- [28] F. Parastesh, et al. A simple chaotic model for development of HIV virus. *Scientia Iranica*. Special issue on collective behavior of nonlinear dynamical networks (2021) 1643–1652.
- [29] A. Wolf, J. B. Swift, H. L. Swinney and J. A. Vastano. Determining Lyapunov exponents from a time series. *Physica D: nonlinear phenomena* **16** (3) (1985) 285–317.
- [30] W. Hahn. *Stability of Motion*. Springer, Berlin, New York, 1967.



An Efficient DCA Algorithm for Solving Non-Monotone Affine Variational Inequality Problem

A. Noui^{1*}, Z. Kebaili² and M. Achache²

¹ *Geology Department, Setif 1 University, Setif 19000, Algeria.*

² *Fundamental and Numerical Mathematics Laboratory, Setif 1 University, Setif 19000, Algeria.*

Received: November 20, 2023; Revised: July 5, 2024

Abstract: In this paper, we propose a method for solving a non monotone affine variational inequality problem (AVI). We consider an equivalent optimization model, which is formulated as a DC program, and we apply DCA for solving it. The process consists of solving a successive convex quadratic program. The efficiency of the proposed approach is illustrated by the numerical experiments on several test problems in terms of the quality of the obtained solutions and their convergence.

Keywords: *affine variational inequality problem; quadratic program; DC programming; DCA (Difference of Convex functions Algorithms).*

Mathematics Subject Classification (2010): 90C20, 90C30, 90C90, 49J40.

1 Introduction

The variational inequality problem (VIP) remains a prominent and highly sought-after research focus within the realm of numerical optimization. Our objective is to develop a more comprehensive and less restrictive theoretical framework while devising appropriate algorithms to address it. Both the affine variational inequality problem (AVI) and the standard linear complementarity problem bear a close connection to the Karush-Kuhn-Tucker conditions commonly encountered in quadratic programming. Let us define some essential notations: We denote by \mathbb{R}^n and \mathbb{R}^m the finite-dimensional Euclidean spaces, and $\mathbb{R}^{n \times n}$ and $\mathbb{R}^{m \times n}$ represent, respectively, the spaces of $(n \times n)$ -matrices and $(m \times n)$ -matrices. The following constitutes an affine variational inequality problem (AVI):

$$\begin{cases} \text{Find } x \in C \\ \text{such that } \langle Mx + q, y - x \rangle \geq 0, \text{ for all } y \in C. \end{cases} \quad (1)$$

* Corresponding author: <mailto:a.noui@univ-setif.dz>

Here $(M, A, q, b) \in D = \mathbb{R}^{n \times n} \times \mathbb{R}^{m \times n} \times \mathbb{R}^n \times \mathbb{R}^m$ represents the data of the problem, the convex polyhedron $C = \{x \in \mathbb{R}^n : Ax \geq b\}$ is the constraint set of the problem and $\langle x, y \rangle = x^T y$ denotes the usual scalar product in \mathbb{R}^n . If $C = \mathbb{R}_+^n$, then the AVI becomes the linear complementarity problem

$$x^T (Mx + q) = 0, Mx + q \geq 0, x \geq 0. \quad (2)$$

This problem is often denoted as the Linear Complementarity Problem (LCP). Over time, a multitude of methods have been put forth to address the affine variational inequality problem (AVI), as documented in references [2, 4, 6, 7, 10, 13]. While the AVI is not inherently framed as an optimization problem, the literature contains several optimization models and methodologies designed to tackle it. Broadly speaking, the resultant optimization problem of the AVI is non-convex, rendering it extremely challenging to solve using global approaches, particularly in large-scale settings. In this paper, we delve into a novel and highly effective local optimization strategy for addressing the affine variational inequality problem (AVI). This approach leverages DC programming (Difference of Convex functions programming) and DCA (DC Algorithms). The foundations of DC programming and DCA were initially laid by Pham Dinh Tao in a preliminary form in 1985 and have since undergone extensive development, particularly in the works of Tao Pham Dinh, as documented in references [14, 15, 18–20], and in related works cited therein. These methods have now become classics and are widely adopted by many researchers, as evidenced by references [10, 11, 17, 21, 22]. The motivation behind our work stems from the successful application of DCA (DC Algorithms) to numerous large-scale non-convex programs, both smooth and non-smooth, across various domains in applied sciences. The DCA has proven itself to be a reliable approach, often yielding global solutions and demonstrating superior robustness and efficiency compared to standard methods.

In our study, we adopt an optimization perspective for the affine variational inequality problem (AVI). We demonstrate that this optimization problem can be cast as a DC (Difference of Convex functions) program, making it amenable to DCA.

A DC program involves the minimization of a DC function, typically expressed as $f = g - h$, over a convex set. Here, g and h are convex functions that constitute the DC components. It is noteworthy that the construction of DCA revolves around the convex DC components, namely g and h , "rather than the DC function f " itself.

In this work, we propose a suitable DC formulation for optimizing the AVI and investigate the implications of this DC decomposition in terms of the mentioned properties. To evaluate the efficiency of both the optimization model and the corresponding DC formulation, as well as the resulting DCA schemes, we conduct tests using several benchmark datasets.

The paper is structured as follows.

Section 2: This section delves into the relationship between a quadratic program and the affine variational inequality (AVI).

Section 3: This section provides a brief introduction to DC programming and DCA, offering insights into the solution methods for addressing the optimization problem associated with the AVI using DC programming and DCA.

Section 4: In this section, we present the numerical results obtained from experiments conducted on several test problems, providing insights into the practical performance of the proposed methods.

2 Optimization and AVI

The relationship between optimization and the Affine Variational Inequality (AVI) lies in the fact that the AVI can be formulated as an optimization problem, while the AVI is not explicitly an optimization problem, it can often be transformed into a quadratic optimization problem when the matrix M is symmetric (see [1,5,6,9]), and this opens the door for applying various optimization techniques to find solutions efficiently. Researchers leverage optimization principles and methodologies to tackle the AVI and obtain solutions that meet certain criteria or objectives. The AVI problem is equivalent to the first-order conditions of the following quadratic program:

$$\min_{x \in C} f(x) = \frac{1}{2}x^T Mx + q^T x. \quad (3)$$

3 Overview of DC Programs and DCA

DC programming and DCA indeed serve as fundamental tools in both smooth and non-smooth non-convex programming, including global optimization. These methods are particularly valuable when dealing with optimization problems where the objective function is expressed as the difference between two convex functions, either over the entire space \mathbb{R}^n or within a specified set $C \subset \mathbb{R}^n$. In a general sense, a DC program can be represented by the following mathematical form:

$$\alpha = \min_{x \in \mathbb{R}^n} (f(x) = g(x) - h(x)), \quad (4)$$

where both $g(x)$ and $h(x)$ are convex functions. The necessary local optimality condition for the primal DC program (4) is

$$\partial h(x^*) \subset \partial g(x^*), \quad (5)$$

where $\partial h(x)$ and $\partial g(x)$ denote the sub-differential of $h(x)$ and $g(x)$ at the point x .

A point x^* satisfies the generalized Kuhn-Tucker condition (a critical point of $g - h$) if

$$\partial g(x^*) \cap \partial h(x^*) = \emptyset. \quad (6)$$

The DCA (DC Algorithm) is the algorithmic framework employed to address these DC programming problems. It iteratively approximates the non-convex objective function using convex components, optimizes the convexified subproblems, and updates the solution until convergence is achieved. The DCA has demonstrated its utility in handling challenging non-convex optimization problems, making it a valuable tool in various fields of applied mathematics and optimization. Based on optimality conditions and duality in the DCA, the idea of the DCA is quite simple: each iteration k of the DCA approximates the concave part $-h$ by its affine majorization, which corresponds to taking

$$y^k \in \partial h(x^k),$$

and minimizes the resulting convex function, which is equivalent to determining the unique solution of the problem (4):

$$x^{k+1} \in \partial g^*(y^k)$$

with g^* being the conjugate function of g . The generic form of a DC algorithm is stated as follows.

Algorithm 3.1 Initialization: Let $x \in \mathbb{R}^n$ be the best guess, $k \rightarrow 0$.

Repeat.

Calculate $y^k \in \partial h(x^k)$.

Calculate $x^{k+1} \in \arg \min (g(x) - h(x^k) - \langle x - x^k, y^k \rangle : x \in \mathbb{R}^n)$.

$k \rightarrow k + 1$

Until convergence of $\{x^k\}$.

The convergence characteristics of the DCA and its underlying theoretical foundation can be found in the following cited sources [14, 16, 19, 20].

3.1 DCA for addressing AVI

In the context of a general non-convex quadratic program, various DC formulations have been introduced in [14, 16]. In this paper, we employ the following DC decomposition, which appears to be the most intuitive: $f(x) = g(x) - h(x)$, where

$$\begin{cases} g(x) = \varkappa_C(x) + \frac{\rho}{2} \|x\|^2 + \langle q, x \rangle, \\ h(x) = \frac{\rho}{2} \|x\|^2 - \frac{1}{2} \langle Mx, x \rangle, \end{cases} \quad \text{and } \rho \geq \lambda_{\max}.$$

In this context, λ_{\max} represents the largest eigenvalue of the matrix M , while $\varkappa_C(\cdot)$ represents the indicator function associated with the set C . It is evident that both g and h are convex functions, rendering problem (1) a DC program in the standard form

$$\min_{x \in \mathbb{R}^n} \{g(x) - h(x)\}. \tag{7}$$

Following the generic DCA scheme, along with its properties and theoretical foundation detailed in [9, 12, 15, 16], at each step $k \geq 0$, the computation of y^k is performed as

$$y^k = (\nabla h(x^k))^T = (\rho I - M)x^k \tag{8}$$

and subsequently, the unique solution denoted as x^{k+1} is determined for the convex minimization problem

$$\min_{x \in \mathbb{R}^n} \{g(x) - [h(x^k) + \langle x - x^k, y^k \rangle]\}.$$

So, at every step $k \geq 0$, the point is computed as follows:

$$x^{k+1} = P_c \left(x^k - \frac{1}{\rho} (Mx^k - q) \right).$$

This is the unique solution corresponding to the problem (7). The latter can be equivalently expressed as

$$\min \left\{ \left\| x - \frac{1}{\rho} (y^k - q) \right\|^2, Ax \geq b \right\}$$

with $y^k = (\rho I - M)x^k$.

The primary operation at each iteration of the algorithm involves solving a quadratic program. The application of the DCA to (7) can be outlined as follows.

Algorithm 3.2 Step 0. Let $\epsilon > 0$ be a sufficiently small positive number, Let $x^0 \in C$ be a starting point, set $k = 0$,
For $k = 0, 1, \dots$

Step 1. Compute $y^k = (\rho I - M)x^k$,

Step 2. Compute x^{k+1} as an optimal solution of the following optimization program:

$$\min \left\{ \left\| x - \frac{1}{\rho} (y^k - q) \right\|^2, Ax \geq b \right\}$$

If either $\|x^{k+1} - x^k\| \leq \epsilon$ or $\|f(x^{k+1}) - f(x^k)\| \leq \epsilon$, **then stop**,
otherwise, set $k = k + 1$ and go to **Step 1**.

The main operation at each iteration of the algorithm consists of solving one quadratic program.

3.2 Convergence of the algorithm

Theorem 3.1 [14]

1) The DCA generates the sequence $\{x_k\}$ in C such that the sequence $\{f(x_k)\}$ is decreasing.

2) If the optimal value of problem (7) is finite, then the sequence $\{x_k\}$ converges to x^* satisfying the necessary local optimality condition $\partial h(x^*) \subset \partial g(x^*)$.

4 Computational Results

To provide a better understanding of our algorithm's performance, we implemented it in Matlab and applied it to a set of examples that have been previously studied in the literature. We designate the initial point as x^0 . These examples were tested with various values of ρ and x^0 . In our implementation, we set the tolerance parameter to $\epsilon = 10^{-6}$.

Example 4.1 [12] Consider the following AVI problem, where its data is given by

$$M = \begin{bmatrix} 1 & 0 \\ 0 & -2 \end{bmatrix}, \quad A = \begin{bmatrix} 1 & 0 \\ 0 & 1 \\ -1 & -1 \end{bmatrix}, \quad q = \begin{pmatrix} -1 \\ 0 \end{pmatrix}, \quad b = \begin{pmatrix} 0 \\ 0 \\ -2 \end{pmatrix}.$$

The optimal solution set of Example 4.1 is $Sol(M, A, q, b) = \{(0, 2)^T, (1, 0)^T\}$.

In the implementation, we take $\rho_{\max} = 1$ and we use two starting points such as $x_1^0 = (0.5, 0.5)^T$ and $x_2^0 = (-10, -10)^T$. The numerical results obtained by the algorithm are summarized in Table 1.

Example 4.2 [12] The data of the AVIs is given by

$$M = \begin{bmatrix} 1 & 0 \\ 0 & -1 \end{bmatrix}, \quad A = \begin{bmatrix} 1 & 2 \\ 1 & 2 \\ 1 & 0 \end{bmatrix}, \quad q = \begin{pmatrix} -1 \\ 0 \end{pmatrix}, \quad b = \begin{pmatrix} 0 \\ 0 \\ 2 \end{pmatrix}.$$

The optimal solution set is given by $Sol(M, A, q, b) = \{(2, -1)^T, (2, 1)^T, (2, 0)^T\}$.

We take $\rho_{\max} = 1$ and the initial points $x_1^0 = (4, 0)^T$ and $x_2^0 = (-0.5, -10)^T$. The obtained numerical results are then summarized in Table 2.

Example 4.3 [18] The data of the AVIs is deduced from a non-convex quadratic program, where

ρ	x_1^0		x_2^0	
	4 iter	CPU (s)	iter	CPU (s)
-1	7	0.0389	8	0.0422
0.5	3	0.0155	12	0.0630
1	3	0.0178	13	0.0701
1.5	4	0.0289	16	0.0773
2	4	0.0184	19	0.0724
4	6	0.0525	30	0.2047
10	12	0.0853	60	0.3669
100	103	0.5227	476	3.5156

Table 1: Example 4.1.

ρ	x_1^0		x_2^0	
	4 iter	CPU (s)	iter	CPU (s)
0.01	2	0.0224	3	0.0278
0.1	2	0.0246	3	0.0583
0.5	2	0.0095	3	0.01992
1	2	0.0093	5	0.0390
2	3	0.1899	8	0.0457
10	12	0.1395	26	0.1926
100	111	0.6902	210	0.7789

Table 2: Example 4.2.

$$M = \begin{pmatrix} 263 & -97 & 62 & 217 & 52 & 621 & 935 & 258 & -61 & -10 \\ -97 & 299 & -17 & 9 & 4 & -123 & -17 & -40 & -3 & 37 \\ 62 & -17 & 178 & 71 & -118 & -83 & -110 & 9 & -56 & 42 \\ 217 & 9 & 71 & 143 & -5 & 842 & 228 & 42 & 58 & -41 \\ 52 & -4 & -118 & -5 & 177 & 102 & -15 & 120 & 13 & -52 \\ 621 & -123 & -83 & 842 & 102 & 219 & 574 & 22 & 73 & -53 \\ 935 & -17 & -110 & 228 & -15 & 574 & 457 & 154 & -25 & 84 \\ 258 & -40 & 9 & 42 & 120 & 22 & 154 & 473 & 18 & -29 \\ -61 & -3 & -56 & 58 & 13 & 73 & -25 & 18 & -4 & -79 \\ -10 & 37 & 42 & -41 & -52 & -53 & 84 & -29 & -79 & 224 \end{pmatrix},$$

$$A = \begin{pmatrix} I \\ -I \end{pmatrix}, \quad b = (0, 0, 0, 0, 0, -1, -1, -1, -1, -1)^T,$$

and

$$q = (-20, -314, 46, -83.45, -128.7, 41.3, 43.85, 341.8, 34.05, -34.6)^T.$$

The optimal solution set of Example 3 is given by

$$Sol(M, A, q, b) = \left\{ (0, 1, 0.5, 0, 0.75, 0, 0, 0.6, 1, 0.49)^T \right\}.$$

Here $\rho_{\max} = 2081.7$ and the initial starting points are given by

$x_1^0 = (-1, \dots, -1)^T$ and $x_2^0 = (0.5, \dots, 0.5)^T$. The obtained numerical results for this problem are summarized in Table 3.

ρ	x_1^0		x_2^0	
	4 iter	CPU (s)	iter	CPU (s)
500	40	0.02951	97	0.06440
1000	81	0.2974	262	0.0308
2000	4	0.0646	3	0.0545
2081.7	4	0.0652	3	0.0581
2500	7	0.1137	4	0.0711
3000	7	0.1178	7	0.1216

Table 3: Example 4.3.

Example 4.4 [8] (Variable Size Example). Consider the following quadratic program:

$$\left\{ \begin{array}{l} \min \left[-\sum_{i=1}^n x_i^2 \right] \\ \text{Such that} \\ \sum_{i=1}^n x_i \geq j, \quad j = 1, 2, \dots, n, \\ x_i \geq 0, \quad i = 1, 2, \dots, n. \end{array} \right.$$

The data of the corresponding variational problem are

$$M = \begin{pmatrix} -2 & 0 & 0 & \cdot & \cdot & \cdot & 0 \\ 0 & -2 & 0 & \cdot & \cdot & \cdot & 0 \\ 0 & 0 & -2 & \cdot & \cdot & \cdot & 0 \\ \cdot & \cdot & \cdot & \cdot & \cdot & \cdot & \cdot \\ \cdot & \cdot & \cdot & \cdot & \cdot & \cdot & \cdot \\ \cdot & \cdot & \cdot & \cdot & \cdot & \cdot & \cdot \\ 0 & 0 & 0 & \cdot & \cdot & \cdot & -2 \end{pmatrix}, \quad q = \begin{pmatrix} 0 \\ 0 \\ 0 \\ \cdot \\ \cdot \\ \cdot \\ 0 \end{pmatrix},$$

$$A = \begin{pmatrix} -1 & 0 & 0 & \cdot & \cdot & \cdot & 0 \\ -1 & -2 & 0 & \cdot & \cdot & \cdot & 0 \\ -1 & -2 & -3 & \cdot & \cdot & \cdot & 0 \\ \cdot & \cdot & \cdot & \cdot & \cdot & \cdot & \cdot \\ \cdot & \cdot & \cdot & \cdot & \cdot & \cdot & \cdot \\ \cdot & \cdot & \cdot & \cdot & \cdot & \cdot & \cdot \\ -1 & -2 & -3 & \cdot & \cdot & \cdot & n \\ 1 & 0 & 0 & \cdot & \cdot & \cdot & 0 \\ 0 & 1 & 0 & \cdot & \cdot & \cdot & 0 \\ 0 & 0 & 1 & \cdot & \cdot & \cdot & 0 \\ \cdot & \cdot & \cdot & \cdot & \cdot & \cdot & \cdot \\ \cdot & \cdot & \cdot & \cdot & \cdot & \cdot & \cdot \\ \cdot & \cdot & \cdot & \cdot & \cdot & \cdot & \cdot \\ 0 & 0 & 0 & \cdot & \cdot & \cdot & 1 \end{pmatrix}, \quad b = \begin{pmatrix} -1 \\ -2 \\ -3 \\ \cdot \\ \cdot \\ \cdot \\ -n \\ 0 \\ 0 \\ 0 \\ \cdot \\ \cdot \\ \cdot \\ 0 \end{pmatrix}.$$

The results of this example are quoted in the following table for various values of the dimension n .

n	iteration number	CPU (s)
5	2	0.01026
10	2	0.0292
50	2	0.0751
100	2	0.1048
300	2	0.4333
700	2	2.2656
1000	2	6.1662
1500	2	19.3652
3000	2	207.7703

Table 4: Example 4.4.

5 Conclusion

Our investigation is centered around a nonconvex programming approach that relies on DC programming and DCA algorithms to tackle a non-monotone Affine Variational Inequality problem (AVIP). To address the AVIP, we formulated an optimization model and leveraged DCA algorithms for its resolution. Employing a suitable decomposition for this model, we devised a straightforward DCA algorithmic scheme, involving the successive solution of convex quadratic programs. Our numerical experiments, conducted on a variety of test problems, provided compelling evidence for the efficiency and effectiveness of the proposed approach. We successfully applied our approach to solve the model presented above, and it has demonstrated its capability to be employed in addressing large-scale mathematical problems.

References

- [1] M. Achache. A new primal-dual path-following method for convex quadratic programming. *Computational & Applied Mathematics* **25** (2006) 97–110.
- [2] M. Achache. Complexity analysis and numerical implementation of a short-step primal-dual algorithm for linear complementarity problems. *Applied Mathematics and computation* **216** (2010) 1889–1895.
- [3] N. Anane, Z. Kebaili and M. Achache. A DC Algorithm for Solving non-Uniquely Solvable Absolute Value Equations. *Nonlinear Dynamics and Systems Theory* **23** (2) (2023) 119–128.
- [4] Y. Censor, A.N. Iusem and A.S. Zenios. An interior-point method with Bregman functions for the variational inequality problem with paramonotone operators. *Mathematical Programming* **81** (1998) 373–400.
- [5] D. den Hertog, B. Roos and T. Terlaky. A Polynomial Method of Weighted Centers for Convex Quadratic Programming. *Journal of Information and Optimization Sciences* **12** (1991) 187–205.
- [6] F. Facchinei and J.S. Pang. Finite-dimensional Variational Inequalities and Complementarity Problems, vol. I, II. In: Springer Series in Operations Research. Springer-Verlag, New York, 2003.
- [7] F. Fukushima. Equivalent differentiable optimization problems and descent methods for asymmetric variational inequality problems. *Mathematical Programming* **53** (3) (1992) 99–110.

- [8] Li Ge and Sanyang Liu. An accelerating algorithm for globally solving non convex quadratic programming. *Journal of Inequalities and Applications* **178** (2018).
- [9] P.T. Harker and B. Xiao. A polynomial-time algorithm for affine variational inequalities. *Applied Mathematical Letters*. **3** (4) (1991) 31–34.
- [10] Z. Kebaili and M. Achache. On solving non monotone affine variational inequalities problem by DC programming and DCA. *Asian-European Journal of Mathematics* **1** (1) (2010) 1–8.
- [11] N. Krause and Y. Singer. Leveraging the margin more carefully In: Proceedings of the 21st International Conference on Machine Learning, ICML, 2004, Banff, Alberta, Canada, (2004) p. 63. ISBN:1-58113-828-5.
- [12] G.M. Lee and N.N. Tam. Continuity of the Solution Map in Parametric Affine Variational Inequalities. *Set-Valued Analysis* **15** (2007) 105–123.
- [13] Gui-Hua Lin and Zun-Quan Xia. Some improved convergence results for variational inequality problems. *Journal of Interdisciplinary Mathematics* **2** (1) (1999) 81–88.
- [14] H.A. Le Thi and T. Pham Dinh. On solving linear complementarity problems by DC programming and DCA. *Computational Optimization and Applications* **50** (3) (2011) 507–524.
- [15] H.A. Le Thi and T. Pham Dinh. Solving a Class of Linearly Constrained Indefinite Quadratic Problems by D.C. Algorithms. *Journal of global optimization* **11** (3) (1997) 253–285.
- [16] H.A. Le Thi and T. Pham Dinh. The DC (Difference of Convex Functions) Programming and DCA Revisited with DC Models of Real World Nonconvex Optimization Problems. *Annals of Operations Research* **133** (3) (2005) 23–46.
- [17] Y. Liu, X. Shen and H. Doss. Multicategory ψ -learning and support vector machine: Computational tools. *Journal of Computational and Graphical Statistics* **14** (2005) 219–236.
- [18] A. Malek and N. Hosseinipour-Mahani. Solving a class of non-convex quadratic problems based on generalized KKT conditions and neurodynamic optimization technique. *Kybernetika* **51** (5) (2015) 890–908.
- [19] T. Pham Dinh and H.A. Le Thi. Convex analysis approach to dc programming. Theory, algorithms and applications. *Acta Math. Vietnam* **22** (1) (1997) 289–355.
- [20] T. Pham Dinh and H.A. Le Thi. A DC optimization algorithm for solving the trust-region subproblem. *SIAM Journal on Optimization* **8** (2) (1998) 476–505.
- [21] C. Ronan, S. Fabian, W. Jason and B. Léon. Trading convexity for scalability. In: Proceedings of the 23rd International Conference on Machine Learning, ICML 2006, Pittsburgh, Pennsylvania, 2006. 201–208. ISBN:1-59593-383-2.
- [22] T. Schüle, C. Schnörr, S. Weber and J. Hornegger. Discrete tomography by convex-concave regularization and D.C. programming. *Discrete Applied Mathematics* **151** (2005) 151–229.



A Novel Numerical Approach for Solving Nonlinear Volterra Integral Equation with Constant Delay

K. Rouibah^{1*}, S. Kaouache¹ and A. Bellour²

¹ *Laboratory of Mathematics and Their Interactions, Abdelhafid Boussouf Center University, Mila 43000, Algeria.*

² *Laboratory of Applied Mathematics and Didactics, Ecole Normale Supérieure de Constantine 25000, Algeria.*

Received: January 14, 2024; Revised: June 6, 2024

Abstract: In this paper, we discuss the application of an iterative collocation method based on the Lagrangian polynomials to the numerical solution of a class of nonlinear Volterra integral equations with constant delay. This application contains, but is not limited to, many important Volterra delay integral equations that arise in physical and biological modeling processes and that are widely used in the analysis of dynamical systems. In addition, the approximate solution is given in a suitable polynomial spline space by using explicit formulas without resorting to solving any algebraic system. The proposed technique is efficient and easy to implement. The error analysis of the proposed numerical method is studied theoretically. Finally, illustrative examples are given to demonstrate the efficiency of the proposed method.

Keywords: *nonlinear delay Volterra integral equation; collocation method; iterative method; Lagrange polynomials.*

Mathematics Subject Classification (2010): 45J05, 45G10, 65R20, 70K99.

1 Introduction

In this paper, we study a numerical method for the solution of Volterra integral nonlinear equations with constant delay $\tau > 0$,

$$x(t) = f(t) + \int_0^t k_1(t, s, x(s))ds + \int_0^{t-\tau} k_2(t, s, x(s))ds, t \in I = [0, T], \quad (1)$$

* Corresponding author: <mailto:r.khoula@centre-univ-mila.dz>

where $x(t) = \Phi(t)$, $t \in [-\tau, 0]$, f , k_1 , k_2 and Φ are the functions being sufficiently smooth. Equation (1) is frequently encountered in physical and biological modeling processes [1]. The monograph [2] presents a historical survey of mathematical models in biology, which can be described by Volterra integral equations with constant delays.

Now, some results on the numerical solutions of Volterra integral equations have been investigated [3–10]. Different methodologies have been proposed to approximate the solution of (1). For example, Ali et al. [11] proposed a spectral method for pantograph-type delay integral equations by using the Legendre collocation method. Brunner [2] applied the polynomial collocation method to approximate the solution of (1). Caliò et al. [12,13] proposed a deficient spline collocation method, Birem et al. [16] developed an algorithm for solving first kind two-dimensional Volterra integral equations by using the collocation method, Horvat [14] used the spline collocation method to find a numerical solution of (1) in the spline space $S_{m+d}^{(d)}(\Pi_N)$ and Rouibah et al. [15] provided a new numerical approach based on the use of continuous collocation Lagrange polynomials for the numerical solution of nonlinear Volterra integral equations.

On the other hand, the Taylor polynomial method for approximating the solution of integral equations has been proposed in the recent years. For example, Bellour and Rawashdeh [17] used the Taylor method to find an approximate solution for first kind integral equations. Darania and Ivaz [18], Maleknejad and Mahmoudi [19], K. Al-Khaled and M.H. Yousef applied the Sumudu decomposition method [20], Sezer and Gülsu [21] applied the Taylor method to certain linear and nonlinear Volterra integral equations.

This paper is concerned with a piecewise polynomial collocation method based on the Lagrangian polynomials. Our goal is to develop an iterative explicit solution to approximate the solution of the Volterra integral equation with a constant delay (1).

The main advantages of the current collocation method are:

1. A more direct and convergent algorithm is introduced to compute the approximation solution and this provides an explicit numerical solution of the equation (1), which is a basic motivation for using an iterative collocation method.

2. In the current method, there is no algebraic system needed to be solved, which makes the proposed algorithm very effective, easy to implement and the calculation cost low.

The rest of the paper is organized as follows. In Section 2, we divide the interval $[0, T]$ into subintervals, and we approximate the proposed solution in each interval by using Lagrange polynomials. Global convergence is established in Section 3, and three numerical examples are provided in Section 4. Finally, conclusion is given in Section 5.

2 Description of the Collocation Method

Let Π_N be a uniform partition of the interval $I = [0, T]$ defined by

$$t_n^i = i\tau + nh, \quad i = 0, \dots, r-1, \quad n = 0, \dots, N-1, \quad (2)$$

where the stepsize is given by

$$\frac{\tau}{N} = h \text{ and } \tau = \frac{T}{r}.$$

Let $0 \leq c_1 < \dots < c_m \leq 1$ be the collocation parameters, and $t_{n,j}^i = t_n^i + c_j h$, $j = 1, \dots, m$, $i = 0, \dots, r-1$, $n = 0, \dots, N-1$ be the collocation points.

Define the subintervals as $\sigma_n^i = [t_n^i, t_{n+1}^i]$, and $\sigma_{N-1}^i = [t_{N-1}^i, t_N^i]$. Denote by π_m the set of all real polynomials of degree not exceeding m . We define the real polynomial

spline space of degree m as follows:

$$S_{m-1}^{(-1)}(I, \Pi_N) = \{u : u_n = u|_{\sigma_n^i} \in \pi_{m-1}, n = 0, \dots, N - 1, i = 0, \dots, r - 1\}. \tag{3}$$

It is easy to show that for any $y \in C^m([0, T])$,

$$y(t_n^i + sh) = \sum_{j=1}^m L_j(s)y(t_{n,j}^i) + \epsilon_n(s), \quad \epsilon_n(s) = h^m \frac{y^m(\zeta_n)(s)}{m!} \prod_{j=1}^m (s - c_j), \tag{4}$$

where $s \in [0, 1]$ and $L_j(v) = \prod_{l \neq j} \frac{v - c_l}{c_j - c_l}$ are the Lagrange polynomials associate with the parameters $c_j, j = 1, \dots, m$.

Inserting (4) into (1), we get

$$\begin{aligned} x(t_{n,j}^i) = & f(t_{n,j}^i) + h \sum_{l=0}^{i-1} \sum_{p=0}^{N-1} \sum_{v=1}^m b_v k_1(t_{n,j}^i, t_{pv}^l, x(t_{pv}^l)) + h \sum_{p=0}^{n-1} \sum_{v=1}^m b_v k_1(t_{n,j}^i, t_{pv}^i, x(t_{pv}^i)) \\ & + h \sum_{v=1}^m a_{j,v} k_1(t_{n,j}^i, t_{n,v}^i, x(t_{n,v}^i)) + h \sum_{l=0}^{i-2} \sum_{p=0}^{N-1} \sum_{v=1}^m b_v k_2(t_{n,j}^i, t_{pv}^l, x(t_{pv}^l)) \\ & + h \sum_{p=0}^{n-1} \sum_{v=1}^m b_v k_2(t_{n,j}^i, t_{pv}^{i-1}, x(t_{pv}^{i-1})) + h \sum_{v=1}^m a_{j,v} k_2(t_{n,j}^i, t_{n,v}^{i-1}, x(t_{n,v}^{i-1})) \\ & + o(h^m), \end{aligned}$$

where $j = 1, \dots, m, i = 0, \dots, r - 1, n = 0, \dots, N - 1$, such that

$$a_{j,v} = \int_0^{c_j} L_v(\eta) d\eta$$

and

$$b_v = \int_0^1 L_v(\eta) d\eta.$$

It holds for any $u \in S_{m-1}^{-1}(I, \Pi_N)$ that

$$u(t_n^i + sh) = \sum_{j=1}^m L_j(s)u(t_{n,j}^i), s \in [0, 1]. \tag{5}$$

Now, we approximate the exact solution x by $u \in S_{m-1}^{-1}(I, \Pi_N)$ such that $u(t_{n,j}^i)$ satisfy the following nonlinear system:

$$\begin{aligned} u(t_{n,j}^i) = & f(t_{n,j}^i) + h \sum_{l=0}^{i-1} \sum_{p=0}^{N-1} \sum_{v=1}^m b_v k_1(t_{n,j}^i, t_{pv}^l, u(t_{pv}^l)) + h \sum_{p=0}^{n-1} \sum_{v=1}^m b_v k_1(t_{n,j}^i, t_{pv}^i, u(t_{pv}^i)) \\ & + h \sum_{v=1}^m a_{j,v} k_1(t_{n,j}^i, t_{n,v}^i, u(t_{n,v}^i)) + h \sum_{l=0}^{i-2} \sum_{p=0}^{N-1} \sum_{v=1}^m b_v k_2(t_{n,j}^i, t_{pv}^l, u(t_{pv}^l)) \\ & + h \sum_{p=0}^{n-1} \sum_{v=1}^m b_v k_2(t_{n,j}^i, t_{pv}^{i-1}, u(t_{pv}^{i-1})) + h \sum_{v=1}^m a_{j,v} k_2(t_{n,j}^i, t_{n,v}^{i-1}, u(t_{n,v}^{i-1})), \end{aligned}$$

where $v = 1, \dots, m$, $n = 0, \dots, N - 1$, $i = 0, \dots, r - 1$, and $u(t) = \phi(t) \in [-\tau, 0]$.

According to the nonlinearity of the previous system, we can use an iterative collocation solution $u^q \in S_{m-1}^{-1}(I, \Pi_N)$, $q \in \mathbb{N}$, to approximate the exact solution of (1) such that

$$u^q(t_n^i + sh) = \sum_{j=1}^m L_j(s) u^q(t_{n,j}^i), s \in [0, 1], \quad (6)$$

where the coefficients $u^q(t_{n,j}^i)$ are given by

$$\begin{aligned} u^q(t_{n,j}^i) &= f(t_{n,j}^i) + h \sum_{l=0}^{i-1} \sum_{p=0}^{N-1} \sum_{v=1}^m b_v k_1(t_{n,j}^i, t_{p,v}^l, u^q(t_{p,v}^l)) \\ &+ h \sum_{p=0}^{n-1} \sum_{v=1}^m b_v k_1(t_{n,j}^i, t_{p,v}^i, u^q(t_{p,v}^i)) + h \sum_{v=1}^m a_{j,v} k_1(t_{n,j}^i, t_{n,v}^i, u^{q-1}(t_{n,v}^i)) \\ &+ h \sum_{l=0}^{i-2} \sum_{p=0}^{N-1} \sum_{v=1}^m b_v k_2(t_{n,j}^i, t_{p,v}^l, u^q(t_{p,v}^l)) + h \sum_{p=0}^{n-1} \sum_{v=1}^m b_v k_2(t_{n,j}^i, t_{p,v}^{i-1}, u^q(t_{p,v}^{i-1})) \\ &+ h \sum_{v=1}^m a_{j,v} k_2(t_{n,j}^i, t_{n,v}^{i-1}, u^q(t_{n,v}^{i-1})), \end{aligned}$$

where the initial values $u^0(t_{n,j}^i) \in J$ (J is a bounded interval). The above formula is explicit and the approximate solution u^q is given without needing to solve any algebraic system.

In the following section, we prove the convergence of the approximate solution u^q to the exact solution x of (1). Moreover, we can show that the order of convergence is m for all $q \geq m$.

3 Convergence Analysis

Here, we assume that the functions k_1 and k_2 satisfy the Lipschitz condition with respect to the third variable; i.e., there exists $L_i \geq 0$ ($i = 1, 2$) such that

$$|k_i(t, s, y_1) - k_i(t, s, y_2)| \leq L_i |y_1 - y_2|.$$

The following lemmas are very important.

Lemma 3.1 (*Discrete Gronwall-type inequality [2]*)

Let $\{k_j\}_{j=0}^n$ be a given non-negative sequence and the sequence $\{\varepsilon_n\}$ satisfy $\varepsilon_0 \leq p_0$ and

$$\varepsilon_n \leq p_0 + \sum_{i=0}^{n-1} k_i \varepsilon_i, \quad n \geq 1,$$

where $p_0 \geq 0$, then ε_n can be bounded by

$$\varepsilon_n \leq p_0 \exp \left(\sum_{j=0}^{n-1} k_j \right), \quad n \geq 1.$$

Lemma 3.2 (Discrete Gronwall-type inequality [22])

If $\{f_n\}_{n \geq 0}$, $\{g_n\}_{n \geq 0}$ and $\{\varepsilon_n\}_{n \geq 0}$ are non negative sequences and

$$\varepsilon_n \leq f_n + \sum_{i=0}^{n-1} g_i \varepsilon_i, \quad n \geq 0,$$

then

$$\varepsilon_n \leq f_n + \sum_{i=0}^{n-1} f_i g_i \exp \left(\sum_{k=0}^{n-1} g_k \right), \quad n \geq 0.$$

The following result gives the existence and uniqueness of the bounded solution for the nonlinear system (2).

Lemma 3.3 For sufficiently small h , the nonlinear system (2) has a unique solution $u \in S_{m-1}^{-1}$. Moreover, the function u is bounded.

Proof. 1. The nonlinear system (2) has a unique solution in S_{m-1}^{-1} . We will use the induction combined with the Banach fixed point theorem.

- (i) On the interval $\sigma_0^0 = [t_0^0, t_1^0]$, for $j = 1 \dots m$, where $x(t) = \Phi(t)$ for $t \in [-\tau, 0]$, we have

$$u(t_{0,j}^0) = f(t_{0,j}^0) + h \sum_{v=1}^m a_{j,v} k_1(t_{0,j}^0, t_{0,v}^0, u(t_{0,v}^0)) + h \sum_{v=1}^m a_{j,v} k_2(t_{0,j}^0, t_{0,v}^0 - \tau, \phi(t_{0,v}^0)).$$

Let $F_0^0 : R^m \rightarrow R^m$ for $j = 1 \dots m$, so

$$F_{0,j}^0(x) = f(t_{0,j}^0) + h \sum_{v=1}^m a_{j,v} k_1(t_{0,j}^0, t_{0,v}^0, x_v) + h \sum_{v=1}^m a_{j,v} k_2(t_{0,j}^0, t_{0,v}^0 - \tau, \phi(t_{0,v}^0)).$$

From the Banach fixed point theorem, we have

$$\|F_0^0(x) - F_0^0(y)\| \leq hL_1 \|x - y\|,$$

which ensures the existence and uniqueness of $u \in \sigma_0^0$ for h being sufficiently small.

- (ii) Suppose that u exists and is unique on each interval σ_k^l , $l = 0, \dots, i-1$, $k = 0, \dots, N -$

1, and we show that u exists and is unique on $\sigma_n^i = [t_n^i, t_{n+1}^i]$, $j = 1, \dots, m$. Hence

$$\begin{aligned} F_{n,j}^i(x) &= f(t_{n,j}^i) + h \sum_{l=0}^{i-1} \sum_{p=0}^{N-1} \sum_{v=1}^m b_v k_1(t_{n,j}^i, t_{pv}^l, u(t_{pv}^l)) \\ &\quad + h \sum_{p=0}^{n-1} \sum_{v=1}^m b_v k_1(t_{n,j}^i, t_{pv}^i, u(t_{pv}^i)) \\ &\quad + h \sum_{v=1}^m a_{j,v} k_1(t_{n,j}^i, t_{n,v}^i, x_v) \\ &\quad + h \sum_{l=0}^{i-2} \sum_{p=0}^{N-1} \sum_{v=1}^m b_v k_2(t_{n,j}^i, t_{pv}^l, u(t_{pv}^l)) \\ &\quad + h \sum_{p=0}^{n-1} \sum_{v=1}^m b_v k_2(t_{n,j}^i, t_{pv}^{i-1}, u(t_{pv}^{i-1})) \\ &\quad + h \sum_{v=1}^m a_{j,v} k_2(t_{n,j}^i, t_{n,v}^{i-1}, u(t_{n,v}^{i-1})). \end{aligned}$$

For all $i = 0 \dots r-1$, $n = 0 \dots N-1$, $j = 1 \dots m$, we have

$$\|F_{n,j}^i(x) - F_{n,j}^i(y)\| \leq hL_1 \|x - y\|,$$

which ensures the existence and uniqueness of $u \in \sigma_n^i$ for h being sufficiently small.

2. The solution u is bounded. We have

$$\begin{aligned} |u(t_{n,j}^i)| &\leq \alpha + hL_1 \sum_{l=0}^{i-1} \sum_{p=0}^{N-1} \sum_{v=1}^m b_v |u(t_{pv}^l)| + hL_2 \sum_{l=0}^{i-2} \sum_{p=0}^{N-1} \sum_{v=1}^m b_v |u(t_{pv}^l)| \\ &\quad + hL_1 \sum_{p=0}^{n-1} \sum_{v=1}^m b_v |u(t_{pv}^i)| + hL_2 \sum_{p=0}^{n-1} \sum_{v=1}^m b_v |u(t_{pv}^{i-1})| \\ &\quad + hL_1 \sum_{v=1}^m a_{j,v} |u(t_{n,v}^i)| + hL_2 \sum_{v=1}^m a_{j,v} |u(t_{n,v}^{i-1})|. \end{aligned}$$

Let $\alpha = \|f\| + (\tau + T + h)(\|k_1\| + \|k_2\|)$ and let $y_n^i = \max\{u(t_{n,p}^i), p = 1 \dots m\}$. We have

$$\begin{aligned} y_n^i - hL_1 y_n^i &\leq \alpha + hL_1 \sum_{l=0}^{i-1} \sum_{p=0}^{N-1} y_p^l + hL_2 \sum_{l=0}^{i-2} \sum_{p=0}^{N-1} y_p^l \\ &\quad + hL_2 \sum_{p=0}^{n-1} y_p^{i-1} + hL_2 y_n^{i-1} + hL_1 \sum_{p=0}^{n-1} y_p^i \\ &\leq \alpha + h(L_1 + 3L_2) \sum_{l=0}^{i-1} \sum_{p=0}^{N-1} y_p^l + hL_1 \sum_{p=0}^{n-1} y_p^i. \end{aligned}$$

Hence, for all $h \in (0, \frac{1}{2L_1}]$, we get

$$y_n^i \leq 2\alpha + hL_3 \sum_{l=0}^{i-1} \sum_{p=0}^{N-1} y_p^l + hL_4 \sum_{p=0}^{n-1} y_p^i, \tag{7}$$

where $L_3 = 6L_2 + 2L_1$ and $L_4 = 2L_1$. Then, by Lemma 3.1, we obtain

$$\begin{aligned} y_n^i &\leq (2\alpha + hL_3 \sum_{l=0}^{i-1} \sum_{p=0}^{N-1} y_p^l) \exp(\tau L_4) \\ &\leq \alpha_2 + hL_5 \sum_{l=0}^{i-1} \sum_{p=0}^{N-1} y_p^l. \end{aligned}$$

We put $z_n^i = \max\{y_n^i, n = 0, \dots, N-1\}$, we have $z^i \leq \alpha_2 + hL_5 \sum_{l=0}^{i-1} N z^l$. Therefore, by Lemma 3.1, we obtain $z^i \leq \alpha_2 \exp(\tau L_5)$. So $(u(t_{n,j}^i))$ is bounded.

The following result gives the convergence of the approximate solution u to the exact solution x .

Theorem 3.1 *Let f, k_1, k_2 and Φ be m times continuously differentiable on their respective domains. Then for sufficiently small h , the collocation solution u converges to the exact solution x , and the resulting error function $e = x - u$ satisfies $\|e\|_{L^\infty(I)} \leq Ch^m$, where C is a finite constant independent of h .*

Proof. We calculate the error between x and the approximate solution u for $v = 1, 2, \dots, m, n = 0, 1, 2, \dots, N-1$ and $i = 0, 1, \dots, r-1$. By setting $e = x - u$ as the collocation error, we get

$$\begin{aligned} |e(t_{n,j}^i)| &\leq hL_1 \sum_{l=0}^{i-1} \sum_{p=0}^{N-1} \sum_{v=1}^m b_v |e(t_{p,v}^l)| + hL_2 \sum_{l=0}^{i-2} \sum_{p=0}^{N-1} \sum_{v=1}^m b_v |e(t_{p,v}^l)| \\ &\quad + hL_1 \sum_{p=0}^{n-1} \sum_{v=1}^m b_v |e(t_{p,v}^i)| + hL_2 \sum_{p=0}^{n-1} \sum_{v=1}^m b_v |e(t_{p,v}^{i-1})| \\ &\quad + hL_1 \sum_{v=1}^m a_{j,v} |e(t_{n,v}^i)| + hL_2 \sum_{v=1}^m a_{j,v} |e(t_{n,v}^{i-1})|. \end{aligned}$$

Let $e_n^i = \max\{e(t_{n,v}^i), v = 1, \dots, m\}$, we have

$$e_n^i \leq hL_3 \sum_{l=0}^{i-1} \sum_{p=0}^{N-1} e_p^l + hL_1 \sum_{p=0}^{n-1} e_p^i + o(h^m), \text{ where } L_3 = 3L_2 + L_1.$$

Hence, for all $h \in (0, \frac{1}{2L_1}]$, we get

$$e_n^i \leq 2hL_3 \sum_{l=0}^{i-1} \sum_{p=0}^{N-1} e_p^l + 2hL_1 \sum_{p=0}^{n-1} e_p^i + 2o(h^m). \tag{8}$$

By Lemma 3.1, one can obtain

$$e_n^i \leq (2hL_3 \sum_{l=0}^{i-1} \sum_{p=0}^{N-1} e_p^l + 2o(h^m)) \exp(2hL_1N) \leq h\alpha \sum_{l=0}^{i-1} \sum_{p=0}^{N-1} e_p^l + ch^m,$$

where $\alpha = 2hL_3 \exp(2hL_1N)$.
 Let $e^i = \max\{e_n^i, n = 0 \dots N - 1\}$. So

$$e^i \leq \tau\alpha \sum_{l=0}^{i-1} e_p^l + ch^m \leq ch^m \exp(T\alpha) \leq Ch^m.$$

Thus, the proof is completed by taking $C = c \exp(T\alpha)$. The following result gives the convergence of the iterative solution u^q to the exact solution x .

Theorem 3.2 *For any initial condition $u^0(t_{n,j}^i) \in J$, the sequence $u^q(t_{n,j}^i)$ converges to the exact solution x . Moreover, the following error estimates hold:*

$$|u^q(t_{n,j}^i) - x| \leq (hd)^q |(u)^0 - x| + Cd^q h^{m+q} + Ch^m, \tag{9}$$

where $d = L_1 \exp(\tau L_1) + rL_1 \exp(\tau L_1) \tau(L_1 + 2L_2) \exp(\tau L_1) \exp(r\tau(L_1 + 2L_2) \exp(\tau L_1))$.

Proof. Let $(e_n^i)^q = \max |u^{q+1}(t_{p,v}^l) - u(t_{p,v}^l)| v = 1 \dots m$. So

$$\begin{aligned} (e_n^i)^{q+1} &\leq hL_1 \sum_{l=0}^{i-1} \sum_{p=0}^{N-1} (e_p^l)^{q+1} + hL_1 \sum_{p=0}^{n-1} (e_p^i)^{q+1} + hL_1 (e_n^i)^q \\ &+ hL_2 \sum_{l=0}^{i-2} \sum_{p=0}^{N-1} (e_p^l)^{q+1} + hL_2 \sum_{p=0}^{n-1} (e_p^{i-1})^{q+1} + hL_2 (e_n^{i-1})^{q+1} \\ &\leq hL_3 \sum_{l=0}^{i-1} \sum_{p=0}^{N-1} (e_p^l)^{q+1} + hL_1 (e_n^i)^q + hL_1 \sum_{p=0}^{n-1} (e_p^i)^{q+1}, \end{aligned}$$

where $L_3 = L_1 + 3L_2$.

Let $e^i = \max\{e_n^i, n = 0 \dots N - 1\}$. This implies

$$(e_n^i)^{q+1} \leq hL_1 (e^i)^q + \tau L_3 \sum_{l=0}^{i-1} (e^l)^{q+1} + hL_1 \sum_{p=0}^{n-1} (e_p^i)^{q+1}.$$

In view of the well-known result on discrete Gronwall inequalities 3.1, we get

$$\begin{aligned} (e_n^i)^{q+1} &\leq (hL_1 (e^i)^q + \tau L_3 \sum_{l=0}^{i-1} (e^l)^{q+1}) \exp(\tau L_1) \\ &\leq hL_4 (e^i)^q + L_5 \sum_{l=0}^{i-1} (e^l)^{q+1}, \end{aligned}$$

where $L_4 = L_1 \exp(\tau L_1)$ and $L_5 = \tau L_3 \exp(\tau L_1)$. By Lemma 3.2, one can obtain

$$(e^i)^{q+1} \leq hL_4 (e^i)^q + \sum_{l=0}^{i-1} hL_4 (e^l)^q L_5 \exp(rL_5). \tag{10}$$

Let $(e)^q = \max\{(e^i)^q, i = 0, 1, \dots, r - 1\}$, we have

$$\begin{aligned} (e)^{q+1} &\leq hL_4(e)^q + hrL_4(e)^qL_5 \exp(rL_5), \\ &\leq hd(e)^q \quad d = L_4 + rL_4L_5 \exp(rL_5), \\ &\leq (hd)^q |(u)^0 - x| + Cd^qh^{m+q}, \end{aligned}$$

where $j = 1, \dots, m, i = 0, \dots, r - 1, n = 0, \dots, N - 1, q \in N^*$. This implies

$$\begin{aligned} |u^q(t_{n,j}^i) - x(t_{n,j}^i)| &\leq |u^q(t_{n,j}^i) - u(t_{n,j}^i)| + |u(t_{n,j}^i) - x(t_{n,j}^i)| \\ &\leq (hd)^q |(u)^0 - x| + Cd^qh^{m+q} + Ch^m. \end{aligned}$$

4 Numerical Examples

In order to verify the theoretical results, we present the following examples with $\tau = 0.5$ and $T = 1$. All the exact solutions x are already known. In each example, we calculate the error between x and the iterative collocation solution u^m .

Example 4.1 Consider the nonlinear Volterra delay integral equation

$$x(t) = f(t) + \int_0^t k_1(t, s, x(s))ds + \int_0^{t-\tau} k_2(t, s, x(s))ds, \quad t \in [0, 1], \tag{11}$$

where $k_1(t, s, z) = s \sin(t + 2z - s)$, $k_2(t, s, z) = \frac{se^{t-z}}{1+t}$ and f is chosen so that the exact solution is $x(t) = 2t + 1$.

The absolute errors for $(m, N) = \{(4, 4), (5, 5), (6, 6), (8, 8)\}$, for $t = 0, 0.2, \dots, 1$ are shown in Table 1. From columns 2, 3, 4, we note that the absolute error reduces as m increases, and from columns 4, 5, we note that the absolute error reduces as N increases.

t	$m = 4, N = 5$	$m = 5, N = 5$	$m = 7, N = 5$	$m = 7, N = 10$
0.0	0.146×10^{-5}	0.69×10^{-7}	0.25×10^{-7}	0.33×10^{-7}
0.2	0.145×10^{-4}	0.342×10^{-6}	0.68×10^{-7}	0.6×10^{-8}
0.4	0.272×10^{-4}	0.75×10^{-7}	0.34×10^{-7}	0.6×10^{-8}
0.6	0.256×10^{-4}	0.82×10^{-6}	0.27×10^{-7}	0.4×10^{-8}
0.8	0.193×10^{-4}	0.20×10^{-5}	0.59×10^{-7}	0.56×10^{-7}
1.0	0.147×10^{-3}	0.13×10^{-4}	0.39×10^{-6}	0.7×10^{-7}

Table 1: Absolute errors of Example 4.2.

Example 4.2 The given functions in equation (1) are

$$\begin{aligned} k_1(t, s, z) &= 2 \cos(t + z - s)s^2, \\ k_2(t, s, z) &= \frac{stz}{1+t^2}, \text{ and } x(t) = \sin(t) + 1. \end{aligned}$$

The absolute errors for $(m, N) = \{(2, 5), (4, 5), (5, 5), (6, 10)\}$, for $t = 0, 0.2, \dots, 1$ are shown in Table 2. From columns 2, 3, 4, we note that the absolute error reduces as m increases, and from columns 4, 5, we note that the absolute error reduces as both m and N increase.

t	$m = 2, N = 5$	$m = 4, N = 5$	$m = 5, N = 5$	$m = 6, N = 10$
0.2	0.123×10^{-3}	0.81×10^{-7}	0.14×10^{-7}	0.1×10^{-8}
0.2	0.472×10^{-3}	0.16×10^{-6}	0.17×10^{-7}	0.2×10^{-8}
0.4	0.794×10^{-3}	0.34×10^{-6}	0.4×10^{-8}	0.41×10^{-7}
0.6	0.232×10^{-2}	0.58×10^{-5}	0.19×10^{-7}	0.12×10^{-7}
0.8	0.813×10^{-2}	0.83×10^{-4}	0.312×10^{-6}	0.52×10^{-7}
1	0.599×10^{-2}	0.22×10^{-4}	0.245×10^{-6}	0.1×10^{-7}

Table 2: Absolute errors of Example 4.3.

Example 4.3 ([23,24]) Consider the following nonlinear Volterra integral equation:

t	Method in [23]		Method in [24]		Our method	
	$N = 10$	$N = 20$	$N = 10$	$N = 20$	$N = 10$	$N = 20$
0.1	1.0×10^{-5}	1.5×10^{-6}	1.2×10^{-5}	2.5×10^{-8}	9.8×10^{-8}	5.5×10^{-9}
0.2	2.4×10^{-5}	3.2×10^{-6}	1.6×10^{-6}	3.4×10^{-7}	1.4×10^{-7}	3.3×10^{-9}
0.3	3.6×10^{-5}	4.7×10^{-6}	2.0×10^{-4}	9.1×10^{-7}	2.0×10^{-7}	1.4×10^{-8}
0.4	4.6×10^{-5}	5.8×10^{-6}	2.0×10^{-5}	1.4×10^{-6}	2.7×10^{-7}	1.6×10^{-8}
0.5	5.2×10^{-5}	6.6×10^{-6}	3.8×10^{-5}	1.8×10^{-6}	3.5×10^{-7}	2.2×10^{-8}
0.6	5.5×10^{-5}	6.9×10^{-6}	5.1×10^{-5}	2.1×10^{-6}	4.3×10^{-7}	2.6×10^{-8}
0.7	5.5×10^{-5}	6.9×10^{-6}	7.2×10^{-5}	1.8×10^{-6}	5.1×10^{-7}	3.4×10^{-8}
0.8	5.2×10^{-5}	6.4×10^{-6}	6.4×10^{-5}	6.4×10^{-6}	5.6×10^{-7}	3.2×10^{-8}
0.9	4.6×10^{-5}	5.7×10^{-6}	1.9×10^{-5}	1.0×10^{-4}	6.0×10^{-7}	4.5×10^{-8}
01	3.9×10^{-5}	4.7×10^{-6}	6.3×10^{-4}	9.2×10^{-4}	4.6×10^{-7}	2.4×10^{-8}

Table 3: Comparison of the absolute errors of Example 4.3

$$x(t) = 1 + (\sin(t))^2 - \int_0^t 3 \sin(t-s)(x(s))^2 ds, \quad t \in [0, 1],$$

which is a particular case of Equation (1), where $k_1(t, s, z) = -3 \sin(t-s)z^2$ and $k_2(t, s, z) = 0$. Here $x(t) = \cos(t)$ is the exact solution.

The absolute errors for $N = 10, 20$ and $m = 4$ at $t = 0, 0.1, \dots, 1$ are displayed in Table 3. The numerical results of the present method are considerably accurate in comparison with the numerical results obtained in [23, 24]. From Table 3, it is easy to see that the results obtained by the present method are very superior to those obtained by the methods in [23, 24].

5 Conclusion

In this paper, an iterative collocation method based on Lagrangian polynomials has been developed to achieve numerical solution of nonlinear Volterra delay integral equations in a suitable spline space. This method is easy to implement and the coefficients of the approximation solution are determined by using iterative formulas without the need to solve any system of algebraic equations. Numerical examples show that the method is

convergent with a good accuracy. In addition, the results in these examples confirm the theoretical results. Moreover, from Tables 1 and 2, we note that the absolute error reduces as N or m increases.

Acknowledgements

This research was supported by the Algerian General Directorate for Scientific Research and Technological Development (DG-RSDT).

References

- [1] K. L. Cooke. An epidemic equation with immigration. *Math. Biosci.* **29** (1976) 135–158.
- [2] H. Brunner. *Collocation Methods for Volterra Integral and Related Functional Differential Equations*. Cambridge university press, Cambridge, 2004.
- [3] H. Brunner. The discretization of neutral functional integro-differential equations by collocation methods. *Journal of analysis and its applications* **18** (1999) 393–406.
- [4] H. Brunner. Iterated collocation methods for Volterra integral equations with delay arguments. *Mathematics of Computation* **62** (1994) 581–599.
- [5] H. Brunner. Collocation and continuous implicit Runge-Kutta methods for a class of delay Volterra integral equations. *Journal of Computational and Applied Mathematics* **53** (1994) 61–72.
- [6] H. Brunner and Y. Yatsenko. Spline collocation methods for nonlinear Volterra integral equations with unknown delay. *Journal of Computational and Applied Mathematics* **71** (1996) 67–81.
- [7] Q. Hu. Multilevel correction for discrete collocation solutions of Volterra integral equations with delay arguments. *Applied Numerical Mathematics* **31** (1999) 159–171.
- [8] B. Cahlon and L. J. Nachman. Numerical solutions of Volterra integral equations with a solution dependant delay. *Journal of Mathematical Analysis and Applications* **112** (1985) 541–562.
- [9] A. Bellour and M. Bousselsal. A Taylor collocation method for solving delay integral equations. *Numer. Algor.* **65** (2014) 843–857.
- [10] H. Laïb, A. Bellour and A. Boulmerka, Taylor collocation method for high-order neutraldelay Volterra integro-differential equations. *J. Innov. Appl. Math. Comput. Sci.* **2** (1) (2022) 53–77.
- [11] I. Ali, H. Brunner and T. Tang. Spectral methods for pantograph-type differential and integral equations with multiple delays. *Front. Math. China* **4** (2009) 49–61.
- [12] F. Caliò, E. Marchetti and R. Pavani. About the deficient spline collocation method for particular differential and integral equations with delay. *Rend. Sem. Mat. Univ. Pol. Torino* **61** (2003) 287–300.
- [13] F. Caliò, E. Marchetti, R. Pavani and G. Micula. About some Volterra problems solved by a particular spline. *Studia Univ. Babeş-Bolyai* **48** (2003) 45–52.
- [14] V. Horvat. On collocation methods for Volterra integral equations with delay arguments. *Mathematical Communications* **4** (1999) 93–109.
- [15] K. Rouibah, A. Bellour, P. Lima and E. Rawa Shdeh. Iterative continuous collocation method for Solving nonlinear Volterra integral equations. *Kragujevac Journal of Mathematics* **64** (4) (2022) 635–648.

- [16] F. Birem, A. Boulmarka, H. Laib and C. Hennous. An algorithm for solving first-kind two dimensional voltera integral equations using collocation method. *Nonlinear Dynamics and Systems Theory* **23** (5) (2023) 475–486.
- [17] A. Bellour and E. Rawashdeh. Numerical solution of first kind integral equations by using Taylor polynomials. *Journal of Inequalities and Special Functions* **1** (2) (2010) 23–29.
- [18] P. Darania and K. Ivaz. Numerical solution of nonlinear Volterra-Fredholm integro-differential equations. *Computers and Mathematics with Applications* **56** (9) (2008) 2197–2209.
- [19] K. Maleknejad and Y. Mahmoudi. Taylor polynomial solution of high-order nonlinear Volterra-Fredholm integro-differential equations. *Applied Mathematics and Computation* **2** (2003) 641–653.
- [20] K. Al-Khaled and M.H. Yousef. Sumudu decomposition method for solving higher-order nonlinear Volterra-Fredholm fractional integro-differential equations. *Nonlinear Dynamics and Systems Theory* **19** (3) (2019) 348–361.
- [21] M. Sezer and M. Gülsu. Polynomial solution of the most general linear Fredholm-Volterra integro-differential difference equations by means of Taylor collocation method. *Applied Mathematics and Computation* **185** (2007) 646–657.
- [22] R.P. Agrwal. *Difference equations and inequalities: Theory, Methods and Applications*. Second edition. Marcel Dekker, Inc. New York, 2000.
- [23] N. Ebrahimi and J. Rashidinia. Collocation method for linear and nonlinear Fredholm and Volterra integral equations. *Appl. Math. Comput.* **270** (2015) 156–164.
- [24] S.H. Javadi, A. Davari and E. Babolian. Numerical implementation of the Adomian decomposition method for nonlinear Volterra integral equations of the second kind. *Int. J. Comput. Math.* **84** (2007) 75–79.